Supported Re catalysts for the transformation of CO_2 to value-added chemicals

Ting Kah Wei

Graduate School of Chemical Sciences and Engineering

Hokkaido University

2022

Acknowledgements

I would like to extend my deepest gratitude to my supervisor Prof. Ken-ichi Shimizu for presenting me with the chance of being a part of his laboratory, and also for generously providing me with his knowledge and expertise. I would also like to express my sincerest gratitude to Asst. Prof. Takashi Toyao for his invaluable advice and continuous guidance throughout the years in this lab, and consistently steering me into the right direction whenever necessary. I am also deeply indebted to Mr. Wataru Onodera and Dr. Ken-ichi Kon, former research assistants of Shimizu Lab, for providing me with various assistance both technically and morally. I am also extremely grateful and indebted to Prof. Atsushi Urakawa and Dr. Nat Phongprueksathat from TU Delft, Prof. Hiroshi Kondoh and Asst. Prof. Ryo Toyoshima from Keio University, and Dr. Shinya Mine, postdoctoral fellow from Shimizu Lab for aiding me with their technical expertise to make this work possible. My appreciation also goes to the Iwatani Naoji Foundation and Japan Society for the Promotion of Science for the studentship that allowed me to continue my PhD studies. I would also like to thank my fellow lab members, both former and present, for making my study and life here a wonderful time. Last but not least, I would like to thank my loved ones and my significant other for their encouragement and support throughout this journey.

Table of contents

Chapter 1

General Introduction

1.1 Environmental impact of CO_2 emission

Carbon dioxide (CO_2), one of the main constituents of greenhouse gases, is widely considered to be the primary driver of global warming and climate change. CO_2 accounts for approximately 76% of global greenhouse gases emissions, mainly from the usage of fossil fuels and industrial processes.[1]

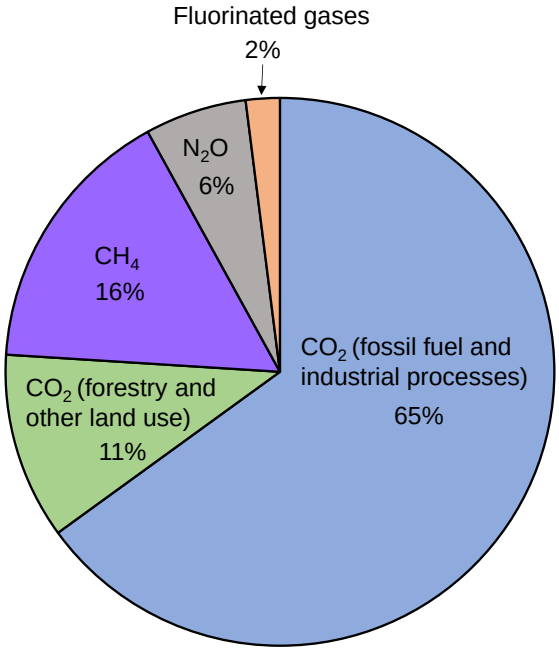

Figure 1. Global anthropogenic greenhouse gas emission by group of gases. Based on data from 2010. Source : IPCC 5th assessment report (2014).

The Paris Agreement has called on nations to limit global warming to well below 2°C, preferably 1.5 °C compared to pre-industrial levels. Anthropogenic CO_2 emission has been rising exponentially ever since the dawn of the industrial revolution. According to the special report on global warming of the Intergovernmental Panel on Climate Change (IPCC), human activities are estimated to have caused approximately 1.0 °C of global warming above pre-industrial levels, and is likely to reach 1.5°C if the rate of increasing follows the current trajectory.[2] Therefore, the common consensus is that the global carbon emission has to be greatly reduced before reaching a point of no return in order to prevent catastrophic climate disaster that will potentially threaten the very existence of human species.

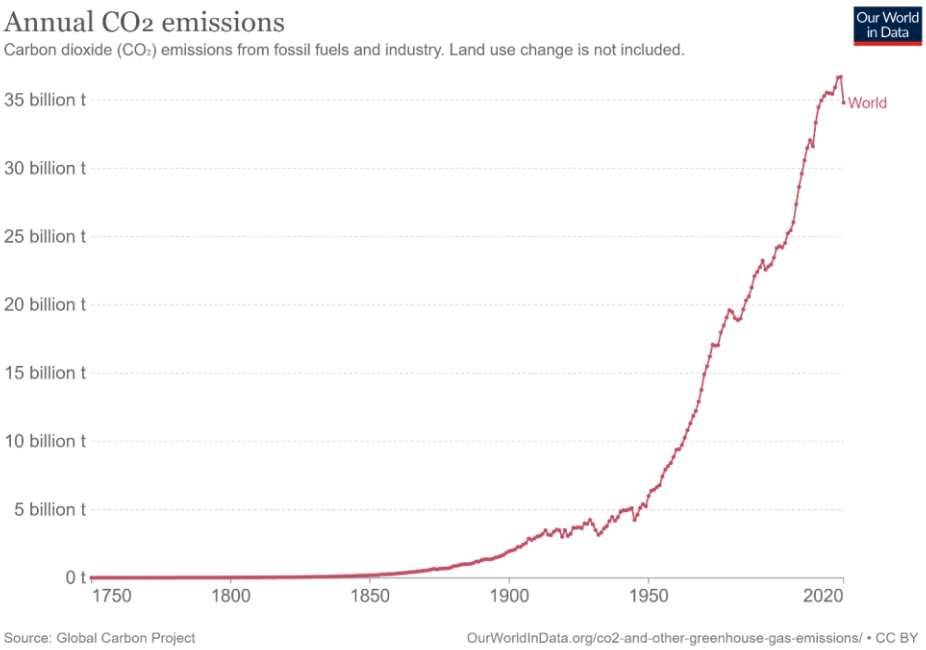

Figure 2. Annual production-based emissions of CO_2. Data from 1750 to 2021 is shown. Source: Hannah Ritchie, Max Roser and Pablo Rosado (2020) - "CO_2 and Greenhouse Gas Emissions". Published online at OurWorldInData.org. Retrieved from: 'https://ourworldindata.org/co2-and-other-greenhouse-gas-emissions'.

1.2 Carbon capture, utilization, and storage (CCUS)

Carbon capture and sequestration, or more commonly known as carbon capture and storage (CCS),[3–10] together with carbon capture and utilization (CCU)[11–19] have become increasingly important for the reduction of carbon emission. CCS technologies involve mainly 3 steps: CO_2 capture, transportation, and storage. In essence, CO_2 is captured from point sources with high carbon emissions such as power plants and industrial plants, and is transported mainly using pipelines to a suitable geological site for permanent storage. However, there are major issues associated with CCS technology that have to be solved for it to become mainstream. From an economic point of view, the deployment of CCS infrastructure requires high capital investment for something that offers virtually little to no profitability, due to the fact that permanent storage of CO_2 itself does not offer much in terms of business opportunity. Moreover, on the technical aspect, CCS is not always a viable option due to geographical constraints, since finding a suitable storage site is a challenging task.[20,21]

Amidst the ever-growing concern on climate change and depletion of fossil resources, CCU technology has garnered broad attention in both academic and industrial sectors due to the prospect of converting CO_2 into valuable products such as fuels or chemicals, while simultaneously contributing to climate change mitigation. The implementation of CO_2 as C_1 source in the petrochemical industries as an alternative to non-renewable fossil feedstock is promising for the realization of a closed carbon cycle, and it is potentially more profitable than CCS due to the fact that value-added products can be sold commercially. Although it may sound like CCU is the “dream” technology to reduce CO_2 emissions, converting CO_2 into various products is a challenging task as the process is extremely energy intensive due to the high thermodynamic stability of CO_2 ($\Delta_f H^\circ_{298K}$ = -393.47 kJ mol^{-1}). Furthermore, at current stage, the largest scale chemical utilization of CO_2 is for the production of urea, which consumes approximately 140 Mt CO_2 yr^{-1}.[18] This is merely a drop in the ocean when compared to the annual CO_2 emission of more than 30 Gt CO_2 yr^{-1} (*vide infra*) in current era. Nevertheless, effective utilization of CO_2 as a carbon feedstock remains a highly attractive prospect for truly enabling a sustainable future, and both CCS and CCU can be integrated and developed in tandem to achieve this goal.

1.3 Catalytic hydrogenation of CO_2

Utilization of CO_2 as a feedstock for the production of chemicals and fuels requires a reduction process to turn CO_2 into various oxygenates and hydrocarbons. Catalytic hydrogenation of CO_2 has been studied extensively because hydrogenation process is arguably the most practical method for CO_2 conversion; the process is straightforward and effective when compared to other methods such as photochemical or electrochemical conversion, and the process is essentially carbon-neutral on the premise that H_2 originates from renewable energy sources (i.e., green hydrogen).[22–29] Furthermore, effective utilization of H_2 is also in line with the concept of "Hydrogen Society" as advocated by the Government of Japan.[30–33]

The synthesis of value-added products via CO_2 hydrogenation follows several possible upgrade pathways as shown in **Figure 3**. Considerable progress has been made in the research for CO_2 hydrogenation to C_1 products. Among them, CO_2 hydrogenation to methanol[34–41] has received widespread attention owing to the concept of "methanol economy" as proposed by the late Nobel prize laureate, George A. Olah.[42] Methanol, as the simplest alcohol, is one of the most important commodity chemicals in the world. Methanol is used as a precursor to many other important chemicals such as formaldehyde, acetic acid, and methyl methacrylate. Methanol can also be used for the production of synthetic fuels such as ethylene and propylene via the methanol-to-hydrocarbons (MTH) process,[43–47] or employed as a fuel itself by mixing with gasoline. Additionally, methanol can be converted to dimethyl ether (DME), a clean fuel that is non-toxic and non-corrosive, via dehydration.[48–51] Similar to methanol, DME is also an important building block for the production of many commonly used chemicals such as methyl acetate, dimethyl sulphate, and can also be converted to light olefins and gasoline. Therefore, the direct synthesis of DME via CO_2 hydrogenation has also been studied alongside CO_2-to-methanol.

CO_2 hydrogenation to higher alcohols, especially ethanol, have also been gaining attention lately,[52–58] albeit to a lesser extent than CO_2-to-methanol as ethanol synthesis is a far more challenging process which requires C−C coupling. The same could be said about Fischer-Tropsch (FT) synthesis using CO_2 to produce synthetic fuels,[59–64] which usually occurs in parallel with CO_2 hydrogenation to higher alcohols, and as a consequence, lowering the selectivity of the desired product(s). For these

processes, the ability to maintain a high yield and selectivity remains a daunting task, and more studies are needed for these technologies to become viable.

Another classical example of CO_2 hydrogenation is methanation reaction, also known as the Sabatier reaction.[65–69] Since methane is the primary component of natural gas, there was a growing interest in CO_2 methanation as a way to produce synthetic natural gas (SNG) in the past. In recent years however, against the backdrop of shale revolution in the USA, the synthesis of methane via CO_2 hydrogenation simply does not make much sense economically, leading to the diminishing of interest in large scale production of SNG.

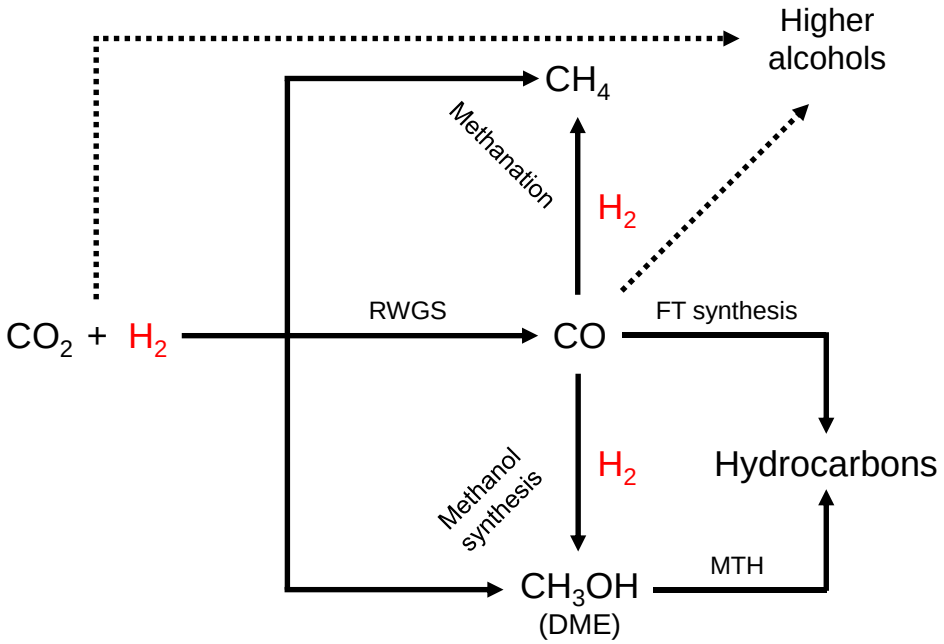

Figure 3. Various pathway for the hydrogenation of CO_2 into value-added products.

1.4 Application of CO_2/H_2 as methylating agent

Aside from direct synthesis of commodity chemicals via CO_2 hydrogenation, the application of CO_2 and H_2 as methylating agent has emerged to be a popular strategy to achieve higher equilibrium conversion of CO_2 for various CO_2 valorization process. For example, *N*-methylation of amines using CO_2 for the synthesis of methylamines have been widely studied.[70–78] However, reports on *C*-methylation using CO_2/H_2 are relatively scarce when compared to *N*-methylation due to the fact that C–C bond formation is far more challenging than C–N coupling as a consequence of the weaker nature of carbon nucleophiles. The very first *C*-methylation was reported in 2014 by Beller and coworkers, in which the direct catalytic methylation of heteroarenes using CO_2/H_2 over Ru-based homogenous catalysts was demonstrated.[79] More recently, multiple reports on the catalytic methylation of common aromatic hydrocarbons such as benzene, toluene, or naphthalene using CO_2/H_2 have also emerged[80–82], signaling the growing interest of methylation using CO_2/H_2 as a method for upgrading low-value commodity chemicals.

1.5 Rhenium as a catalyst

Rhenium (Re) catalysts are of great technological importance in heterogeneous catalysis. Supported rhenium catalysts are reported to be active and highly selective for hydrogenation of carboxylic acid.[83,84] Rhenium is also widely used as an active catalyst for valorization of a vast variety of biomass-derived chemicals.[85–88] One of the most well-known applications of Re as a catalyst is Pt-Re bimetallic catalyst used in petroleum reforming.[89,90]

Rhenium is situated in group VII in the periodic table of elements, which is the same as manganese (Mn), another frequently used element in catalysis. However, rhenium is considerably different from manganese in terms of its chemical and catalytic properties. For example, the most stable oxidation for manganese is +2, whereas for rhenium its most stable oxidation state is +7. Rhenium is known to occupy a variety of oxidation states from 0 to +7, which can be linked to its catalytic multifunctionality. Unlike other noble metals, Re is strongly oxophilic, which makes the determination of its oxidation state highly challenging.

1.6 Thesis outline

In this thesis, the attention will be focused on TiO_2-supported rhenium (Re/TiO_2) catalyst, which shows promising performance for various CO_2 hydrogenation reaction. This thesis will be divided into the following chapters:

Chapter 2: Low temperature hydrogenation of CO_2 to methanol.

Low temperature CO_2-to-methanol reaction over Re/TiO_2 catalyst in batch reactor and fixed-bed flow reactor were explored. The performance of Re/TiO_2 was tested against various other supported metal catalyst, which included the conventional Cu-based methanol synthesis catalyst. The possible active sites and reaction mechanisms were also identified using a combination of *operando* spectroscopic techniques and isotopic labelling experiments.

Chapter 3: Catalytic methylation of aromatic hydrocarbons using CO_2/H_2.

Using a combination of Re/TiO_2 and zeolite, methylation of aromatic hydrocarbons (benzene, toluene, *m*-xylene) was carried out. Various other combination of zeolite and supported metal catalyst were also tested and evaluated. Machine learning method were employed on our accumulated datasets for further catalyst optimization.

Chapter 4: Characterization of Re/support catalysts and mechanistic study employing both experimental and theoretical methods.

DFT calculations were conducted to investigate support-metal interactions between rhenium and various support oxide. The reason for the high dispersion of Re species on TiO_2 was revealed.

1.7 References

(1) Eickemeier, P.; Schlömer, S.; Farahani, E.; Kadner, S.; Brunner, S.; Baum, I.; Kriemann, B. *IPCC, 2012: Summary for Policymakers*; **2019**.

(2) Masson-Delmotte, V. . P. Z. H.-O. P. D. R. J. S. P. R. S. A. P. W. M.-O. C. P. R. P. S. C. J. B. R. M. Y. C. X. Z. M. I. G. E. L. T. M. M. T. and T. W. (eds. . Summary for Policymakers. In Global Warming of 1.5°C: IPCC Special Report on Impacts of Global Warming of 1.5°C above Pre-Industrial Levels in Context of Strengthening Response to Climate Change, Sustainable Development, and Efforts to Eradicate Poverty). *Glob. Warm. 1.5°C* **2018**, 1–24.

(3) Bui, M.; Adjiman, C. S.; Bardow, A.; Anthony, E. J.; Boston, A.; Brown, S.; Fennell, P. S.; Fuss, S.; Galindo, A.; Hackett, L. A.; et al. Carbon Capture and Storage (CCS): The Way Forward. *Energy Environ. Sci.* **2018**, *11* (5), 1062–1176.

(4) Anderson, S.; Newell, R. Prospects for Carbon Capture and Storage Technologies. *Annu. Rev. Environ. Resour.* **2004**, *29*, 109–142.

(5) Boot-Handford, M. E.; Abanades, J. C.; Anthony, E. J.; Blunt, M. J.; Brandani, S.; Mac Dowell, N.; Fernández, J. R.; Ferrari, M. C.; Gross, R.; Hallett, J. P.; et al. Carbon Capture and Storage Update. *Energy Environ. Sci.* **2014**, *7* (1), 130–189.

(6) Lau, H. C.; Ramakrishna, S.; Zhang, K.; Radhamani, A. V. The Role of Carbon Capture and Storage in the Energy Transition. *Energy and Fuels* **2021**, *35* (9), 7364–7386.

(7) Gibbins, J.; Chalmers, H. Carbon Capture and Storage. *Energy Policy* **2008**, *36* (12), 4317–4322.

(8) Roussanaly, S.; Berghout, N.; Fout, T.; Garcia, M.; Gardarsdottir, S.; Nazir, S. M.; Ramirez, A.; Rubin, E. S. Towards Improved Cost Evaluation of Carbon Capture and Storage from Industry. *Int. J. Greenh. Gas Control* **2021**, *106* (January), 103263.

(9) Heddle, G.; Herzog, H.; Klett, M. The Economics of Carbon Dioxide Storage. **2003**, 115.

(10) Rackley, S. Carbon Capture and Storage. *Carbon Capture and Storage* **2009**, *325* (September), 1–392.

(11) Aresta, M.; Dibenedetto, A.; Angelini, A. The Changing Paradigm in CO2 Utilization. *J. CO2 Util.* **2013**, *3–4*, 65–73.

(12) Cuéllar-Franca, R. M.; Azapagic, A. Carbon Capture, Storage and Utilisation Technologies: A Critical Analysis and Comparison of Their Life Cycle Environmental Impacts. *J. CO2 Util.* **2015**, *9*, 82–102.

(13) Meylan, F. D.; Moreau, V.; Erkman, S. CO2 Utilization in the Perspective of Industrial Ecology, an Overview. *J. CO2 Util.* **2015**, *12*, 101–108.

(14) Psarras, P. C.; Comello, S.; Bains, P.; Charoensawadpong, P.; Reichelstein, S.; Wilcox, J. Carbon Capture and Utilization in the Industrial Sector. *Environ. Sci. Technol.* **2017**, *51* (19), 11440–11449.

(15) Gabrielli, P.; Gazzani, M.; Mazzotti, M. The Role of Carbon Capture and Utilization, Carbon Capture and Storage, and Biomass to Enable a Net-Zero-CO2 Emissions Chemical Industry. *Ind. Eng. Chem. Res.* **2020**, *59* (15), 7033–7045.

(16) Thonemann, N.; Pizzol, M. Consequential Life Cycle Assessment of Carbon Capture and Utilization Technologies within the Chemical Industry. *Energy Environ. Sci.* **2019**, *12* (7), 2253–2263.

(17) Mac Dowell, N.; Fennell, P. S.; Shah, N.; Maitland, G. C. The Role of CO2 Capture and Utilization in Mitigating Climate Change. *Nat. Clim. Chang.* **2017**, *7* (4), 243–249.

(18) Hepburn, C.; Adlen, E.; Beddington, J.; Carter, E. A.; Fuss, S.; Mac Dowell, N.; Minx, J. C.; Smith, P.; Williams, C. K. The Technological and Economic Prospects for CO2 Utilization and Removal. *Nature* **2019**, *575* (7781), 87–97.

(19) Zhu, Q. Developments on CO2-Utilization Technologies. *Clean Energy* **2019**, *3* (2), 85–100.

(20) Bachu, S. CO2 Storage in Geological Media: Role, Means, Status and Barriers to Deployment. *Prog. Energy Combust. Sci.* **2008**, *34* (2), 254–273.

(21) Bachu, S.; Bonijoly, D.; Bradshaw, J.; Burruss, R.; Holloway, S.; Christensen, N. P.; Mathiassen, O. M. CO2 Storage Capacity Estimation: Methodology and Gaps. *Int. J. Greenh. Gas Control* **2007**, *1* (4), 430–443.

(22) Saeidi, S.; Najari, S.; Hessel, V.; Wilson, K.; Keil, F. J.; Concepción, P.; Suib, S. L.; Rodrigues, A. E. Recent Advances in CO2 Hydrogenation to Value-Added Products — Current Challenges and Future Directions. *Prog. Energy Combust. Sci.* **2021**, *85*, 100905.

(23) Álvarez, A.; Bansode, A.; Urakawa, A.; Bavykina, A. V.; Wezendonk, T. A.; Makkee, M.; Gascon, J.; Kapteijn, F. Challenges in the Greener Production of Formates/Formic Acid, Methanol, and DME by Heterogeneously Catalyzed CO2 Hydrogenation Processes. *Chem. Rev.* **2017**, *117* (14), 9804–9838.

(24) Yang, H.; Zhang, C.; Gao, P.; Wang, H.; Li, X.; Zhong, L.; Wei, W.; Sun, Y. A Review of the Catalytic Hydrogenation of Carbon Dioxide into Value-Added Hydrocarbons. *Catal. Sci. Technol.* **2017**, *7* (20), 4580–4598.

(25) Ye, R. P.; Ding, J.; Gong, W.; Argyle, M. D.; Zhong, Q.; Wang, Y.; Russell, C. K.; Xu, Z.; Russell, A. G.; Li, Q.; et al. CO2 Hydrogenation to High-Value Products via Heterogeneous Catalysis. *Nat. Commun.* **2019**, *10* (1).

(26) Nezam, I.; Zhou, W.; Gusmão, G. S.; Realff, M. J.; Wang, Y.; Medford, A. J.; Jones, C. W. Direct Aromatization of CO2via Combined CO2hydrogenation and Zeolite-Based Acid Catalysis. *J. CO2 Util.* **2021**, *45* (December 2020).

(27) Wang, W.-H.; Himeda, Y.; Muckerman, J. T.; Manbeck, G. F.; Fujita, E. CO 2 Hydrogenation to Formate and Methanol as an Alternative to Photo- and Electrochemical CO 2 Reduction . *Chem. Rev.* **2015**, *115* (23), 12936–12973.

(28) Roy, S.; Cherevotan, A.; Peter, S. C. Thermochemical CO2 Hydrogenation to Single Carbon Products: Scientific and Technological Challenges. *ACS Energy Lett.* **2018**, *3* (8), 1938–1966.

(29) Kattel, S.; Liu, P.; Chen, J. G. Tuning Selectivity of CO2 Hydrogenation Reactions at the Metal/Oxide Interface. *J. Am. Chem. Soc.* **2017**, *139* (29), 9739–9754.

(30) Behling, N.; Williams, M. C.; Managi, S. Fuel Cells and the Hydrogen Revolution: Analysis of a Strategic Plan in Japan. *Econ. Anal. Policy* **2015**, *48*, 204–221.

(31) Matsuda, S.; Kubota, H. The Feasibility of a “Hydrogen Society.” *Glob. J. Res. Eng.* **2016**, *16* (3).

(32) Nagashima, M. *Japan’s Hydrogen Strategy and Its Economic and Geopolitical Implications*; 2018.

(33) Yoshida, T.; Kojima, K. Toyota MIRAI Fuel Cell Vehicle and Progress toward a Future Hydrogen Society. *Electrochem. Soc. Interface* **2015**, *24* (2), 45–49.

(34) Khan, M. U.; Wang, L.; Liu, Z.; Gao, Z.; Wang, S.; Li, H.; Zhang, W.; Wang, M.; Wang, Z.; Ma, C.; et al. Pt3Co Octapods as Superior Catalysts of CO2Hydrogenation. *Angew. Chemie - Int. Ed.* **2016**, *55* (33), 9548–9552.

(35) Wesselbaum, S.; Vom Stein, T.; Klankermayer, J.; Leitner, W. Hydrogenation of Carbon Dioxide to Methanol by Using a Homogeneous Ruthenium-Phosphine Catalyst. *Angew. Chemie - Int. Ed.* **2012**, *51* (30), 7499–7502.

(36) Huff, C. A.; Sanford, M. S. Cascade Catalysis for the Homogeneous Hydrogenation of CO2 to Methanol. *J. Am. Chem. Soc.* **2011**, *133* (45), 18122–18125.

(37) Jessop, P. G.; Ikariya, T.; Noyori, R. Homogeneous Hydrogenation of Carbon Dioxide. *Chem. Rev.* **1995**, *95* (2), 259–272.

(38) Gothe, M. L.; Pérez-Sanz, F. J.; Braga, A. H.; Borges, L. R.; Abreu, T. F.; Bazito, R. C.; Gonçalves, R. V.; Rossi, L. M.; Vidinha, P. Selective CO2hydrogenation into Methanol in a Supercritical Flow Process. *J. CO2 Util.* **2020**, *40* (May), 101195.

(39) Kar, S.; Sen, R.; Goeppert, A.; Prakash, G. K. S. Integrative CO2Capture and Hydrogenation to Methanol with Reusable Catalyst and Amine: Toward a Carbon Neutral Methanol Economy. *J. Am. Chem. Soc.* **2018**, *140* (5), 1580–1583.

(40) Rodriguez, J. A.; Liu, P.; Stacchiola, D. J.; Senanayake, S. D.; White, M. G.; Chen, J. G. Hydrogenation of CO2to Methanol: Importance of Metal-Oxide and Metal-Carbide Interfaces in the Activation of CO2. *ACS Catal.* **2015**, *5* (11), 6696–6706.

(41) Ting, K. W.; Toyao, T.; Siddiki, S. M. A. H.; Shimizu, K. I. Low-Temperature Hydrogenation of CO 2 to Methanol over Heterogeneous TiO 2 -Supported Re Catalysts. *ACS Catal.* **2019**, *9* (4), 3685–3693.

(42) Olah, G. A. Beyond Oil and Gas: The Methanol Economy. *Angew. Chemie - Int. Ed.* **2005**, *44* (18), 2636–2639.

(43) Sto, M. Methanol-to-Hydrocarbons : Catalytic Materials and Their Behavior1. *Microporous Mesoporous Mater.* **1999**, *29*, 3–48.

(44) Keil, F. J. Methanol-to-Hydrocarbons: Process Technology. *Microporous Mesoporous Mater.* **1999**, *29* (1–2), 49–66.

(45) Tian, P.; Wei, Y.; Ye, M.; Liu, Z. Methanol to Olefins (MTO): From Fundamentals to Commercialization. *ACS Catal.* **2015**, *5* (3), 1922–1938.

(46) Olsbye, U.; Svelle, S.; Bjrgen, M.; Beato, P.; Janssens, T. V. W.; Joensen, F.; Bordiga, S.; Lillerud, K. P. Conversion of Methanol to Hydrocarbons: How Zeolite Cavity and Pore Size Controls Product Selectivity. *Angew. Chemie - Int. Ed.* **2012**, *51* (24), 5810–5831.

(47) Yang, M.; Fan, D.; Wei, Y.; Tian, P.; Liu, Z. Recent Progress in Methanol-to-Olefins (MTO) Catalysts. *Adv. Mater.* **2019**, *31* (50), 1–15.

(48) Xu, M.; Lunsford, J. H.; Goodman, D. W.; Bhattacharyya, A. Synthesis of Dimethyl Ether (DME) from Methanol over Solid-Acid Catalysts. *Appl. Catal. A Gen.* **1997**, *149* (2), 289–301.

(49) Pontzen, F.; Liebner, W.; Gronemann, V.; Rothaemel, M.; Ahlers, B. CO2-Based Methanol and DME - Efficient Technologies for Industrial Scale Production. *Catal. Today* **2011**, *171* (1), 242–250.

(50) Fu, Y.; Hong, T.; Chen, J.; Auroux, A.; Shen, J. Surface Acidity and the Dehydration of Methanol to Dimethyl Ether. *Thermochim. Acta* **2005**, *434* (1–2), 22–26.

(51) Yaripour, F.; Baghaei, F.; Schmidt, I.; Perregaard, J. Catalytic Dehydration of Methanol to Dimethyl Ether (DME) over Solid-Acid Catalysts. *Catal. Commun.* **2005**, *6* (2), 147–152.

(52) Bai, S.; Shao, Q.; Wang, P.; Dai, Q.; Wang, X.; Huang, X. Highly Active and Selective Hydrogenation of CO2 to Ethanol by Ordered Pd-Cu Nanoparticles. *J. Am. Chem. Soc.* **2017**, *139* (20), 6827–6830.

(53) Kusama, H.; Okabe, K.; Sayama, K.; Arakawa, H. Ethanol Synthesis by Catalytic Hydrogenation of CO2 over Rh-Fe/SiO2 Catalysts. *Energy* **1997**, *22* (2–3), 343–348.

(54) Wang, L.; Wang, L.; Zhang, J.; Liu, X.; Wang, H.; Zhang, W.; Yang, Q.; Ma, J.; Dong, X.; Yoo, S. J.; et al. Selective Hydrogenation of CO2 to Ethanol over Cobalt Catalysts. *Angew. Chemie - Int. Ed.* **2018**, *57* (21), 6104–6108.

(55) He, Z.; Qian, Q.; Ma, J.; Meng, Q.; Zhou, H.; Song, J.; Liu, Z.; Han, B. Water-Enhanced Synthesis of Higher Alcohols from CO2 Hydrogenation over a Pt/Co3O4 Catalyst under Milder Conditions. *Angew. Chemie - Int. Ed.* **2016**, *55* (2), 737–741.

(56) Xu, D.; Yang, H.; Hong, X.; Liu, G.; Edman Tsang, S. C. Tandem Catalysis of Direct CO2Hydrogenation to Higher Alcohols. *ACS Catal.* **2021**, *11* (15), 8978–8984.

(57) Schemme, S.; Breuer, J. L.; Samsun, R. C.; Peters, R.; Stolten, D. Promising Catalytic Synthesis Pathways towards Higher Alcohols as Suitable Transport Fuels Based on H2 and CO2. *J. CO2 Util.* **2018**, *27* (July), 223–237.

(58) Zeng, F.; Mebrahtu, C.; Xi, X.; Liao, L.; Ren, J.; Xie, J.; Heeres, H. J.; Palkovits, R. Catalysts Design for Higher Alcohols Synthesis by CO2 Hydrogenation: Trends and Future Perspectives. *Appl. Catal. B Environ.* **2021**, *291* (March), 120073.

(59) Liu, J.; Zhang, A.; Jiang, X.; Liu, M.; Sun, Y.; Song, C.; Guo, X. Selective CO2 Hydrogenation to Hydrocarbons on Cu-Promoted Fe-Based Catalysts: Dependence on Cu-Fe Interaction. *ACS Sustain. Chem. Eng.* **2018**, *6* (8), 10182–10190.

(60) Zhou, W.; Cheng, K.; Kang, J.; Zhou, C.; Subramanian, V.; Zhang, Q.; Wang, Y. New Horizon in C1 Chemistry: Breaking the Selectivity Limitation in Transformation of Syngas and Hydrogenation of CO2 into Hydrocarbon Chemicals and Fuels. *Chem. Soc. Rev.* **2019**, *48* (12), 3193–3228.

(61) Guo, L.; Sun, J.; Ge, Q.; Tsubaki, N. Recent Advances in Direct Catalytic Hydrogenation of Carbon Dioxide to Valuable C2+ Hydrocarbons. *J. Mater. Chem. A* **2018**, *6* (46), 23244–23262.

(62) Ding, F.; Zhang, A.; Liu, M.; Zuo, Y.; Li, K.; Guo, X.; Song, C. CO2 Hydrogenation to Hydrocarbons over Iron-Based Catalyst: Effects of Physicochemical Properties of Al2O3 Supports. *Ind. Eng. Chem. Res.* **2014**, *53* (45), 17563–17569.

(63) Guo, L.; Sun, S.; Li, J.; Gao, W.; Zhao, H.; Zhang, B.; He, Y.; Zhang, P.; Yang, G.; Tsubaki, N. Boosting Liquid Hydrocarbons Selectivity from CO2 Hydrogenation by Facilely Tailoring Surface Acid Properties of Zeolite via a Modified Fischer-Tropsch Synthesis. *Fuel* **2021**, *306* (August), 121684.

(64) Zhang, Z.; Huang, G.; Tang, X.; Yin, H.; Kang, J.; Zhang, Q.; Wang, Y. Zn and Na Promoted Fe Catalysts for Sustainable Production of High-Valued Olefins by CO2 Hydrogenation. *Fuel* **2022**, *309* (July 2021), 122105.

(65) Guerra, L.; Rossi, S.; Rodrigues, J.; Gomes, J.; Puna, J.; Santos, M. T. Methane Production by a Combined Sabatier Reaction/Water Electrolysis Process. *J. Environ. Chem. Eng.* **2018**, *6* (1), 671–676.

(66) Su, X.; Xu, J.; Liang, B.; Duan, H.; Hou, B.; Huang, Y. Catalytic Carbon Dioxide Hydrogenation to Methane: A Review of Recent Studies. *J. Energy Chem.* **2016**, *25* (4), 553–565.

(67) Miguel, C. V.; Soria, M. A.; Mendes, A.; Madeira, L. M. Direct CO2 Hydrogenation to Methane or Methanol from Post-Combustion Exhaust Streams - A Thermodynamic Study. *J. Nat. Gas Sci. Eng.* **2015**, *22*, 1–8.

(68) Aziz, M. A. A.; Jalil, A. A.; Triwahyono, S.; Mukti, R. R.; Taufiq-Yap, Y. H.; Sazegar, M. R. Highly Active Ni-Promoted Mesostructured Silica Nanoparticles for CO2 Methanation. *Appl. Catal. B Environ.* **2014**, *147*, 359–368.

(69) Ashok, J.; Pati, S.; Hongmanorom, P.; Tianxi, Z.; Junmei, C.; Kawi, S. A Review of Recent Catalyst Advances in CO2 Methanation Processes. *Catal. Today* **2020**, *356* (November 2019), 471–489.

(70) Beydoun, K.; Thenert, K.; Streng, E. S.; Brosinski, S.; Leitner, W.; Klankermayer, J. Selective Synthesis of Trimethylamine by Catalytic N-Methylation of Ammonia and Ammonium Chloride by Utilizing Carbon Dioxide and Molecular Hydrogen. *ChemCatChem* **2016**, *8* (1), 135–138.

(71) Toyao, T.; Siddiki, S. M. A. H.; Morita, Y.; Kamachi, T.; Touchy, A. S.; Onodera, W.; Kon, K.; Furukawa, S.; Ariga, H.; Asakura, K.; et al. Rhenium-Loaded TiO2: A Highly Versatile and Chemoselective Catalyst for the Hydrogenation of Carboxylic Acid Derivatives and the N-Methylation of Amines Using H2 and CO2. *Chem. - A Eur. J.* **2017**, *23* (59), 14848–14859.

(72) Auer, S. M.; Gredig, S. V.; Köppel, R. A.; Baiker, A. Synthesis of Methylamines from CO2, H2 and NH3 over Cu-Mg-Al Mixed Oxides. *J. Mol. Catal. A Chem.* **1999**, *141* (1–3), 193–203.

(73) Gredig, S. V.; Koeppel, R. A.; Baiker, A. Comparative Study of Synthesis of Methylamines from Carbon Oxides and Ammonia over Cu/Al2O3. *Catal. Today* **1996**, *29* (1–4), 339–342.

(74) Cabrero-Antonino, J. R.; Adam, R.; Beller, M. Catalytic Reductive N-Alkylations Using CO2 and Carboxylic Acid Derivatives: Recent Progress and Developments. *Angew. Chemie - Int. Ed.* **2019**, *58* (37), 12820–12838.

(75) Gredig, S. V.; Koeppel, R. A.; Baiker, A. Synthesis of Methylamines from Carbon Dioxide and Ammonia. *J. Chem. Soc. Chem. Commun.* **1995**, *46* (1), 73–74.

(76) Lin, W.; Cheng, H.; Wu, Q.; Zhang, C.; Arai, M.; Zhao, F. Selective N-Methylation of N-Methylaniline with CO2 and H2 over TiO2-Supported PdZn Catalyst. *ACS Catal.* **2020**, *10* (5), 3285–3296.

(77) Lin, S.; Liu, J.; Ma, L. A Review on Recent Developments in N-Methylation Using CO2. *J. CO2 Util.* **2021**, *54* (August), 101759.

(78) Tlili, A.; Frogneux, X.; Blondiaux, E.; Cantat, T. Creating Added Value with a Waste: Methylation of Amines with CO 2 and H2. *Angew. Chemie - Int. Ed.* **2014**, *53* (10), 2543–2545.

(79) Li, Y.; Yan, T.; Junge, K.; Beller, M. Catalytic Methylation of C-H Bonds Using CO2 and H2. *Angew. Chemie - Int. Ed.* **2014**, *53* (39), 10476–10480.

(80) Wang, Z.; Chang, H.; Zhang, J.; Sun, Z.; Wu, Y.; Liu, Y.; Zhu, Y.; He, H.; Cao, Y.; Bao, X. Tandem Catalytic Methylation of Naphthalene Using CO2 and H2†. *Chem. Commun.* **2022**, *58* (23), 3779–3782.

(81) Shang, X.; Liu, G.; Su, X.; Huang, Y.; Zhang, T. Preferential Synthesis of Toluene and Xylene from CO2Hydrogenation in the Presence of Benzene through an Enhanced Coupling Reaction. *ACS Catal.* **2022**, 13741–13754.

(82) Zuo, J.; Chen, W.; Liu, J.; Duan, X.; Ye, L.; Yuan, Y. Selective Methylation of Toluene Using CO2and H2to Para-Xylene. *Sci. Adv.* **2020**, *6* (34), 1–9.

(83) Toyao, T.; Siddiki, S. M. A. H.; Touchy, A. S.; Onodera, W.; Kon, K.; Morita, Y.; Kamachi, T.; Yoshizawa, K.; Shimizu, K. I. TiO2-Supported Re as a General and Chemoselective Heterogeneous Catalyst for Hydrogenation of Carboxylic Acids to Alcohols. *Chem. - A Eur. J.* **2017**, *23* (5), 1001–1006.

(84) Yoshino, K.; Kajiwara, Y.; Takaishi, N.; Inamoto, Y.; Tsuji, J. Hydrogenation of Carboxylic Acids by Rhenium-Osmium Bimetallic Catalyst. *J. Am. Oil Chem. Soc.* **1990**, *67* (1), 21–24.

(85) Tomishige, K.; Nakagawa, Y.; Tamura, M. Taming Heterogeneous Rhenium Catalysis for the Production of Biomass-Derived Chemicals. *Chinese Chem. Lett.* **2020**, *31* (5), 1071–1077.

(86) Nakagawa, Y.; Shinmi, Y.; Koso, S.; Tomishige, K. Direct Hydrogenolysis of Glycerol into 1,3-Propanediol over Rhenium-Modified Iridium Catalyst. *J. Catal.* **2010**, *272* (2), 191–194.

(87) Nakagawa, Y.; Tamura, M.; Tomishige, K. Recent Development of Production Technology of Diesel- and Jet-Fuel-Range Hydrocarbons from Inedible Biomass. *Fuel Process. Technol.* **2019**, *193* (May), 404–422.

(88) Nakagawa, Y.; Tamura, M.; Tomishige, K. Catalytic Reduction of Biomass-Derived Furanic Compounds with Hydrogen. *ACS Catal.* **2013**, *3* (12), 2655–2668.

(89) Xiao, J.; Puddephatt, R. J. Pt-Re Clusters and Bimetallic Catalysts. *Coord. Chem. Rev.* **1995**, *143* (C), 457–500.

(90) Prestvik, R.; Moljord, K.; Grande, K.; Holmen, A. The Influence of Pretreatment on the Metal Function of a Commercial Pt-Re/Al2O3 Catalyst. *J. Catal.* **1998**, *174* (2), 119–129.

Chapter 2

Low-Temperature Hydrogenation of CO_2 to Methanol over Heterogeneous TiO_2-Supported Re Catalysts

2.1 Introduction

The growing concern about climate change and the depletion of fossil fuels have prompted the search for alternative carbon sources for the generation of energy and the production of chemicals.[1–10] Carbon dioxide (CO_2), which is regarded to be by far the largest contributor to global warming, is a promising prospective for potential applications as a raw material for the production of fine chemicals.[11–19] The direct synthesis of methanol (MeOH) from the hydrogenation of CO_2 has thus attracted significant interest in the scientific community.[20–28] MeOH is used as a precursor for a vast variety of chemical products, which makes it arguably one of the most important commodity chemicals.[29] Additionally, MeOH can be used as a fuel.[30] Traditionally, MeOH is almost exclusively produced from fossil-derived syngas, which primarily consists of CO and H_2 in addition to small amounts of CO_2, by employing Cu-based catalysts, typically under relatively extreme conditions (T > 200 ˚C; p = 5-10 MPa).[31] Industrially, the direct production of MeOH from the hydrogenation of CO_2 has recently been achieved by using similar Cu-based catalysts and reaction conditions.[32] However, this process suffers from a low equilibrium conversion of CO_2 since the hydrogenation reaction is exothermic.[33,34] Consequently, a lower reaction temperature is more favorable for the formation of MeOH.

Several methods for the low-temperature (T ≤ 150 ˚C) hydrogenation of CO_2 to afford MeOH over homogeneous catalysts under mild conditions have recently emerged.[34–46] Although homogeneous catalysts normally exhibit high activity and operate under mild conditions, they typically suffer from product-separation issues and usually require additives in order to achieve high catalytic performance. Methods based on heterogeneous catalysts have also been actively explored recently. However, most methods hitherto reported suffer from low activity.[47–52] Yet some reports on heterogeneous catalytic systems for the low-temperature hydrogenation of CO_2 to MeOH show high activity.[53–57] For instance, Zen and co-workers reported Pt_3Co octapods,[53] $Rh_{75}W_{25}$ nanosheets,[54] and Pt/MoS_2[55] catalysts that produce MeOH with TON > 2000. Carbon-supported Pt_4Co nanowires (Pt_4Co NWs/C)[56] and RhCo porous nanospheres[57] have also been reported recently as active catalysts for the

hydrogenation of CO_2. These processes represent important contributions to the synthesis of CH_3OH under mild conditions. However, in all cases platinum-group metals (PGMs) are employed and the preparation of these catalysts is complicated. Yet, catalysts employed for such selective hydrogenation reactions should be easily accessible. Hence, the development of versatile heterogeneous catalysts that can be operated under mild conditions ($T \leq 150$ °C) is of extreme importance. Moreover, it should be emphasized that the previous reported studies usually do not mention the formation of byproducts such as CO and CH_4. This is especially problematic for dealing with the hydrogenation of CO_2, which usually generates such byproducts to some extent even over homogeneous catalysts.[22]

In this study, a Re/TiO_2 catalyst, which exhibits high activity and product selectivity for i) the hydrogenation of carboxylic acid derivatives, ii) the *N*-methylation of amines using CO_2 and H_2, and iii) the *N*-alkylation of amines with carboxylic acids or esters in the presence of H_2,[58,59] was employed for the hydrogenation of CO_2 to MeOH at low temperature (T = 150 °C). A series of Re/TiO_2 catalysts with different Re loadings, which ensured a wide range of Re dispersion, were prepared and evaluated with respect to their performance in the hydrogenation of CO_2. Whereas a Re loading of 5 wt% ($Re(5)/TiO_2$) furnished the best performance in previous studies,[58,59] the best performance under the conditions applied in this study (*vide infra*) was achieved using a catalyst containing 1 wt% of Re ($Re(1)/TiO_2$). A comparison of the performance of the $Re(1)/TiO_2$ catalyst to that of various other catalysts, including the industrially used methanol synthesis catalyst $Cu/Zn/Al_2O_3$, revealed that $Re(1)/TiO_2$ surpassed the performance of all the other catalysts tested.

2.2 Experimental section

2.2.1 Materials and catalyst preparation

Organic and inorganic compounds were purchased from common commercial suppliers (Tokyo Chemical Industry, Kanto Chemical, Wako Pure Chemical Industries, Nacalai Tesque, and SigmaAldrich) and used without further purification. TiO_2 (ST-01) was obtained from Ishihara Sangyo Co., Ltd. Its BET specific surface area is 188 m^2 g^{-1}. ZrO_2 (JRC-ZRO-2), MgO (JRC-MGO-3), and SiO_2-Al_2O_3 (JRC-SAL-2, Al_2O_3 = 13.75 wt%) were supplied by the Catalysis Society of Japan. Conversely, γ-Al_2O_3 were prepared by calcination of γ-AlOOH (Catapal B Alumina, Sasol) for 3 h at T = 900 °C. CeO_2 was prepared by calcination (T = 600 °C, t = 3 h, in air) of CeO_2 supplied from Daiichi Kigenso Kagaku Kogyo Co., Ltd (Type A). SiO_2 (Q-10) was supplied by Fuji Silysia Chemical Ltd. The carbon support (Kishida Chemical) was commercially obtained. SnO_2 was prepared by calcination (T = 500 °C, t = 3 h) of H_2SnO_3 (Kojundo Chemical Laboratory Co., Ltd.). HZSM-5:SiO_2/Al_2O_3 = 22:1 and HY:SiO_2/Al_2O_3 = 5.5:1 were obtained from TOSOH Co., Ltd. NH_4ReO_4 and metallic Re were purchased from SigmaAldrich. ReO_2 and Re_2O_7 were supplied from Hydrus Chemical Inc. and Strem Chemicals Inc., respectively. Cu/Zn/Al_2O_3 (MDC-7; 34 wt% Cu) was supplied by Clariant Catalysts (Japan).

Precursors of M/TiO_2 (M = 1 wt% Re, Pt, Ir, Rh, Ru, Pd, Ag, Cu, Ni, or Co) and Re/MOx (1 wt% Re; MOx = metal oxides, zeolites, or carbon) were prepared by mixing the support material with the metal sources, i.e., an aqueous solution of NH_4ReO_4, nitrates of Ag, Ni, Cu, Co, $RuCl_3$ or $IrCl_3 \cdot nH_2O$, or aqueous HNO_3 solutions of $Pt(NH_3)_2(NO_3)_2$, $Rh(NO_3)_3$, or $Pd(NH_3)_2(NO_3)_2$. For the preparation of Re/TiO_2, typically 0.072 g of NH_4ReO_4 were added to a glass vessel (500 mL) containing 100 mL of deionized water ([Re] = 0.0027 M). After sonication (1 min) to completely dissolve the NH_4ReO_4, TiO_2 (4.95 g) was added to the solution, which was then stirred (200 rpm) for 30 min at room temperature. Subsequently, the reaction mixture was evaporated to dryness at T = 50 °C, followed by drying at T = 110 °C under ambient pressure for t = 12 h. The thus obtained material was calcined (T = 500 °C, t = 3 h, in air). For each experiment, the active catalyst was prepared by reduction in a quartz tube (T = 500 °C, t = 0.5 h) under a flow of H_2 (20 cm^3 min^{-1}). The other M/TiO_2 catalysts were prepared in the same manner as described above.

2.2.2 Characterization of catalysts

X-ray diffraction (XRD; Rigaku Miniflex) measurements were conducted using CuKα radiation. Re L_3-edge X-ray absorption fine structure (XAFS) measurements were performed at the BL14B2 line (SPring-8) using a Si(111) double crystal monochromator operated at 8 GeV (proposal 2018A1757). Scanning transmission electron microscopy (STEM) images were recorded on a JEM-ARM200F microscope (JEOL) at an acceleration voltage of 200 kV. The Cs-corrector CESCOR (CEOS) was used in the STEM mode. The samples were prepared by dropping ethanol suspensions of the catalysts on carbon-supported copper grids.

Ambient pressure X-ray photoelectron spectroscopy (AP-XPS) measurements were performed at beamline 13B of Photon Factory (PF) at the High Energy Accelerator Research Organization (KEK). A powder of Re/TiO2 with Re loading of 3 wt%, pre-reduced under H_2 at 500 °C for 30 min, were coated on a Si substrate by using deionized water as a dispersant with a drop-and-dry method. The temperature of samples was measured by using a thermocouple directly attached to the sample holder in the analysis chamber. The gases were introduced into the chamber by using variable leak valves. The samples were pretreated by exposure to H_2 (0.1 Torr) at 450 °C for 30 min followed by cooling to 150 °C under the H_2 atmosphere. Gases were then introduced into analysis chamber and the all the XPS spectra were collected at 150 °C. Re 4f measurements were performed with a photon energy of 630 eV. Binding energy was calibrated using the Ti $2p_{3/2}$ peak of Ti^{4+} species (TiO_2; 485.5 eV). XPS spectra were analyzed with convolution of Gaussian and Lorentzian with a Shirley background in the range of 34-46.5 eV. An asymmetric Doniach–Sunjic peak shape was used to fit the peaks for metallic rhenium.

2.2.3 Catalytic reactions

The following procedure for the hydrogenation reactions can be considered representative: after the reduction with H_2 at T = 500 °C (*cf.* catalyst preparation), the catalyst (0.0054 mmol relative to the Re loading), and a mixture of 1,4-dioxane (1 mL) and *n*-decane (0.15 mmol) as an internal standard were added to a stainless-steel autoclave (30 cm^3). The resulting mixture was magnetically stirred (T = 150 °C; p_{CO2} = 1 MPa; p_{H2} = 5 MPa). MeOH was analyzed using a gas chromatograph with a flame-ionization detector (GC-FID; Shimadzu GC-14B with an Ultra ALLOY capillary column UA±1; Frontier Laboratories Ltd.) while the other products were analyzed using a GC-FID (Shimadzu GC-2014 with a Porapak Q column) with a methanizer (Shimadzu MTN-1).

For catalytic testing using fixed-bed continuous flow reactor, 500 mg of catalyst was packed between quartz wool inside a 1/4-inch stainless-steel tube (ID = 2.79 mm). The catalyst was reduced *in situ* at 450 °C with 90%H_2/Ar (25 mL min^{-1}) for 1 h under atmospheric pressure. After cooling down to room temperature, a H_2/CO_2/Ar with vol% of 69%/23%/8% was fed into the reactor and pressurized to 360 bar. The total flow rate of the gas mixture is kept at 16.7 mL min^{-1} to achieve a gas-hourly space velocity (GHSV) of 2000 h^{-1} equivalent. The products were analyzed by an online gas chromatograph (Bruker, GC-450) equipped with a flame ionization detector for methanol, methyl formate, diethyl ether, and other hydrocarbons, and a thermal conductivity detector for permanent gases (CO_2, H_2, Ar, CO, CH_4).

2.2.4 Operando DRIFTS and XAFS measurement

Gas flow (H_2, CO_2, He) is controlled by 6 mass flow controllers (Bronkhorst). Switching between two different reactant gas streams is done using a 4-way valve. The pressure of the two gas streams (to cell and vent) is controlled by back pressure regulators (Bronkhorst). The outlet gas stream is analyzed by a Pfeiffer Omnistar GSD 300C mass spectrometer.

Operando XAFS measurement were carried out using a fixed-bed capillary reactor (ID = 2 mm) at 150 °C, 10 bar, and H_2:CO_2 = 3:1 coupled with detected of the formed products using mass spectrometer. XAFS measurement for Re L_3-edge was performed at X10DA (SuperXAS) beamline of Swiss Light Source (SLS) at Paul Scherrer Institute (PSI).

For *operando* DRIFTS, catalyst powder is (10-15 mg) is loaded in a cylindrical cavity (3 mm in diameter and 3 mm vertical length) of a custom-made high-pressure reaction cell. The cell is mounted in a Harrick Praying Mantis diffuse reflection (DRIFTS) accessory. The spectra were collected using a Thermo Scientific Nicolet 6700 FT-IR spectrometer equipped with a liquid-nitrogen-cooled MCT detector at 4 cm^{-1} resolution for every 10 seconds. No baseline correction was applied to the time-resolved spectra due to the baseline movement. Prior to spectra collection, sample is reduced *in situ* at 500 °C under a H_2 stream (20 mL min^{-1}) for 1 h and subsequently cooled to the targeted reaction temperature of 150 °C under He stream. The cell is pressurized to 10-20 bar and immediately exposed to reactant mixture (CO_2:H_2 = 1:3, total flow = 20 mL min^{-1}) at the same pressure by switching valve.

2.3. Results and discussion

2.3.1 Characterization of Re/TiO_2

$Re(1)/TiO_2$ was synthesized using a facile impregnation method employing NH_4ReO_4 and TiO_2, followed by H_2 reduction at 500 °C. Powder X-ray diffraction (XRD) and scanning transmission electron microscopy (STEM) measurements were carried out in order to characterize $Re(1)/TiO_2$. As given in **Fig. 1**, a XRD pattern of the reduced $Re(1)/TiO_2$ catalyst was essentially identical to that of pristine TiO_2, while peaks associated with Re species were not observed. It should be noted that its structure was confirmed to be anatase. **Figure 2** shows the annular bright field STEM (ABF-STEM) image and high-angle annular dark-field STEM (HAADF-STEM) images of $Re(1)/TiO_2$. These images show that the Re loaded on the TiO_2 support forms highly dispersed sub-nanometer clusters. It is also observed that some Re species exist as single atoms in the matrix of TiO_2.[60–62]

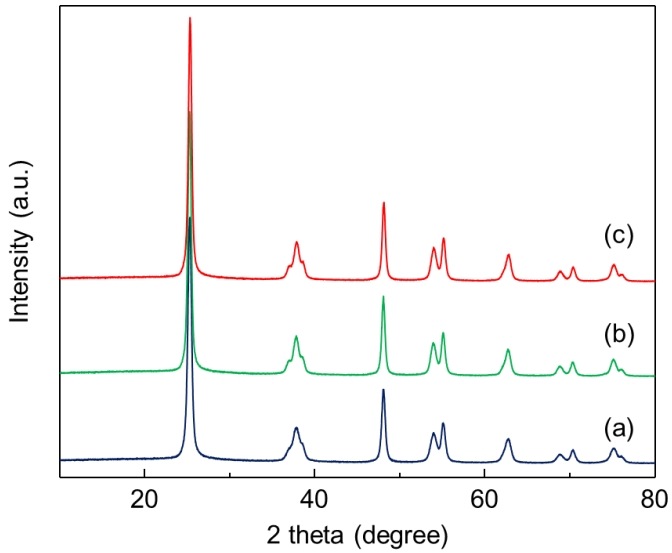

Figure 1. XRD patterns of a) TiO_2; b) NH_4ReO_4-impregnated TiO_2 calcined at 500 °C in air; c) after reduction of (b) at 500 °C under H_2 flow ($Re(1)/TiO_2$).

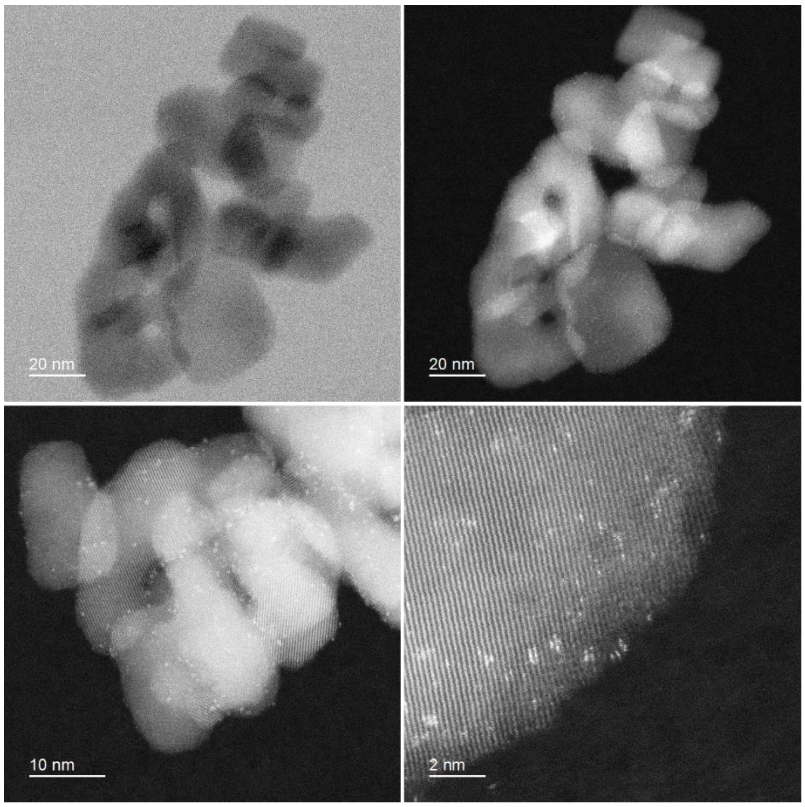

Figure 2. ABF- and HAADF-STEM images for Re(1)/TiO_2.

2.3.2 Low temperature hydrogenation of CO_2 in batch reactor

Hydrogenations of CO_2 were carried out in order to screen the properties of various catalysts. Following pre-treatment of the catalysts with H_2 at 500 °C, these reactions were carried out using a catalyst (0.0054 mmol of catalytically active metal) in a stainless autoclave (V = 30 cm^3; p_{CO2} = 1 MPa; p_{H2} = 5 MPa; T = 150 ˚C; t = 24 h). The obtained results are summarized in **Table 1**. Re(1)/TiO_2 afforded a total turnover number (TON) of 44 with 82% MeOH selectivity (**entry 1**). As minor byproducts, CO and CH_4 were obtained. In contrast, using TiO_2 or various other TiO_2-supported metal catalysts (**entries 2-10**) did not afford significant amounts of MeOH. CO and/or CH_4 were produced as the main products over these catalysts. No reaction occurred when pristine TiO_2 was used as the catalyst (**entry 11**). Various supported Re catalysts were also tested for the direct hydrogenation of CO_2 (**entries 12-21**). The obtained total TONs were lower than that for Re(1)/TiO_2, while the formation of MeOH was not observed. The industrial Cu-based catalyst Cu/Zn/Al_2O_3 supplied by Clariant Catalysts (MDC-7; 34 wt% Cu) was also tested and found to be ineffective under the reaction conditions tested in this study (**entry 22**). Moreover, unsupported Re catalysts including metallic Re, NH_4ReO_4, ReO_2, ReO_3, and Re_2O_7 did not efficiently catalyze the hydrogenation of CO_2 (**entries 23-27**). It should be noted here that the catalytic tests were also carried out after a H_2 reduction at 300 °C, given that a H_2 reduction at 500 °C may not be appropriate for some of the catalysts.[19] Still, it was confirmed that Re(1)/TiO_2 is the most effective catalyst for the direct hydrogenation of CO_2 to afford MeOH. These results clearly demonstrate that the combination of Re as the catalytically active species and TiO_2 as the support is particularly effective for the synthesis of MeOH from the hydrogenation of CO_2.

Table 1. Results of the hydrogenation of CO_2 catalyzed by a variety of catalysts.[a]

Entry	Catalyst	Total TON	Selectivity (%)		
			MeOH	CO	CH_4
1	$Re(1)/TiO_2$	44	82	16	2
2	$Pt(1)/TiO_2$	64	<1	87	13
3	$Pd(1)/TiO_2$	21	<1	88	12
4	$Rh(1)/TiO_2$	41	<1	100	<1
5	$Ir(1)/TiO_2$	5	<1	89	11
6	$Ru(1)/TiO_2$	3	<1	100	<1
7	$Ni(1)/TiO_2$	4	<1	100	<1
8	$Co(1)/TiO_2$	2	<1	100	<1
9	$Ag(1)/TiO_2$	<1	-	-	-
10	$Cu(1)/TiO_2$	<1	-	-	-
11	TiO_2	<1	-	-	-
12	$Re(1)/ZrO_2$	8	<1	65	35
13	$Re(1)/Al_2O_3$	2	<1	9	91
14	$Re(1)/SiO_2$	1	<1	65	35
15	Re(1)/Carbon	1	<1	36	64
16	$Re(1)/CeO_2$	<1	-	-	-
17	Re(1)/MgO	<1	-	-	-
18	$Re(1)/SiO_2$-Al_2O_3	<1	-	-	-
19	$Re(1)/SnO_2$	<1	-	-	-
20	Re(1)/HZSM-5(22)	1	<1	92	8
21	Re(1)/HY(5.5)	<1	-	-	-
22	$Cu/Zn/Al_2O_3$[b]	<1	-	-	-
23[c]	Metallic Re	<1	-	-	-
24[c]	NH_4ReO_4[c]	2	<1	2	98
25[c]	ReO_2[c]	1	<1	4	96
26[c]	ReO_3[c]	2	<1	<1	100
27[c]	Re_2O_7[c]	10	<1	<1	100

[a]Pre-treatment: H_2 (30 mL min^{-1}), 500 ˚C, 0.5 h; reaction conditions: 0.0054 mmol of catalytically active metal, 1,4-dioxane (1 mL), CO_2 (1 MPa), H_2 (5 MPa), 150 ˚C, 24 h; TONs were calculated based on the total amount of metal atoms used. [b] 34 wt% of Cu. [c] Reactions were carried out without pre-treatment.

2.3.3 Mechanistic study

The time-course plot of the hydrogenation of CO_2 shows that the concentration of all the products (MeOH, CO, and CH_4) increases with increasing the reaction time, as given in **Fig. 3**. It should also be noted that other possible byproducts such as formic acid (HCOOH) and formaldehyde (HCOH) were not observed when using a GC-FID apparatus equipped with a methanizer. In order to get further insight into the specifics of the reaction, hydrogenation reactions employing CO or HCOOH as a starting substrate were carried out (**Scheme 1**). The hydrogenation of CO, carried out at lower pressure (0.5 MPa) for safety reasons, hardly proceeded, whereas that of CO_2 (0.5 MPa) afforded MeOH at a formation rate of 0.8 mmol $mmol_{Re}^{-1}$ h^{-1} based on the Re used. This result indicates that the potentially produced CO is not an intermediate for the formation of MeOH. On the other hand, the reaction of HCOOH afforded MeOH, suggesting that the derivatives of HCOOH (e.g. $HCOO^-$) adsorbed on the catalyst surface could serve as intermediates for the formation of MeOH.

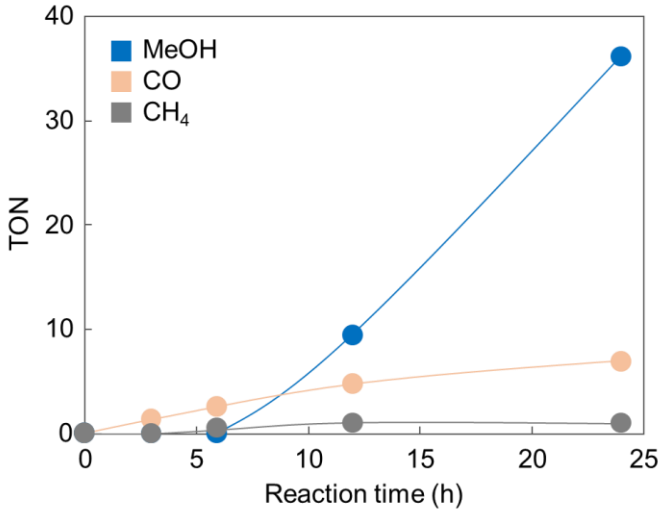

Figure 3. Time-course plot of the hydrogenation of CO_2 catalyzed by Re(1)/TiO_2. Pre-treatment: H_2 (30 mL min^{-1}), 500 ˚C, 0.5 h; reaction conditions: 0.0054 mmol Re, 1,4-dioxane (1 mL), CO_2 (1 MPa), H_2 (5 MPa), 150 ˚C.

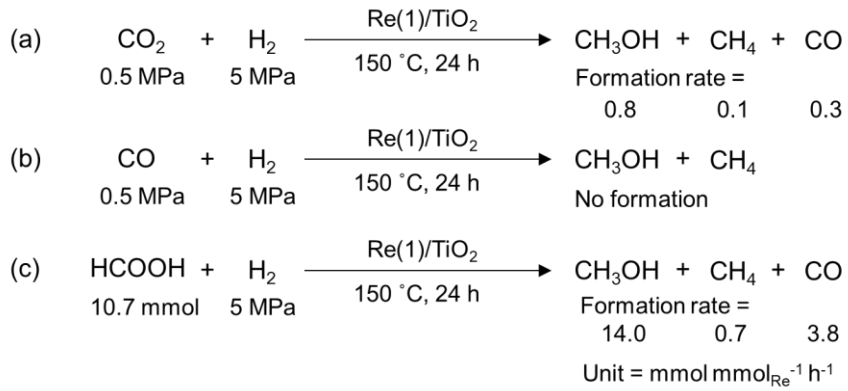

Scheme 1. Hydrogenation of model substrates over Re(1)/TiO_2. (a) CO_2, (b) CO, and (c) HCOOH. Pre-treatment: H_2 (30 mL min^{-1}), 500 ˚C, 0.5 h; reaction conditions: 0.0054 mmol Re, 1,4-dioxane (1 mL).

2.3.4 Structure-activity relationship

Subsequently, the hydrogenation of CO_2 was carried out using Re(x)/TiO_2 (x = 0.2, 1.0, 5.0, 10, and 20 wt%) in order to i) determine the optimal Re loading and ii) investigate the effect of the size of the Re species on the hydrogenation reaction. The corresponding HAADF-STEM images for Re(x)/TiO_2 (x = 0.2, 1, 5, 10, and 20 wt%) are shown in **Fig. 4**. The highest formation rate and selectivity for MeOH was achieved using Re(1)/TiO_2 (**Fig. 5**). With increasing Re loading, the MeOH selectivity is gradually shifting toward CH_4. This could be attributed to the fact that larger clusters of Re nanoparticles favor the formation of CH_4, while isolated atoms (single atoms) of Re mainly seen for Re(x)/TiO_2 with low Re loadings favor the formation of CO. This notion is in accordance with the results of a previous study on the hydrogenation of CO_2 over Rh/TiO_2.[64] Moreover, our results indicate that the formation of MeOH should be favored over Re/TiO_2 given the sub-nanometer size of the Re species. These considerations could explain why Re(1)/TiO_2 serves as the most effective catalyst for the formation of MeOH in this study.

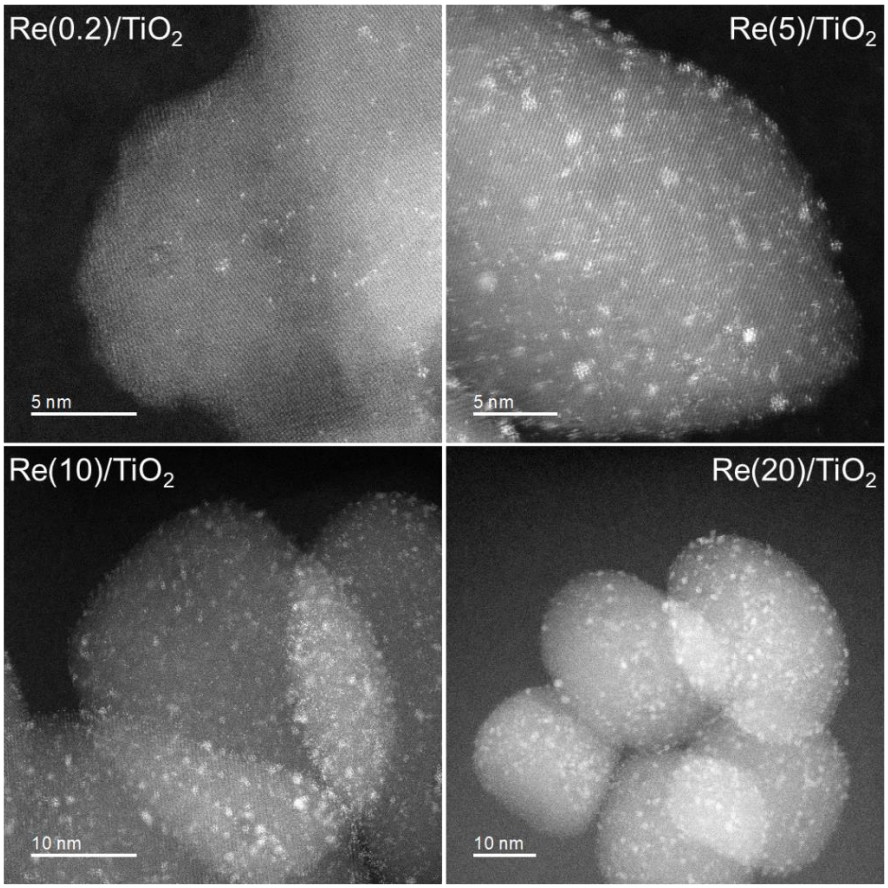

Figure 4. HAADF-STEM images of Re(x)/TiO_2 (x = 0.2, 5, 10, and 20 wt%).

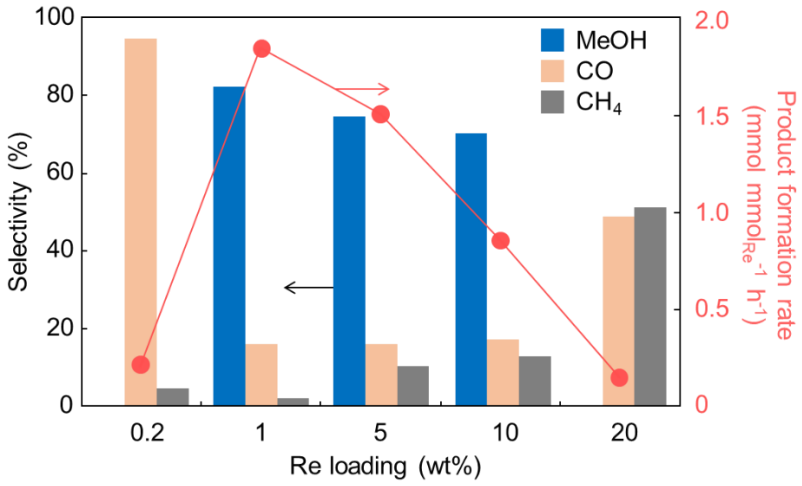

Figure 5. Effect of the Re loading on the hydrogenation of CO_2 catalyzed by Re(x)/TiO_2 (x = 0.2, 1, 5, 10, and 20 wt%). Pre-treatment: H_2 (30 mL min^{-1}), 500 ˚C, 0.5 h; reaction conditions: 0.0054 mmol of Re, 1,4-dioxane (1 mL), CO_2 (1 MPa), H_2 (5 MPa), 150 ˚C, 24 h.

Finally, we tested Re(1)/TiO_2 for the hydrogenation of CO_2 after a reduction with H_2 at different temperatures (200, 300, 500, 700, and 900 ˚C), as shown in **Fig. 6**. The results show that the best performance is observed for Re(1)/TiO_2 pre-treated at 500 ˚C. X-ray absorption near edge structure (XANES) measurements were measured in order to determine the oxidation states of Re species, as given in **Fig. 7**. Note that the XANES spectra were collected at room temperature without exposure to air after the H_2 reduction by sealing the samples in a glove bag filled with N_2. Chemical shifts of the binding energy as a function of the reduction temperature are also plotted.[65] The shifts for reference samples ReO_3, ReO_2, and Re metallic powder are shown with dotted lines. The obtained results suggest that the valence of the Re species decreases with increasing reduction temperature, which implies that the average oxidation state of the Re species responsible for the catalytic formation of MeOH should be higher than 0 and below +4. It is well-known that Re often shows high dispersion on supports, that it is difficult to be reduced, and exhibits a variety of oxidation states.[66-68] These features render research on catalytically active Re components highly challenging, and consequently, little is known about the chemical identity of such catalytically active Re species.[69] The precise nature of the catalytically active Re species remains unknown and the catalyst may contain a variety of Re species in different oxidation states. At present, we cannot exclude the possibility that these mixtures of Re species in different oxidation states and the interfaces between them are necessary for the efficient progression of the reaction. HAADF-STEM measurements suggest that reduction

temperatures beyond 500 ˚C should lead to sintering of the Re species, which would prevent the formation of MeOH (**Figs. 8 and 9**).

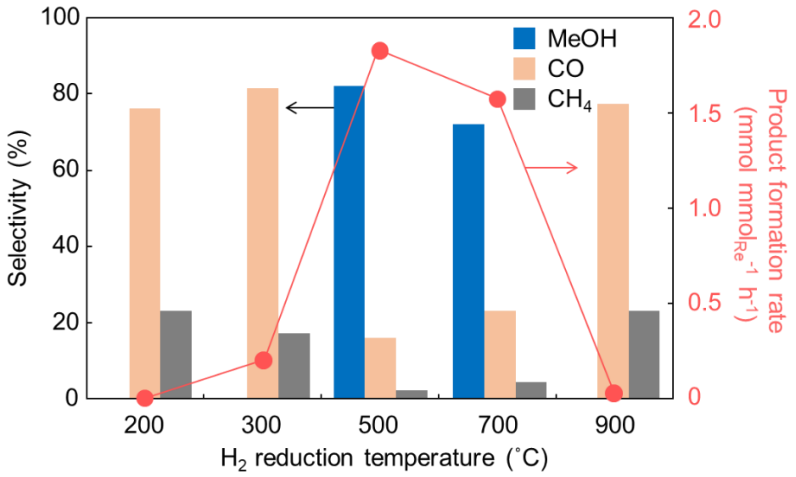

Figure 6. Effect of the pre-treatment reduction temperature on the CO_2 hydrogenation catalyzed by Re(1)/TiO_2 catalysts. Pre-treatment: H_2 (30 mL min^{-1}), 0.5 h; reaction conditions: 0.0054 mmol of Re, 1,4-dioxane (1 mL), CO_2 (1 MPa), H_2 (5 MPa), 150 ˚C, 24 h.

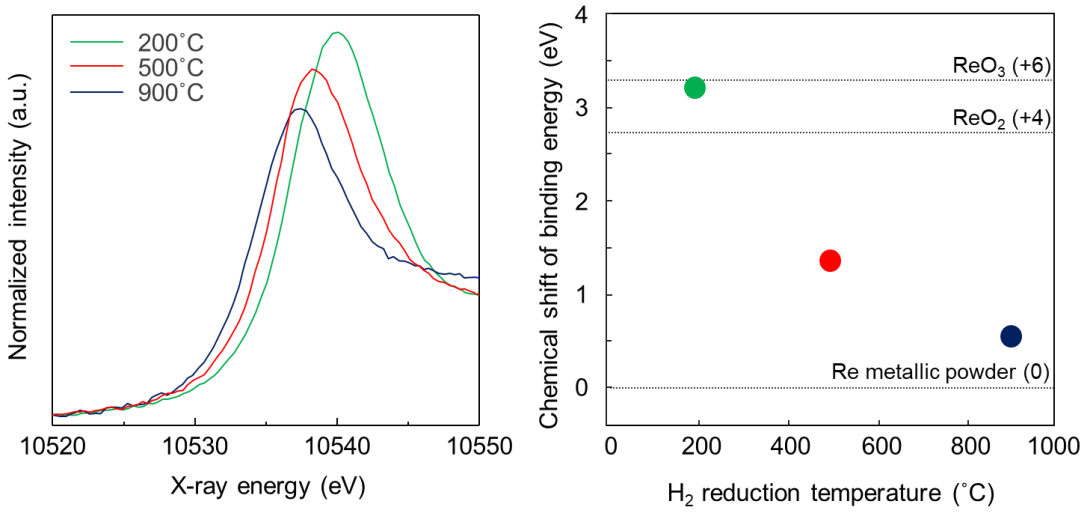

Figure 7. Re L_3-edge XANES spectra of Re(1)/TiO_2 after temperature-dependent reductions (left) and the chemical shift of the binding energy as a function of the reduction temperature (right). The samples were treated at 200, 500, or 900 °C under a flow of H_2. The XANES spectra were taken at room temperature without exposure to air after the reduction treatment by sealing the samples under N_2.

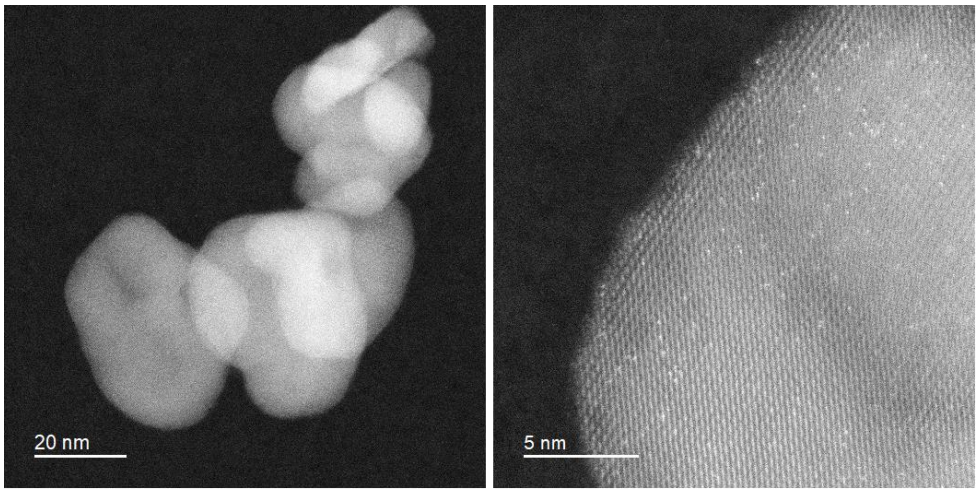

Figure 8. HAADF-STEM images of Re(1)/TiO_2 after reduction at 200 °C under a flow of H_2.

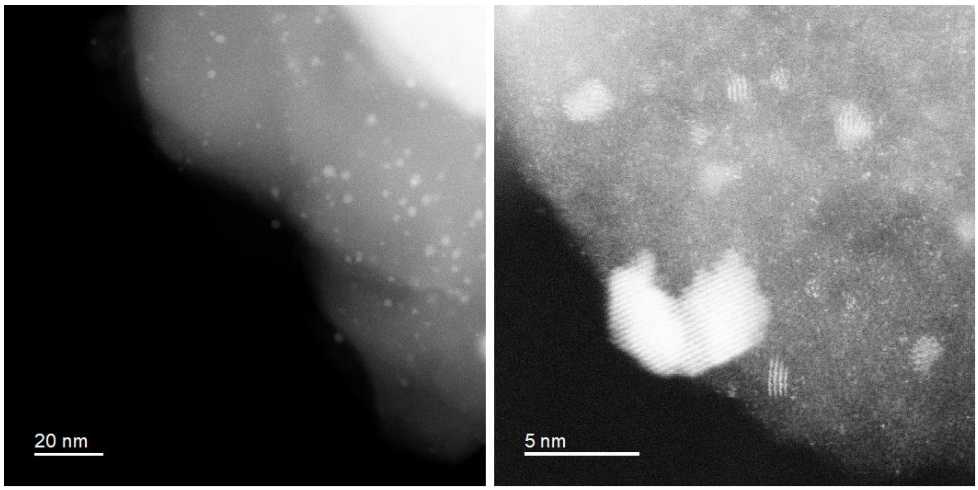

Figure 9. HAADF-STEM images of Re(1)/TiO_2 after reduction at 900 °C under a flow of H_2.

2.3.5 Low temperature hydrogenation of CO_2 in fixed-bed flow reactor

The catalytic performance of Re(3)/TiO_2 and commercial Cu/ZnO/Al_2O_3 were tested and compared using a fixed-bed continuous flow reactor at a H_2/CO_2 ratio of 3, 150 °C and 360 bar for 24h (**Figure 10**). Initially, both catalysts showed higher CO_2 conversion that declined with time-on-stream, more prominently for Cu/ZnO/Al_2O_3. Re/TiO_2 showed a comparable and higher CO_2 conversion to Cu/ZnO/Al_2O_3 over time despite significantly lower metal loading. CH_3OH selectivity displayed three distinguished stages within the 24 h experiment: activation (0-10 h), stable performance (10-20 h), and stabilization and deactivation (>20 h). During the activation period, methyl formate ($HCOOCH_3$) is the main product over Cu/ZnO/Al_2O_3. After initial >60% selectivity followed by a decrease, methyl formate selectivity reaches ca. 47% at ca. 8 h before a rapid decline to less than 5%. Along with the decrease of methyl formate selectivity, CH_3OH and CO selectivities gradually increase and become stable. On the other hand, Re/TiO_2 shows a high initial CH_4 selectivity (>40%) that rapidly declines within 5 h. $HCOOCH_3$ selectivity over Re/TiO_2 is lower than that of Cu/ZnO/Al_2O_3 during the first 10 h, but it becomes higher over time. Generally, the drop in $HCOOCH_3$ selectivity is accompanied with counteracting increase of methanol selectivity, implying their close correlation and balance of the surface intermediates leading to the two products.

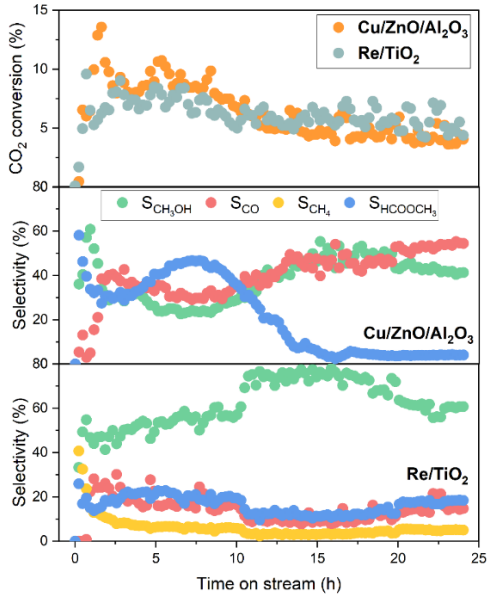

Figure 10. Catalytic activity of Cu/ZnO/Al_2O_3 and Re(3)/TiO_2 in CO_2 hydrogenation. H_2/CO_2 = 3, T = 150 °C, P = 360 bar, and GHSV = 2,000 h^{-1}.

2.3.6 *Operando* DRIFTS

CO_2 hydrogenation over Re/TiO_2 under working conditions of 150 °C and 10 bar was investigated using *operando* DRIFTS, which can provide insights into the temporal evolution of surface species during CO_2 hydrogenation over the freshly reduced catalyst. The *v*(C–H) bands in 2500-3200 cm^{-1} region are presented in **Figure 11a**, while *v*(C–O) bands in 1000-1800 and 1800-2300 cm^{-1} are shown in **Figure 11b** and **11c**. The characteristic IR bands of rhenium hydride (Re–H, 1965 cm^{-1}) and bridging or chelating bidentate formate on TiO_2 (κ^2-HCOO*, 2950, 2869, 1560, and 1357 cm^{-1}) appear immediately after the reaction was initiated. Linear carbonyl species (μ^1-CO*, 2030 cm^{-1}) appear after 0.5 min. Bridge carbonyls (μ^2-CO*, 1936 and 1880 cm^{-1}) appear after 2 min. However, we later confirm that the bands assigned μ^1-CO* and μ^2-CO* are the parts of the rhenium tricarbonyls complex ($Re(CO)_3$). The bands that appeared simultaneously at 2883, 2848, 2732, 1640, and 1405 cm^{-1} can be assigned to adsorbed methyl formate ($HCOOCH_3$*) or adsorbed formic acid (HCOOH*). However, those adsorbed molecules were not usually observed under operando DRIFTS since they are prone to chemically adsorbed in form of κ^2-HCOO*. These bands were later assigned as monodentate formate on Re (κ^1-HCOO*) or bridging formate (μ^2-HCOO*) over Re or Re-O-Ti interface. Methoxy species (CH_3O*, 2829, and 2927 cm^{-1}) appear in the latest order after 10 min of reaction.

In summary, the surface species temporally evolved in the following orders: κ^2-HCOO* = Re-H (0.25 min) → μ^1-CO* (0.5 min) →μ^2-CO* ($Re(CO)_3$ formation) = μ^2-HCOO* (2 min) → CH_3O* (10 min). It should be highlighted that a faster spectral acquisition than 10s is required to distinguish the formation rate between κ^2-HCOO* and Re-H.

The formation of carbonyl species over Re/TiO_2 during the reaction (Figure 4b) indicates the reduction of the Re=O bond, which is generally required to form a coordination complex with CO. The tentatively assigned μ^1-CO* and μ^2-CO* form with distinct kinetics. However, the formation of bridged carbonyls is less favored or not possible on atomically dispersed Re due to the lack of adjacent Re atoms. At the reaction temperature, the adsorption of CO can lead to disruption and dispersion of Re crystallites, and eventually, lead to the formation of rhenium carbonyls complexes like $Re(CO)_3$. Here, based on the spectral features, the carbonyl species are assigned to

$Re(CO)_3$, although the number of carbonyls can fluctuate depending on the coordinating groups and environment around Re.

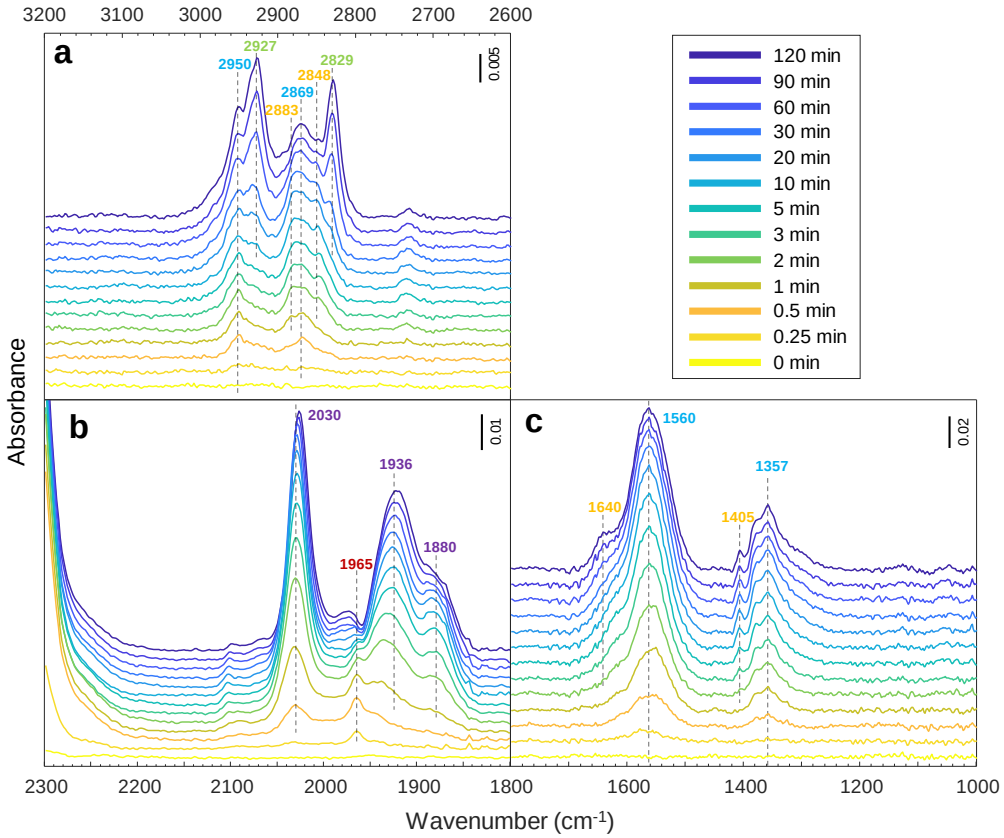

Figure 11. Temporal evolution of surface species obtained from *in situ* DRIFTS during reaction with H_2 + CO_2 over $Re(3)/TiO_2$. Reduction condition: 300 °C under 10 mL min^{-1} of H_2 for 1 h. (Pre-reduced at 500 °C with H_2 and passivated with $1\%O_2/N_2$). Reaction conditions: 10 mg catalyst, H_2/CO = 3, T = 150 °C, P = 10 bar, F_{total} = 10 mL min^{-1}.

The normalized IR bands of surface species and mass spectrometry (MS) signals of gaseous products are compared in **Figure 12**. During the CO_2 hydrogenation,

CH_3OH formation (**Figure 12d**) reaches a steady state within 20 min and its profile is similar to that of κ^2-HCOO* formation (**Figure 12a**). In contrast, CH_3O* formation has shown a significant delay in its increase on the catalyst surface. This suggests that the observed CH_3O* is not required as the intermediate for CH_3OH formation. $^{13}CO_2$ hydrogenation yielded similar temporal evolution of surface and gaseous species to the case of $^{12}CO_2$ (**Figures 12c** and **12f**).

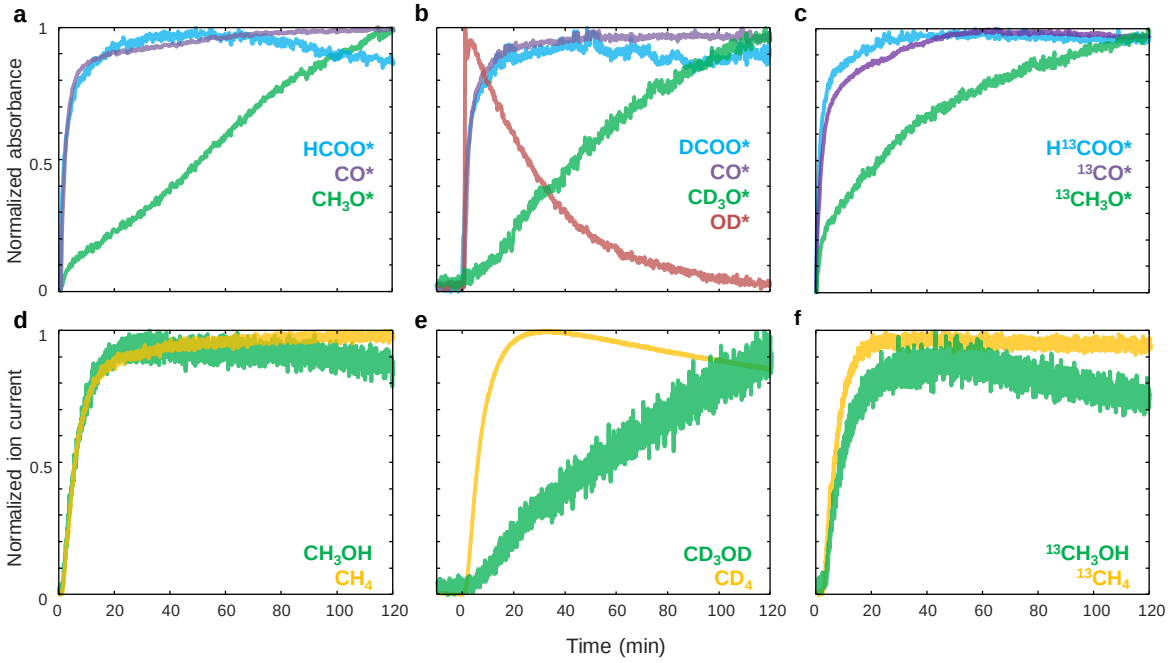

Figure 12. Temporal evolution of normalized absorbance of the main surface species obtained from *operando* DRIFTS during reaction with **a** H_2 + CO_2, **b**, D_2+ CO_2, **c** H_2 + $^{13}CO_2$ over pre-reduced Re(3)/TiO_2. The corresponding normalized ion current signal of methanol and methane obtained from mass spectrometer is shown directly beneath. Wavenumber (cm^{-1}): κ^2-HCOO* (1565), μ^1-CO* (2026), CH_3O* (2830), κ^2-DCOO* (2181), μ^1-CO* (2026), CD_3O* (2063), OD* (2704), κ^2-H^{13}COO* (1527), μ^1-^{13}CO* (1976), $^{13}CH_3O$* (2827). The MS of CD_4 at m/z = 18 is shown instead of m/z = 20 because of overlapping with D_2O and H_2O contribution was assumed to be negligible.

Furthermore, an identical isotopic labeling experiment was performed using D_2 instead of H_2. During the CO_2 hydrogenation with D_2, a similar κ^2-DCOO* (2180 cm^{-1}) formation profile to that of HCOO* is observed, suggesting that CO_2 activation to κ^2-HCOO* is not affected by the KIE (**Figure 12b**). However, the CD_3OD formation (**Figure 12e**) is much slower compared to CH_3OH formation (**Figure 12d**) while CD_4 is virtually unaffected (**Figure 12e**). This indicates completely different formation mechanisms and involved intermediates to form methanol and methane. The CD_3OD signal shows a similar profile to that of CD_3O* (2061 cm^{-1}), which behaves oppositely to the terminal deuteroxyl group (OD*, 2704 cm^{-1}). To understand the location and roles

of this CD_3O^* as well as the correlation between CD_3O^* and OD^*, a CH_3OH adsorption experiment was performed, followed by titration using D_2 (**Figure 13**). After CH_3OH was adsorbed as CH_3O^*, titration of CH_3O^* by D_2 produced CH_3OD and regenerated OD^* similar to the inverted relationship between CD_3O^* and OD^*. This suggested that the observed CH_3O^* species are located on TiO_2 support and originated from CH_3OH adsorption over the Ti-OH sites.

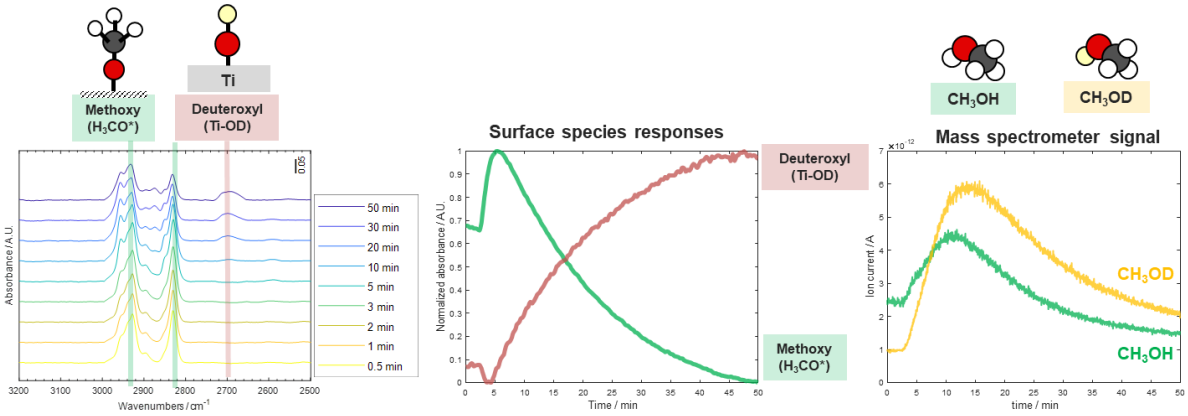

Figure 13. Reaction of CH_3O^* adlayer on Re/TiO_2 with D_2 after flushing with He. Reduction condition: 300 ºC under 10 mL min^{-1} of H_2 for 1 h. (pre-reduced at 500 °C with H_2 and passivated with $1\%O_2/N_2$). Reaction conditions: ca. 10 mg catalyst, 2000 ppm CH_3OH in N_2, T = 150 °C, P = 5 bar, F_{total} = 20 mL min^{-1}.

A similar experiment is performed over TiO_2 support (**Figure 14**). However, the Ti-OD at 2704 cm^{-1} was not observed, which indicates that the formation of the Ti-OH group via heterolytic dissociation of H_2 is not possible over TiO_2, at least at this temperature. This confirms the role of Re for H_2 dissociation and hydride transfer over TiO_2 via H-spillover. Moreover, the CD_3O^* is unreactive to D_2 without Re. From the results above, it is clear that CD_3OD produced during CO_2 hydrogenation (with D_2) reacted with OD^* to form CD_3O^*. Therefore, the slower product formation rate due to CD_3OD adsorption led to delayed detection of CD_3OD compared to CD_4.

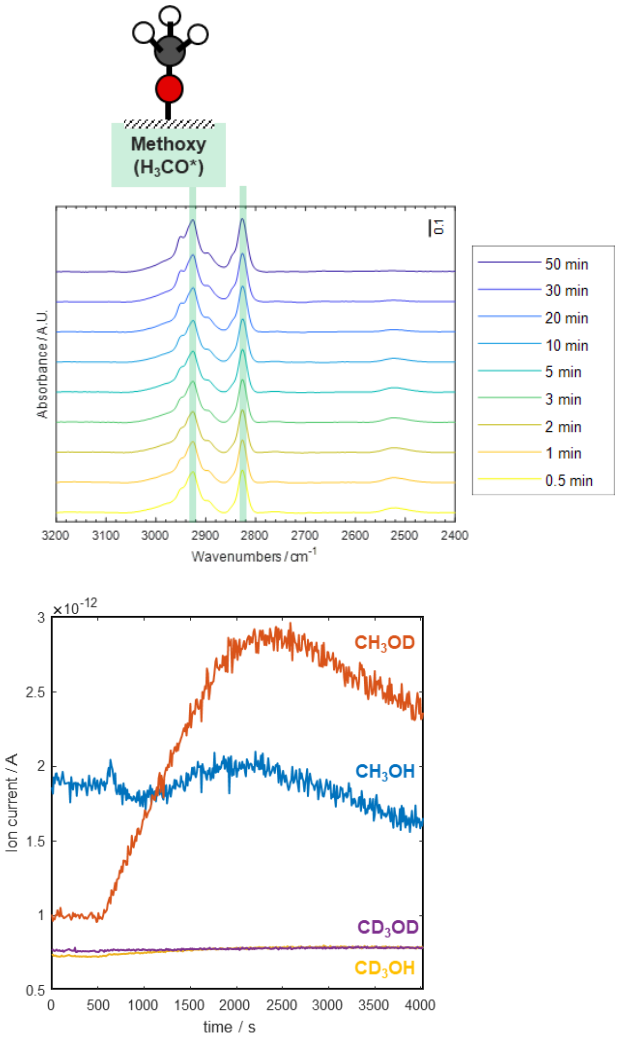

Figure 14. Reaction of CH_3O* adlayer on TiO_2 with D_2 after flushing with He. Reduction condition: 300 ºC under 10 mL min^{-1} of H_2 for 1 h. (pre-reduced at 500 °C with H_2 and passivated with 1%O_2/N_2). Reaction conditions: ca. 10 mg catalyst, 2000 ppm CH_3OH in N_2, T = 150 °C, P = 5 bar, F_{total} = 20 mL min^{-1}.

The instantaneous formation of OD* during CO_2 hydrogenation with D_2 suggests that D-spillover from Re is rapid within the time scale of the experiment compared to the consumption of Re–H (produced during catalyst activation via reduction with H_2) to form DCOO*. The gradual decline of the OD* concentration discarded the Ti-OH role in κ^2-HCOO* formation via CO_2 activation into HCO_3* and its subsequent hydrogenation at low temperatures, since κ^2-HCOO* saturation on the surface was significantly faster than OD* consumption. Notably, the quickly formed OD* on TiO_2 is gradually replaced by CD_3O*.

Additionally, CO hydrogenation was also carried out to understand the mechanistic differences to CO_2 hydrogenation, as shown in **Figure 15**. Compared with

CO_2 hydrogenation, similar $Re(CO)_3$ (2029, 1915, and 1873 cm^{-1}) are observed. The gaseous CO (2169 cm^{-1}) and, additional peaks of $Re_2(CO)^{10}$ (2104 and 1995 cm^{-1}) also appeared. Only a trace amount of adsorbed H_2O, κ^2-HCOO*, and CH_3O* is observed, which indicated the lack of CH_3OH formation. There is no indication of formyl (HCO*) and formaldehyde (H_2CO*) produced via stepwise hydrogenation of carbonyls as the main intermediate for CO hydrogenation. The formate species which is a more natural intermediate in CO_2 hydrogenation via hydride transfer to CO_2 seems indeed the key intermediate in producing methanol over Re/TiO_2.

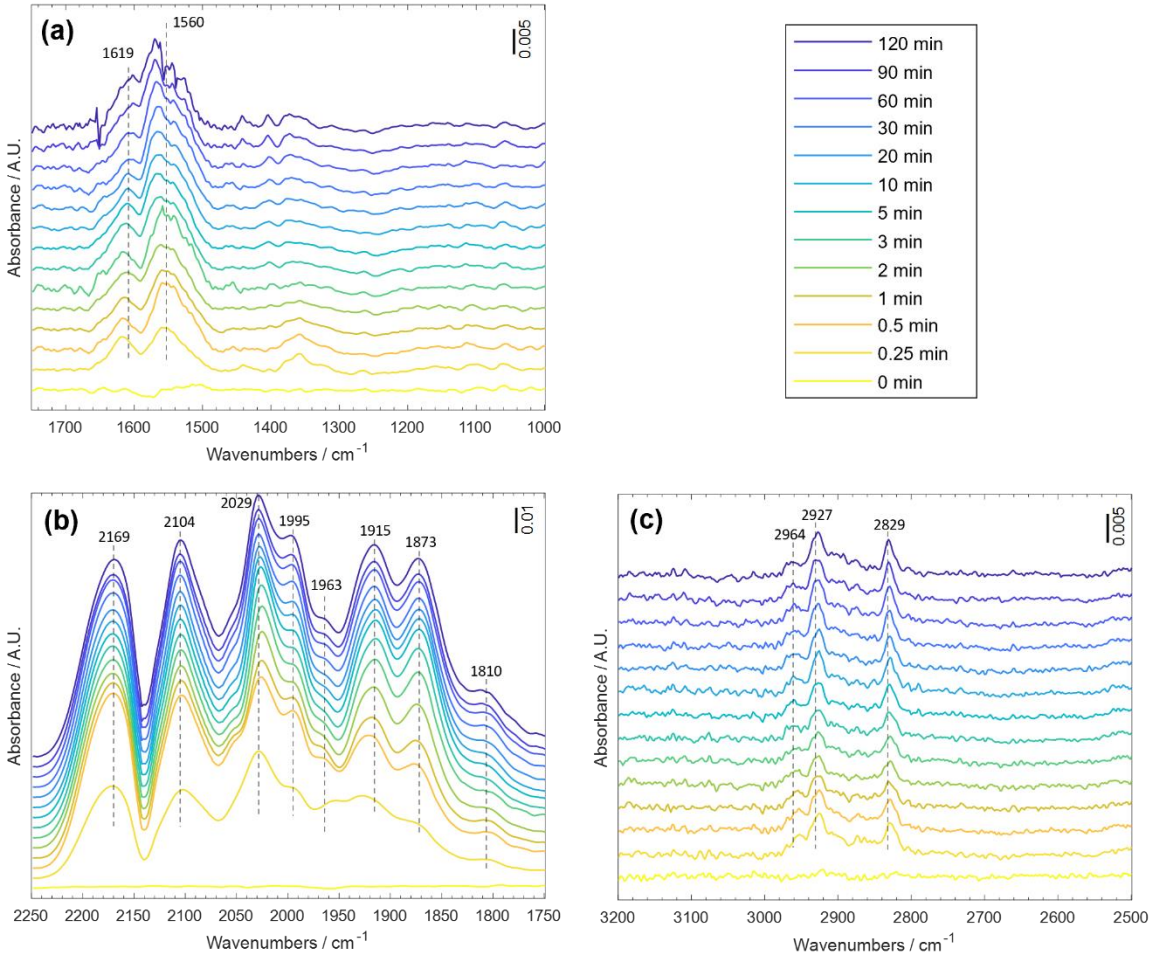

Figure 15 Temporal evolution of surface species obtained from *in situ* DRIFTS during reaction with H_2 + CO over $Re(3)/TiO_2$. Reduction condition: 300 °C under 10 mL min^{-1} of H_2 for 1 h. (Pre-reduced at 500 °C with H_2 and passivated with $1\%O_2/N_2$). Reaction conditions: 10 mg catalyst, H_2/CO = 3, T = 150 °C, P = 10 bar, F_{total} = 10 mL min^{-1}.

2.3.7 Transient experiment: concentration modulation

The transient experiment can utilize not only isotopes but also the drastic changes in the reactant concentration, e.g. passing only one of the reactants momentarily, allowing the detection of surface species responding to periodic perturbation. This technique can improve sensitivity and unveils spectral features that are not accessible by steady-state experiments. The transient experiment requires multiple modulation cycles for the system to reach a quasi-steady state. Such states include the oxidation state of active metal, local structure, surface species coverage, etc. The responses of those states after the quasi-steady state are similar in the following cycles, allowing cycle averaging to improve the signal-to-noise ratio.

The example of a quasi-steady state over Re/TiO_2 is clearly shown in the transient experiment of the modulated flow of H_2+CO_2 vs. CO_2. As shown in **Figure 16a**, the reaction under H_2+CO_2 had reached a steady state (①) before the transient experiment. Modulation with CO_2 induced structural change of Re/TiO_2, leading to an increase in the CH_3OH signal in the gas phase. The structural change reached a quasi-steady state after 3 cycles (②) and remained irreversible after the transient experiment (③). The Re L_3-edge XANES showed a notable increase in the white line intensity compared to the previous steady-state (**Figure 16b**). During the quasi-steady state (②) the change in response to the periodic concentration change was infinitesimal, but the subtle change was confirmed by the phase-resolved spectra obtained by phase sensitive detection (**Figure 16c**). The in-phase and out-of-phase positions are at 10537 eV and 10543.5 eV, but they are assumed to be artificially created peaks to describe the shift of absorption peaks. Rather this study shows that the Re redox state does change, although the extent is small, around the peak around 10540 eV, which can be in the range of Re^0-Re^{4+}.

Representative HAADF-STEM images of reduced and spent Re/TiO_2 (**Figures 17a** and **17b**) show that increased dispersion of Re clusters is responsible for the irreversible change until reaching the quasi-steady state (①). As shown in **Figures 17c** and **17d**, the particle size distribution of Re clusters becomes narrower toward single Re atoms and clusters containing a few Re atoms after the transient reaction. The decomposition and (re)dispersion of metal nanoparticles is often related to the concentration of defect sites that enthalpically stabilize adatoms.

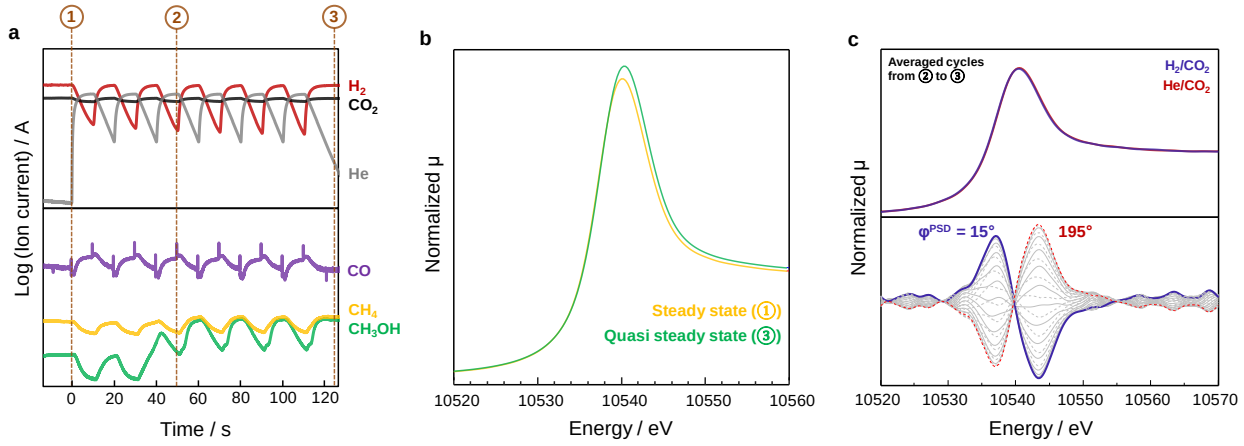

Figure 16. Transient H_2+CO_2 and He+CO_2 experiment. **a** Corresponding normalized ion current signal from a mass spectrometer. **b** operando Re L_3-edge XANES spectra. **c** Phase-resolved amplitude spectra from Re L_3-edge XANES: Spectra is within φ^{PSD}= 0-360° at steps of φ^{PSD}= 15°. He balances are used in the CO_2 phase to maintain partial pressure. Reaction conditions: H_2/CO_2 = 3, T = 150 °C, P = 10 bar, F_{total} = 10 mL min^{-1}.

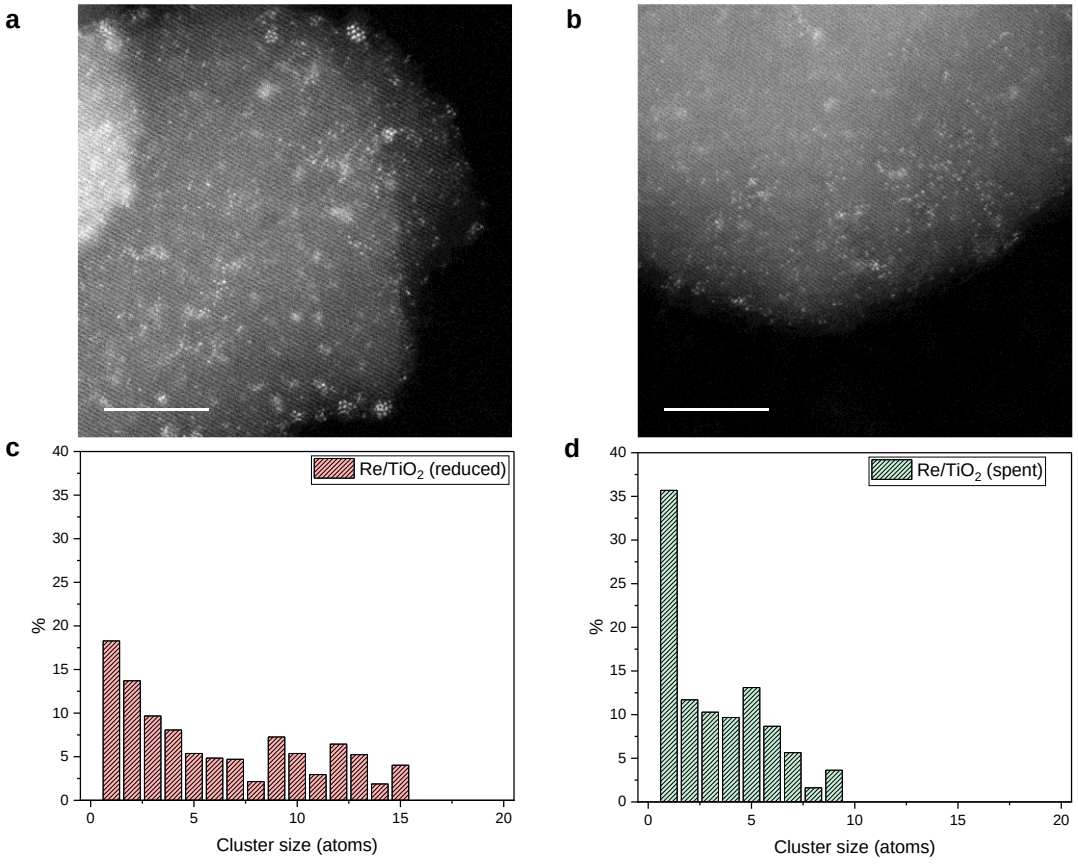

Figure 17. Representative HAADF-STEM images of Re/TiO_2: **a** after reduction (500 °C in H_2) and **b** after transient experiment (150 °C and 10 bar). **c** Re cluster size distribution of Re/TiO_2 was determined from HAADF-STEM: **c** after reduction (500 °C in H_2) and **d** after the transient experiment (150 °C and 10 bar).

To gain more precise insights into the redox state of Re, an AP-XPS study was performed (**Figure 18**). Re/TiO_2 was reduced at 450 °C, which is lower than the standard reduction temperature for the pretreatment, due to a limitation of our experimental setup Re/TiO_2 after reduction at 450 °C was found to contain multiple oxidation states of Re such as Re^0, Re^{2+}, and Re^{4+}. Although Re^{2+} is not known to exist as a stable bulk oxide, it can exist as surface species. Note that other species including Re^{3+} and Re^{1+}, which have been reported as surface species and/or in metal complexes, can also be present although the fitting with Re^0, Re^{2+}, and Re^{4+} gave a sufficient fit in the present study. The amount of surface cationic $Re^{\delta+}$ species increased under CO_2 atmosphere at 150 °C, suggesting the Re^0 oxidation by CO_2 (**Table 2**). Subsequent introduction of H_2 reduced the formed cationic $Re^{\delta+}$ species, followed by reoxidation by CO_2. These results indicate that CO_2 oxidizes the supported Re and the oxidized Re is reduced by H_2 reversibly, suggesting the participation of surface cationic $Re^{\delta+}$ species such as Re^{4+} and Re^{2+} in CO_2 hydrogenation, while the remaining Re^0 plays a role in H_2 activation. We are aware that measurements at low pressures (millibar scale) may lead to different conclusions to identify catalytic species. However, direct observations of the surface Re species under repeated reduction (H_2) – oxidation (CO_2) cycles with XPS techniques can give qualitative insights into redox behavior of the Re species.

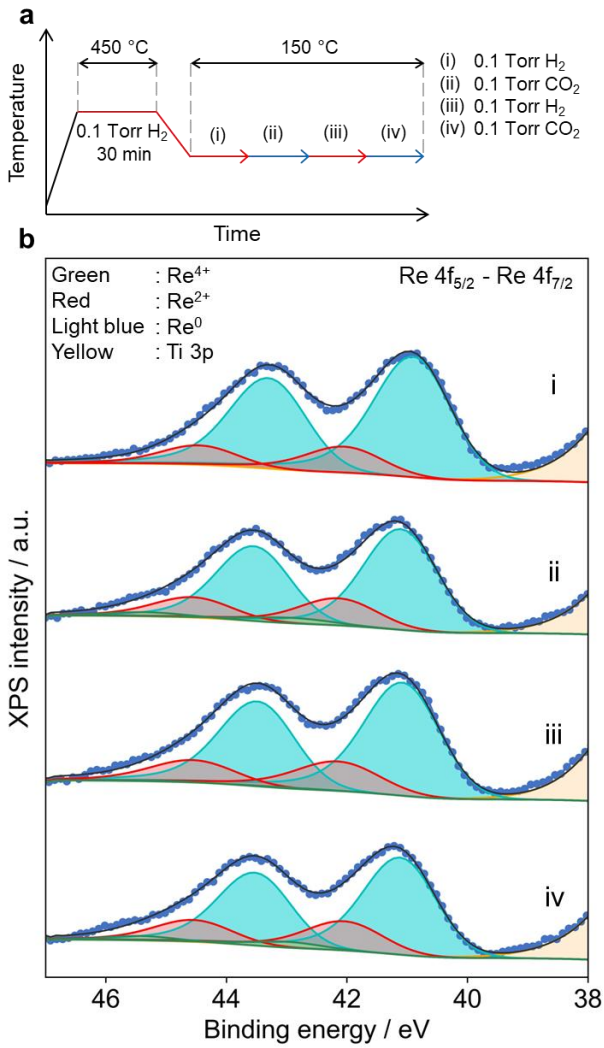

Figure 18. a Experimental conditions during the AP-XPS study. **b** Re 4f AP-XPS spectra of Re/TiO_2 under exposure to (i) H_2, (ii) CO_2, (iii) H_2, and (iv) CO_2 at 150 °C. Blue dots: raw spectrum; black line: sum; green: Re^{4+}; red: Re^{2+}; light blue: Re^0; yellow: Ti 3p.

Table 2. Peak concentrations in the Re 4f AP-XPS spectra of Re/TiO_2 at 150 °C under various gas conditions (**Figure 10**).

Gas condition	Peak concentration / %		
	Re^0	Re^{2+}	Re^{4+}
(i) 0.1 Torr H_2[a]	83.2	14.5	0
(ii) 0.1 Torr CO_2	73.9	20.4	4.4
(iii) 0.1 Torr H_2 (2^{nd})	76.8	22.8	0.4
(iv) 0.1 Torr CO_2 (2^{nd})	74.5	21.6	3.9

[a]Measured at 150 °C right after H_2 reduction at 450 °C.

2.4 Conclusions

The hydrogenation of CO_2 was carried out under mild conditions (T < 150 ˚C; p_{CO2} = 1 MPa; p_{H2} = 5 MPa) using various heterogeneous Re/TiO_2 catalysts and a series of other catalysts that includes TiO_2-supported catalysts, oxide-supported, and unsupported Re catalysts. The highest TON and selectivity for the formation of MeOH was observed for Re(1)/TiO_2, i.e., a TiO_2-supported Re catalyst with a Re loading of 1 wt%. Studies on structure-activity relationship indicates that Re species responsible for the catalytic formation of MeOH should be sub-nanometer size and have oxidation states higher than 0 and below +4. Metallic Re species act as H_2 activator for H-spillover to cationic Re sites. The formation of Re-H is the first step in CO_2 activation to monodentate formate over cationic Re species before its further hydrogenation to CH_3OH or spillover onto TiO_2 support, becoming less reactive bidentate formate (spectator).

2.5 References

(1) Artz, J.; Müller, T. E.; Thenert, K.; Kleinekorte, J.; Meys, R.; Sternberg, A.; Bardow, A.; Leitner, W. Sustainable Conversion of Carbon Dioxide: An Integrated Review of Catalysis and Life Cycle Assessment. *Chem. Rev.* **2018**, *118*, 434–504.

(2) Fujimoto, K.; Yokota, K. Effective Hydrogenation of Carbon Dioxide with Two-Stage Reaction System. *Chem. Lett.* **1991**, *20*, 559–562.

(3) Xu, Q.; He, D.; Fujiwara, M.; Tanaka, M.; Souma, Y.; Yamanaka, H. Hydrogenation of Carbon Dioxide over Fe-Cu-Na/Zeolite Composite Catalysts: Na Migration via Solid-Solid Reaction and Its Effects on the Catalytic Activity. *J. Mol. Catal. A Chem.* **1998**, *136*, 161–168.

(4) Motokura, K.; Naijo, M.; Yamaguchi, S.; Miyaji, A.; Baba, T. Silicone Wastes as Reducing Agents for Carbon Dioxide Transformation: Fluoride-Catalyzed Formic Acid Synthesis from CO_2, H_2O, and Disilanes. *Chem. Lett.* **2015**, *44*, 1464–1466.

(5) Filonenko, G. A.; Vrijburg, W. L.; Hensen, E. J. M.; Pidko, E. A. On the Activity of Supported Au Catalysts in the Liquid Phase Hydrogenation of CO_2 to Formates. *J. Catal.* **2016**, *343*, 97–105.

(6) Gao, P.; Li, S.; Bu, X.; Dang, S.; Liu, Z.; Wang, H.; Zhong, L.; Qiu, M.; Yang, C.; Cai, J.; Wen, W.; Sun, Y. Direct Conversion of CO_2 into Liquid Fuels with High Selectivity over a Bifunctional Catalyst. *Nat. Chem.* **2017**, *9*, 1019–1024.

(7) Kuwahara, Y.; Fujie, Y.; Yamashita, H. Poly(Ethyleneimine)-Tethered Ir Complex Catalyst Immobilized in Titanate Nanotubes for Hydrogenation of CO_2 to Formic Acid. *ChemCatChem* **2017**, *9*, 1906–1914.

(8) Ramirez, A.; Gevers, L.; Bavykina, A.; Ould-Chikh, S.; Gascon, J. Metal Organic Framework-Derived Iron Catalysts for the Direct Hydrogenation of CO_2 to Short Chain Olefins. *ACS Catal.* **2018**, *8*, 9174–9182.

(9) Dang, S.; Gao, P.; Liu, Z.; Chen, X.; Yang, C.; Wang, H.; Zhong, L.; Li, S.; Sun, Y. Role of Zirconium in Direct CO_2 Hydrogenation to Lower Olefins on Oxide/Zeolite Bifunctional Catalysts. *J. Catal.* **2018**, *364*, 382–393.

(10) Mori, K.; Sano, T.; Kobayashi, H.; Yamashita, H. Surface Engineering of a Supported PdAg Catalyst for Hydrogenation of CO_2 to Formic Acid: Elucidating the Active Pd Atoms in Alloy Nanoparticles. *J. Am. Chem. Soc.* **2018**, *140*, 8902–8909.

(11) Honda, M.; Kuno, S.; Sonehara, S.; Fujimoto, K.; Suzuki, K.; Nakagawa, Y.; Tomishige, K. Tandem Carboxylation-Hydration Reaction System from Methanol, CO_2 and Benzonitrile to Dimethyl Carbonate and Benzamide Catalyzed by CeO2. *ChemCatChem* **2011**, *3*, 365–370.

(12) Wang, W. H.; Himeda, Y.; Muckerman, J. T.; Manbeck, G. F.; Fujita, E. CO_2 Hydrogenation to Formate and Methanol as an Alternative to Photo- and Electrochemical CO_2 Reduction. *Chem. Rev.* **2015**, *115*, 12936–12973.

(13) Zhu, P.; Sun, J.; Yang, G.; Liu, G.; Zhang, P.; Yoneyama, Y.; Tsubaki, N. Tandem Catalytic Synthesis of Benzene from CO_2 and H_2. *Catal. Sci. Technol.* **2017**, *7*, 2695–2699.

(14) Liu, X.; Wang, M.; Zhou, C.; Zhou, W.; Cheng, K.; Kang, J.; Zhang, Q.; Deng, W.; Wang, Y. Selective Transformation of Carbon Dioxide into Lower Olefins with a Bifunctional Catalyst Composed of $ZnGa_2O_4$ and SAPO-34. *Chem. Commun.* **2017**, *54*, 140–143.

(15) Toyao, T.; Siddiki, S. M. A. H.; Ishihara, K.; Kon, K.; Onodera, W.; Shimizu, K. Heterogeneous Platinum Catalysts for Direct Synthesis of Trimethylamine by N-Methylation of Ammonia and Its Surrogates with CO_2/H_2. *Chem. Lett.* **2017**, *46*, 68–70.

(16) Mitsudome, T.; Urayama, T.; Fujita, S.; Maeno, Z.; Mizugaki, T.; Jitsukawa, K.; Kaneda, K. A Titanium Dioxide Supported Gold Nanoparticle Catalyst for the Selective N-Formylation of Functionalized Amines with Carbon Dioxide and Hydrogen. *ChemCatChem* **2017**, *9*, 3632–3636.

(17) Li, Y.; Cui, X.; Dong, K.; Junge, K.; Beller, M. Utilization of CO_2 as a C1 Building Block for Catalytic Methylation Reactions. *ACS Catal.* **2017**, *7*, 1077–1086.

(18) Tamura, M.; Miura, A.; Gu, Y.; Nakagawa, Y.; Tomishige, K. Selective N-Methylation of Aniline to N-Methylaniline with CO_2 and H_2 by CeO_2-Supported Cu Sub-Nanoparticle Catalyst. *Chem. Lett.* **2017**, *46*, 1243–1246.

(19) Toyao, T.; Hakim Siddiki, S. M. A.; Kon, K.; Shimizu, K. The Catalytic Reduction of Carboxylic Acid Derivatives and CO_2 by Metal Nanoparticles on Lewis-Acidic Supports. *Chem. Rec.* **2018**, *18*, 1374–1393.

(20) Iizuka, T.; Kojima, M.; Tanabe, K. Support Effects in the Formation of Methanol from Carbon Dioxide and Hydrogen over Rhenium Catalysts. *J. Chem. Soc. Chem. Commun.* **1983**, 638–639.

(21) Xu, Z.; Qian, Z. H.; Tanabe, K.; Hattori, H. Support Effect of Re Catalyst on Methanol Synthesis From CO_2 and H_2 Under a Pressure of 5-Atm. *Bull. Chem. Soc. Jpn.* **1991**, *64*, 1664–1668.

(22) Tominaga, K.; Sasaki, Y.; Kawai, M.; Watanabe, T.; Saito, M. Ruthenium Complex Catalysed Hydrogenation of Carbon Dioxide to Carbon Monoxide, Methanol and Methane. *J. Chem. Soc. Chem. Commun.* **1993**, 629–631.

(23) Álvarez, A.; Bansode, A.; Urakawa, A.; Bavykina, A. V.; Wezendonk, T. A.; Makkee, M.; Gascon, J.; Kapteijn, F. Challenges in the Greener Production of Formates/Formic Acid, Methanol, and DME by Heterogeneously Catalyzed CO_2 Hydrogenation Processes. *Chem. Rev.* **2017**, *117*, 9804–9838.

(24) Rodriguez, J. A.; Liu, P.; Stacchiola, D. J.; Senanayake, S. D.; White, M. G.; Chen, J. G. Hydrogenation of CO_2 to Methanol: Importance of Metal-Oxide and Metal-Carbide Interfaces in the Activation of CO_2. *ACS Catal.* **2015**, *5*, 6696–6706.

(25) Bahruji, H.; Bowker, M.; Hutchings, G.; Dimitratos, N.; Wells, P.; Gibson, E.; Jones, W.; Brookes, C.; Morgan, D.; Lalev, G. Pd/ZnO Catalysts for Direct CO_2 Hydrogenation to Methanol. *J. Catal.* **2016**, *343*, 133–146.

(26) Martin, O.; Martín, A. J.; Mondelli, C.; Mitchell, S.; Segawa, T. F.; Hauert, R.; Drouilly, C.; Curulla-Ferré, D.; Pérez-Ramírez, J. Indium Oxide as a Superior Catalyst for Methanol Synthesis by CO_2 Hydrogenation. *Angew. Chem. Int. Ed.* **2016**, *55*, 6261–6265.

(27) Wang, J.; Li, G.; Li, Z.; Tang, C.; Feng, Z.; An, H.; Liu, H.; Liu, T.; Li, C. A Highly Selective and Stable ZnO-ZrO_2 Solid Solution Catalyst for CO_2 Hydrogenation to Methanol. *Sci. Adv.* **2017**, *3*, e1701290.

(28) Larmier, K.; Liao, W. C.; Tada, S.; Lam, E.; Verel, R.; Bansode, A.; Urakawa, A.; Comas-Vives, A.; Copéret, C. CO_2-to-Methanol Hydrogenation on Zirconia-Supported Copper Nanoparticles: Reaction Intermediates and the Role of the Metal–Support Interface. *Angew. Chem. - Int. Ed.* **2017**, *56*, 2318–2323.

(29) Kattel, S.; Liu, P.; Chen, J. G. Tuning Selectivity of CO_2 Hydrogenation Reactions at the Metal/Oxide Interface. *J. Am. Chem. Soc.* **2017**, *139*, 9739–9754.

(30) Kar, S.; Kothandaraman, J.; Goeppert, A.; Prakash, G. K. S. Advances in Catalytic Homogeneous Hydrogenation of Carbon Dioxide to Methanol. *J. CO2 Util.* **2018**, *23*, 212–218.

(31) Olah, G. A.; Goeppert, A.; Prakash, G. K. S. Chemical Recycling of Carbon Dioxide to Methanol and Dimethyl Ether: From Greenhouse Gas to Renewable, Environmentally Carbon Neutral Fuels and Synthetic Hydrocarbons. *J. Org. Chem.* **2009**, *74*, 487–498.

(32) Saito, M.; Murata, K. Development of High Performance Cu/ZnO-Based Catalysts for Methanol Synthesis and the Water-Gas Shift Reaction. *Catal. Surv. from Asia* **2004**, *8*, 285–294.

(33) Gaikwad, R.; Bansode, A.; Urakawa, A. High-Pressure Advantages in Stoichiometric Hydrogenation of Carbon Dioxide to Methanol. *J. Catal.* **2016**, *343*, 127–132.

(34) Porosoff, M. D.; Yan, B.; Chen, J. G. Catalytic Reduction of CO_2 by H_2 for Synthesis of CO, Methanol and Hydrocarbons: Challenges and Opportunities. *Energy Environ. Sci.* **2016**, *9*, 62–73.

(35) Balaraman, E.; Gunanathan, C.; Zhang, J.; Shimon, L. J. W.; Milstein, D. Efficient Hydrogenation of Organic Carbonates, Carbamates and Formates Indicates Alternative Routes to Methanol Based on CO_2 and CO. *Nat. Chem.* **2011**, *3*, 609–614.

(36) Huff, C. A.; Sanford, M. S. Cascade Catalysis for the Homogeneous Hydrogenation of CO_2 to Methanol. *J. Am. Chem. Soc.* **2011**, *133*, 18122–18125.

(37) Wesselbaum, S.; Vom Stein, T.; Klankermayer, J.; Leitner, W. Hydrogenation of Carbon Dioxide to Methanol by Using a Homogeneous Ruthenium-Phosphine Catalyst. *Angew. Chem. - Int. Ed.* **2012**, *51*, 7499–7502.

(38) Rezayee, N. M.; Huff, C. A.; Sanford, M. S. Tandem Amine and Ruthenium-Catalyzed Hydrogenation of CO_2 into Methanol. *J. Am. Chem. Soc.* **2015**, *137*, 1028−1031.

(39) Wesselbaum, S.; Moha, V.; Meuresch, M.; Brosinski, S.; Thenert, K. M.; Kothe, J.; Stein, T. vom; Englert, U.; Hölscher, M.; Klankermayer, J.; Leitner, W. Hydrogenation of Carbon

Dioxide to Methanol Using a Homogeneous Ruthenium–Triphos Catalyst: From Mechanistic Investigations to Multiphase Catalysis. *Chem. Sci.* **2015**, *6*, 693–704.

(40) Schneidewind, J.; Adam, R.; Baumann, W.; Jackstell, R.; Beller, M. Low-Temperature Hydrogenation of Carbon Dioxide to Methanol with a Homogeneous Cobalt Catalyst. *Angew. Chem. - Int. Ed.* **2017**, *56*, 1890 –1893.

(41) Kar, S.; Goeppert, A.; Kothandaraman, J.; Prakash, G. K. S. Manganese-Catalyzed Sequential Hydrogenation of CO_2 to Methanol via Formamide. *ACS Catal.* **2017**, *7*, 6347−6351.

(42) Ribeiro, A. P. C.; Martins, L. M. D. R. S.; Pombeiro, A. J. L. Carbon Dioxide-to-Methanol Single-Pot Conversion Using a C-Scorpionate Iron(II) Catalyst. *Green Chem.* **2017**, *19*, 4811–4815.

(43) Everett, M.; Wass, D. F. Highly Productive CO_2 Hydrogenation to Methanol-a Tandem Catalytic Approach: Via Amide Intermediates. *Chem. Commun.* **2017**, *53*, 9502–9504.

(44) Kothandaraman, J.; Goeppert, A.; Czaun, M.; Olah, G. A.; Prakash, G. K. S. Conversion of CO_2 from Air into Methanol Using a Polyamine and a Homogeneous Ruthenium Catalyst. *J. Am. Chem. Soc.* **2016**, *133*, 778–781.

(45) Kar, S.; Sen, R.; Goeppert, A.; Prakash, G. K. S. Integrative CO_2 Capture and Hydrogenation to Methanol with Reusable Catalyst and Amine: Toward a Carbon Neutral Methanol Economy. *J. Am. Chem. Soc.* **2018**, *140*, 1580–1583.

(46) Scharnagl, F.; Hertrich, M.; Neitzel, G.; Jackstell, R.; Beller, M. Homogeneous Catalytic Hydrogenation of CO_2 to Methanol – Improvements with Tailored Ligands. *Adv. Synth. Catal.* In Press. doi:10.1002/adsc.201801314.

(47) Zeng, J.; Fujimoto, K.; Tsubaki, N. A New Low-Temperature Synthesis Route of Methanol: Catalytic Effect of the Alcoholic Solvent. *Energy and Fuels* **2002**, *16*, 83–86.

(48) Reller, C.; Pöge, M.; Lißner, A.; Mertens, F. O. R. L. Methanol from CO_2 by Organo-Cocatalysis: CO_2 Capture and Hydrogenation in One Process Step. *Environ. Sci. Technol.* **2014**, *48*, 14799−14804.

(49) Chen, Y.; Choi, S.; Thompson, L. T. Low-Temperature CO_2 Hydrogenation to Liquid Products via a Heterogeneous Cascade Catalytic System. *ACS Catal.* **2015**, *5*, 1717−1725.

(50) Chen, Y.; Choi, S.; Thompson, L. T. Low Temperature CO_2 Hydrogenation to Alcohols and Hydrocarbons over Mo_2C Supported Metal Catalysts. *J. Catal.* **2016**, *343*, 147–156.

(51) He, Z.; Qian, Q.; Ma, J.; Meng, Q.; Zhou, H.; Song, J.; Liu, Z.; Han, B. Water-Enhanced Synthesis of Higher Alcohols from CO_2 Hydrogenation over a Pt/Co_3O_4 Catalyst under Milder Conditions. *Angew. Chem. - Int. Ed.* **2016**, *55*, 737–741.

(52) Kothandaraman, J.; Dagle, R. A.; Dagle, V. L.; Davidson, S. D.; Walter, E. D.; Burton, S. D.; Hoyt, D. W.; Heldebrant, D. J. Condensed-Phase Low Temperature Heterogeneous Hydrogenation of CO_2 to Methanol. *Catal. Sci. Technol.* **2018**, *8*, 5098–5103.

(53) Khan, M. U.; Wang, L.; Liu, Z.; Gao, Z.; Wang, S.; Li, H.; Zhang, W.; Wang, M.; Wang, Z.; Ma, C.; Zeng, J. Pt_3Co Octapods as Superior Catalysts of CO_2 Hydrogenation. *Angew. Chem. - Int. Ed.* **2016**, *55*, 9548 –9552.

(54) Zhang, W.; Wang, L.; Liu, H.; Hao, Y.; Li, H.; Khan, M. U.; Zeng, J. Integration of Quantum Confinement and Alloy Effect to Modulate Electronic Properties of RhW Nanocrystals for Improved Catalytic Performance toward CO_2 Hydrogenation. *Nano Lett.* **2017**, *17*, 788−793.

(55) Li, H.; Wang, L.; Dai, Y.; Pu, Z.; Lao, Z.; Chen, Y.; Wang, M.; Zheng, X.; Zhu, J.; Zhang, W.; Si, R.; Ma, C.; Zeng, J. Synergetic Interaction between Neighbouring Platinum Monomers in CO_2 Hydrogenation. *Nat. Nanotechnol.* **2018**, *13*, 411–417.

(56) Bai, S.; Shao, Q.; Feng, Y.; Bu, L.; Huang, X. Highly Efficient Carbon Dioxide Hydrogenation to Methanol Catalyzed by Zigzag Platinum–Cobalt Nanowires. *Small* **2017**, *13*, 1604311.

(57) Zheng, X.; Lin, Y.; Pan, H.; Wu, L.; Zhang, W.; Cao, L.; Zhang, J.; Zheng, L.; Yao, T. Grain Boundaries Modulating Active Sites in RhCo Porous Nanospheres for Efficient CO_2 Hydrogenation. *Nano Res.* **2018**, *11*, 2357–2365.

(58) Toyao, T.; Siddiki, S. M. A. H.; Touchy, A. S.; Onodera, W.; Kon, K.; Morita, Y.; Kamachi, T.; Yoshizawa, K.; Shimizu, K. TiO_2-Supported Re as a General and Chemoselective Heterogeneous Catalyst for Hydrogenation of Carboxylic Acids to Alcohols. *Chem. - A Eur. J.* **2017**, *23*, 1001–1006.

(59) Toyao, T.; Siddiki, S. M. A. H.; Morita, Y.; Kamachi, T.; Touchy, A. S.; Onodera, W.; Kon, K.; Furukawa, S.; Ariga, H.; Asakura, K.; Yoshizawa, K.; Shimizu, K. Rhenium-Loaded TiO_2: A Highly Versatile and Chemoselective Catalyst for the Hydrogenation of Carboxylic Acid Derivatives and the *N*-Methylation of Amines Using H_2 and CO_2. *Chem. - A Eur. J.* **2017**, *23*, 14848–14859.

(60) Gates, B. C.; Flytzani-Stephanopoulos, M.; DIxon, D. A.; Katz, A. Atomically Dispersed Supported Metal Catalysts: Perspectives and Suggestions for Future Research. *Catal. Sci. Technol.* **2017**, *7*, 4259–4275.

(61) Jones, J.; Xiong, H.; DeLaRiva, A. T.; Peterson, E. J.; Pham, H.; Challa, S. R.; Qi, G.; Oh, S.; Wiebenga, M. H.; Hernández, X. I. P.; Wang, Y.; Datye, A. K. Thermally Stable Single-Atom Platinum-on-Ceria Catalysts via Atom Trapping. *Science* **2016**, *353*, 150–154.

(62) Zhang, Z.; Zhu, Y.; Asakura, H.; Zhang, B.; Zhang, J.; Zhou, M.; Han, Y.; Tanaka, T.; Wang, A.; Zhang, T.; Yan, N. Thermally Stable Single Atom Pt/m-Al_2O_3 for Selective Hydrogenation and CO Oxidation. *Nat. Commun.* **2017**, *8*, 16100.

(63) Bobadilla, L. F.; Santos, J. L.; Ivanova, S.; Odriozola, J. A.; Urakawa, A. Unravelling the Role of Oxygen Vacancies in the Mechanism of the Reverse Water-Gas Shift Reaction by Operando DRIFTS and Ultraviolet-Visible Spectroscopy. *ACS Catal.* **2018**, *8*, 7455−7467.

(64) Matsubu, J. C.; Yang, V. N.; Christopher, P. Isolated Metal Active Site Concentration and Stability Control Catalytic CO_2 Reduction Selectivity. *J. Am. Chem. Soc.* **2015**, *137*, 3076–3084.

(65) Koso, S.; Watanabe, H.; Okumura, K.; Nakagawa, Y.; Tomishige, K. Stable Low-Valence ReOx Cluster Attached on Rh Metal Particles Formed by Hydrogen Reduction and Its Formation Mechanism. *J. Phys. Chem. C* **2012**, *116*, 3079−3090.

(66) Ly, B. K.; Tapin, B.; Aouine, M.; Delichere, P.; Epron, F.; Pinel, C.; Especel, C.; Besson, M. Insights into the Oxidation State and Location of Rhenium in Re-Pd/TiO_2 Catalysts for Aqueous-Phase Selective Hydrogenation of Succinic Acid to 1,4-Butanediol as a Function of Palladium and Rhenium Deposition Methods. *ChemCatChem* **2015**, *7*, 2161–2178.

(67) Thompson, S. T.; Lamb, H. H. Catalysts for Selective Hydrogenation of Furfural Derived from the Double Complex Salt $[Pd(NH_3)_4](ReO_4)_2$ on γ-Al_2O_3. *J. Catal.* **2017**, *350*, 111–121.

(68) Nakagawa, Y.; Tazawa, S.; Wang, T.; Tamura, M.; Hiyoshi, N.; Okumura, K.; Tomishige, K. Mechanistic Study of Hydrogen-Driven Deoxydehydration over Ceria-Supported Rhenium Catalyst Promoted by Au Nanoparticles. *ACS Catal.* **2018**, *8*, 584−595.

(69) Greiner, M. T.; Rocha, T. C. R.; Johnson, B.; Klyushin, A.; Knop-Gericke, A.; Schlögl, R. The Oxidation of Rhenium and Identification of Rhenium Oxides during Catalytic Partial Oxidation of Ethylene: An in-Situ Xps Study. *Zeitschrift fur Phys. Chemie* **2014**, *228*, 521–541.

Chapter 3

Catalytic Methylation of Aromatic Hydrocarbons using CO_2 and H_2 over TiO_2-Supported Re and Zeolite Catalysts: Machine Learning-Assisted Catalyst Optimization

3.1 Introduction

In recent years, because of increasing interest in carbon capture and utilization technology, the implementation of CO_2 as a C_1 source for the production of chemicals has garnered broad attention in both the academic and industrial sectors.[1–7] The conversion of CO_2 via hydrogenation to commodity chemicals such as methanol remains one of the most extensively studied topics because hydrogenation is considered one of the most practical methods of converting CO_2; the process is essentially carbon neutral on the premise that H_2 originates from renewable energy sources.[8–14] The produced methanol is further upgraded to various chemicals such as olefins and hydrocarbons, including aromatics.[15,16] Although methanol production from the hydrogenation of CO_2 has recently been achieved industrially, this process suffers from a low equilibrium conversion of CO_2 because of thermodynamic limitations.[17–19] In this regard, the direct conversion of CO_2 to aromatics, most notably benzene, toluene, and xylenes (BTX), has been attracting attention because the one-pass equilibrium conversion of CO_2 is higher for CO_2-to-aromatics than for CO_2-to-methanol and because BTX have higher added value.[20–28] However, the direct conversion of CO_2 to aromatics requires harsh reaction conditions, typically involving temperatures greater than 300 °C.

The application of CO_2 and H_2 as a methylating agent has emerged as a promising strategy to achieving a higher equilibrium conversion of CO_2. For instance, *N*-methylation of amines using CO_2 for the synthesis of methylamines has been widely explored.[29–36] However, reports on *C*-methylation using CO_2 are relatively scarce compared with the volume of literature on *N*-methylation because C–C bond formation is generally more difficult than C–N bond formation as a consequence of the weaker nature of carbon nucleophiles. In 2014, Beller and coworkers reported the first ever direct catalytic *C*-methylation of heteroarenes using CO_2 and H_2 over Ru-based homogeneous catalysts.[37] Although their work was groundbreaking and impactful, the reported substrate scope was limited to electron-rich arenes and the process required the addition of a Lewis acid. We have recently reported the methylation of benzene using CO_2/H_2 for the one-pot synthesis of methylated benzene derivatives over a mixed catalyst comprising TiO_2-supported Re (Re(1)/TiO_2; Re loading = 1 wt%) as a hydrogenation catalyst and H-MOR zeolite (SiO_2/Al_2O_3 = 90) as a methylation catalyst.[38] We have also carried out the one-pot methylation of naphthalene over

Re(1)/TiO_2 and H-Beta (SiO_2/Al_2O_3 = 40). Compared to the methylation of arenes using syngas (that is, a CO/H_2 mixture),[39–42] this process, which directly uses CO_2, would be beneficial. In addition, our process shows greater productivity of methylated products than the methylation process using methane as a carbon source.[43] More recently, Yuan and coworkers reported the selective methylation of toluene over $ZnZrO_x$–ZSM-5 catalyst at 360 °C and 3 MPa.[44] Although these few reports on *C*-methylation using CO_2/H_2 as a methylation agent are available, the development of a catalyst system for the methylation of common aromatics under mild conditions is needed to efficiently upgrade them to higher value-added products.

In present work, catalytic methylation of toluene and *m*-xylene using CO_2 and H_2 was performed. Toluene and *m*-xylene were chosen as the main starting substrates because of their lower demand in the petrochemical industries. We sought to convert them into more methylated aromatic hydrocarbons using CO_2 as a carbon source. The produced polymethyl benzenes can be further converted to *p*-xylene, which is widely used as a precursor for plastics,[45] using a current petroleum industrial process based on disproportionation/transmethylation over zeolite catalysts.[46,47] After a thorough screening of various combinations of catalysts, the combination of Re(1)/TiO_2 and H-Beta(40) was found to exhibit the best performance under the experimental reaction conditions (p_{CO2} = 1 MPa; p_{H2} = 5 MPa; T = 240 °C) because it achieved the highest yield of methylated products while generating the smallest amount of byproducts such as demethylated and dearomatized products as well as CO and CH_4 in the gas phase when toluene or *m*-xylene was used as the substrate. In addition to the traditional catalysis research approach, we also demonstrate a data-science-based catalyst optimization process using machine learning (ML) techniques.

3.2 Experimental section

3.2.1 Materials and catalyst preparation

Chemical reagents were obtained from commercial suppliers and were used as received (Tokyo Chemical Industry, Wako Pure Chemical Industries, and Sigma-Aldrich). TiO_2 (ST-01) was obtained from Ishihara Sangyo Co. ZrO_2 (JRC-ZRO-5) was provided by the Catalysis Society of Japan. Al_2O_3 was prepared via calcination of boehmite (Catapal B Alumina, Sasol) for 3 h at 900 °C. CeO_2 was prepared by calcination of CeO_2 obtained from Daiichi Kigenso Kagaku Kogyo Co. (Type A) for 3 h at 600 °C in air. SiO_2 (CARiACT Q-10) was purchased from Fuji Silysia Chemical. Activated carbon was obtained from Kishida Chemical Co. H-Beta (SiO_2/Al_2O_3 = 40) and H-Beta (SiO_2/Al_2O_3 = 510) were provided by TOSOH Corp. H-MOR (SiO_2/Al_2O_3 = 90) and H-Beta (SiO_2/Al_2O_3 = 150) were obtained from Clariant Catalysts. H-CHA (SiO_2/Al_2O_3 = 22) was prepared by calcination of NH_4-CHA (SiO_2/Al_2O_3 = 22, TOSOH Corp.) for 1 h at 600 °C in air. H-MFI (SiO_2/Al_2O_3 = 150) was purchased from N. E. Chemcat Corp. Cu/ZnO/Al_2O_3 (MDC-7; 34 wt% Cu) was supplied by Clariant Catalysts.

M/TiO_2 (*M* = 1 wt% Re, Pt, Ir, Rh, Ru, Pd, Ag, Au, Cu, Ni, Co) and Re/Support (1 wt% Re; Support = metal oxide or activated carbon) were prepared using a simple impregnation method in which the support material was mixed with an aqueous solution of the metal precursor (NH_4ReO_4; nitrate of Ag, Ni, Cu, or Co; $RuCl_3$; $IrCl_3 \cdot nH_2O$; $HAuCl_4 \cdot 4H_2O$; aqueous HNO_3 solution of $Pt(NH_3)_2(NO_3)_2$, $Rh(NO_3)_3$, or $Pd(NH_3)_2(NO_3)_2$). As an example, for the preparation of Re(1)/TiO_2, 0.072 g of NH_4ReO_4 was added to a glass vessel (500 mL) containing 400 mL of deionized water. After the NH_4ReO_4 was completely dissolved by stirring, 4.95 g of TiO_2 (ST-01) was added to the solution, followed by stirring at 400 rpm for 30 min at room temperature. Water was subsequently removed from the reaction mixture by evaporation *in vacuo*, followed by drying at 110 °C under ambient pressure for at least 12 h. The resultant material was calcined for 3 h at 500 °C in air. Prior to each experiment, the active catalyst was prepared by reduction in a quartz tube for 0.5 h at 500 °C under flowing H_2 (20 cm^3 min^{-1}). Other *M*/TiO_2 and Re/Support catalysts were also synthesized in the same previously described manner unless otherwise specified. Cu/ZrO_2 with Cu loading = 8 wt% was prepared using a method described elsewhere.[48]

3.2.2 Catalytic reactions

Reactions were carried out via the following procedure. Typically, 0.15 g of a supported metal catalyst (equivalent to 0.0081 mmol of loaded metal) and 0.10 g of zeolite catalyst were thoroughly pre-mixed physically in a quartz tube and then reduced under flowing H_2 for 0.5 h at 500 °C. After the reduced catalyst had sufficiently cooled, 1 mmol of substrate (*m*-xylene or toluene) was added to the tube without exposing the catalyst to air. The tube containing the catalyst/reactant mixture was then loaded into an autoclave, after which the vessel was charged with 1 MPa CO_2 and 5 MPa H_2. The batch reactor was subsequently heated to the desired temperature (240 °C), and the mixture was stirred magnetically at 500 rpm for 20 h. The autoclave was then removed from the heat source and cooled prior to product analysis. Liquid products were extracted using 1,4-dioxane and analyzed using a gas chromatograph equipped with a flame ionization detector (GC-FID; Shimadzu GC-2010; ULBON Xylene Master; Shinwa Chemical Industries). Quantitative analysis was conducted using the internal standard calibration method with *n*-decane as the internal standard. Gaseous products such as CO, CH_4, and lower alkanes were analyzed by GC-FID (Shimadzu GC-2014; Porapak Q column) equipped with a methanizer (Shimadzu MTN-1). Quantitative analysis of gaseous products was conducted using an external standard calibration method. The yields were defined as follows:

$$\text{Substrate-based yield} = \frac{\Sigma\ \text{Amount of methylated product (mmol)}}{\text{Initial amount of substrate (mmol)}} \times 100$$

For the methylation of *m*-xylene, the methylated products include tri-, tetra-, penta-, and hexamethylbenzene; for the methylation of toluene, xylenes and onwards are included.

$$CO_2\text{-based yield} = \frac{\Sigma\ [\text{Amount of benzene-derived product (mmol)} \times \text{Coefficient}]}{\text{Initial amount of } CO_2 \text{ (mmol)}} \times 100$$

Coefficient = Number of methyl groups in product - Number of methyl group in substrate

Benzene-derived products include benzene, toluene, xylenes, and tri-, tetra-, penta-, and hexamethylbenzenes. The coefficient is the change in the number of methyl groups relative to the substrate. For example, for the methylation of *m*-xylene and toluene, the coefficient for benzene is −2 and −1, respectively, and for trimethylbenzene is +1 and +2, respectively. Dearomatized products include cyclohexane and methylcyclohexane.

3.2.3 Machine learning

A widely used package, scikit-learn (http://scikit-learn.org, version 0.23.2), was used for machine learning (ML) implementations.[49] Gradient boosting regression with XGBoost (XGB)[50] (version 0.23.2) was used. The default values of XGBoost were used for tuning hyperparameters except for n_estimators = 500. For evaluation of the predictive capability of the ML model, Monte Carlo cross-validation with 100 random leave-25%-out trials was used. The root-mean-square error (RMSE) between the predicted and true values (ground truth) was calculated for each trial, and the results were averaged to obtain the mean RMSE values.

3.3 Results and discussion

3.3.1 Catalytic methylation of *m*-xylene

Initially, the catalytic methylation of *m*-xylene using CO_2 and H_2 was carried out over combinations of various supported metal catalysts and a fixed H-Beta(40) catalyst; the results are shown in **Figure 1**. Re(1)/TiO_2 exhibited the highest yield of methylated products on the basis of both CO_2 and *m*-xylene as a starting substrate among all the catalysts tested. Polymethylbenzenes, including trimethylbenzenes, tetramethylbenzenes, pentamethylbenzene, and hexamethylbenzene, were obtained as the main products. In addition, a small amount of toluene, as well as the other xylenes (*o*-xylene and *p*-xylene), was detected, suggesting that disproportionation/transmethylation/dealkylation processes also occurred during the reaction. Notably, benzene was not formed when Re(1)/TiO_2 was used as the hydrogenation catalyst, whereas catalysts such as Pd(1)/TiO_2 and Ni(1)/TiO_2 produced relatively large amounts of benzene. In addition, dearomatized products were not observed over the catalytic system with Re(1)/TiO_2, whereas Pd, Rh, and Ag catalysts promoted the dearomatization reaction to produce cyclohexane and methylcyclohexane. Note that Re(1)/Al_2O_3 and Re(1)/SiO_2 produced dearomatized products even though their active metal was Re. Given that Re on TiO_2 is highly dispersed compared with other supports such as Al_2O_3 and SiO_2,[51,52] the observed high selectivity toward the desired polymethylbenzenes rather than dearomatized products is attributable to the high dispersion of the Re species, which is achieved through combination with TiO_2 as a support. This reaction was also attempted using Re/H-Beta(40), which was synthesized by directly depositing 1 wt% of Re on H-Beta(40). The performance of Re/H-Beta(40) was poor, showing not only a mediocre yield, but also low selectivity from the formation of large amount of dearomatized products. For benchmarking purpose, the industrial methanol synthesis catalyst Cu/ZnO/Al_2O_3 was also employed for the reaction and was found to exhibit low activity. Since the Cu content of the Cu/ZnO/Al_2O_3 catalyst is 34 wt%, the amount of catalyst used in this experiment was merely 2 mg, which could be the reason why methylation reaction barely proceeded as the production of methanol was limited. Cu/ZrO_2, another methanol synthesis catalyst,[48] was also tested and showed a relatively high selectivity for methylated products with a yield second only to that of Re(1)/TiO_2, which exhibited the best performance among the investigated catalysts. Cu/ZrO_2 was also found to

promote the dearomatization process, although the amount of dearomatized products obtained was lower when compared with the amount obtained using $Cu/ZnO/Al_2O_3$. To ensure fairer comparisons, experiments using 0.15 g of $Cu/ZnO/Al_2O_3$ and Cu/ZrO_2 were also attempted. The results for both catalysts vastly improved, showing better yields and selectivity for methylated products, although the performance still lag behind that of $Re(1)/TiO_2$. These results indicate that, although Cu is an active metal for the methanol synthesis process and is still a promising candidate as a catalyst component, a catalyst/reaction-condition optimization process that considers both the productivities of polymethylbenzenes and the selectivity is necessary to minimize unwanted reactions such as dearomatization. In the end, $Re(1)/TiO_2$ was chosen as the preferred catalyst for the following reasons: a) $Re(1)/TiO_2$ showed the highest overall yield and selectivity for methylated products, producing relatively low amount of byproducts while maintaining a high substrate conversion. b) Dearomatization of aromatic compounds and the formation of benzene via dealkylation can be prevented using $Re(1)/TiO_2$.

Next, we proceeded with the catalyst screening by testing various combinations of zeolites with $Re(1)/TiO_2$ for the methylation of *m*-xylene (**Figure 2**). H-Beta(40) exhibited the highest yield of methylated products. Irrespective of the SiO_2/Al_2O_3 ratio, H-Beta in general produced relatively lower amount of byproducts than the other tested zeolites, likely because of efficient substrate diffusion. Again, neither the formation of dearomatized products nor total dealkylation of *m*-xylene to benzene was observed. On the basis of the results presented thus far, we concluded that $Re(1)TiO_2$ and H-Beta(40) constituted the best catalyst combination for the methylation of *m*-xylene using CO_2 and H_2.

The effect of Re loading on the catalytic performance was also studied to determine the optimal loading amount of Re. A series of Re/TiO_2 catalysts with a wide range of Re loadings (0.2–20 wt%) and in combination with H-Beta(40) was tested for the methylation of *m*-xylene (**Figure 3**). Catalysts with a lower Re loading (Re < 1 wt%) were found to produce greater amount of CO, whereas a higher Re loading (Re > 1 wt%) appeared to favor the formation of CH_4. These phenomena are attributable to the fact that catalysts with a low Re loading but a large fraction of atomically dispersed Re species have been reported to favor the formation of CO, whereas catalysts with a high Re loading have a higher fraction of large Re clusters/nanoparticles, which enhances the formation of CH_4. The highest yield of methylated products, together with the lowest

amount of byproducts, was achieved when 1 wt% of Re was used. Therefore, among the investigated catalysts, Re(1)/TiO_2 was found to be the most suitable catalyst for our system.

We next investigated the effect of reaction temperature on the methylation reaction catalyzed by Re(1)/TiO_2 and H-Beta(40) (**Figure 4**). The methylation reaction barely proceeded at lower temperatures such as 150 °C. With increasing temperature, yields of methylated products, as determined on the basis of both *m*-xylene and CO_2, increased within the investigated temperature range (to 280 °C). However, the amount of unwanted byproducts such as CH_4 also increased with increasing reaction temperature. Therefore, given the aforementioned issue and our desire to use a milder reaction temperature, we selected 240 °C as the standard reaction temperature for the present study. The effect of the amount of H-Beta(40) was also studied using Re(1)/TiO_2 on the catalytic methylation of *m*-xylene (**Figure 5**). Although higher amount of H-Beta(40) was found to increase the substrate-based yield, the differences in CO_2-based yield and the selectivity to methylated products were minimal. Since lesser amount of catalyst is preferable for actual application, 0.1 g of H-Beta was thus chosen as the standard for this study.

Control experiments for the catalytic methylation of *m*-xylene were conducted using Re(1)/TiO_2 and/or H-Beta(40) under different reaction conditions (**Figure 6**), labeled as A–F. The standard reaction condition (A) is included for ease of comparison. When only Re(1)/TiO_2 was used as a catalyst without H-Beta(40) (B), the major products were CO, CH_4, and CH_3OH, which was expected because Re(1)/TiO_2 is known to catalyze the CO_2 hydrogenation of methanol.[52] However, when Re(1)/TiO_2 was absent and only H-Beta(40) was used (C), various aromatic methylated compounds were detected, indicating that disproportionation/transalkylation of *m*-xylene occurred on H-Beta(40). Control experiments in the absence of CO_2/H_2, which was used as the alkylating agent, were also conducted. In these experiments, the reactor was filled with 1 MPa of N_2 to create a pressurized environment and provide an inert atmosphere. In the absence of H-Beta(40) and the CO_2/H_2 mixture, the methylation reaction barely proceeded, as evident from the extremely low conversion of *m*-xylene (D), demonstrating that CO_2/H_2 was indeed the source of the methyl group for the synthesis of methylated aromatics. When only H-Beta(40) and *m*-xylene were present (E), results similar to those of experiment C were observed, further

demonstrating that the transalkylation occurred on H-Beta(40). Finally, a control experiment in the presence of Re(1)/TiO_2, H-Beta(40) and *m*-xylene (F) showed a nearly identical result to those of experiment C and E, once again proving that a certain degree of disproportionation/transalkylation is bound to occur even in the absence of CO_2. Based on the results above, it can be inferred that irrespective of the availability of CO_2, disproportionation/transalkylation of *m*-xylene is catalyzed by H-Beta(40), thus always forming a fixed ratio of products. The presence of Re(1)/TiO_2 and CO_2/H_2 is needed for the methylation reaction to proceed as Re(1)/TiO_2 is essential for the activation of CO_2. It is worthwhile to highlight the fact that while a rough estimate of product formation via disproportionation/transalkylation can be obtained based on the results of control experiments, determination of the exact ratio for product formation between methylation and disproportionation/transalkylation under the standard reaction condition (i.e. in the presence of CO_2/H_2) is a difficult task.

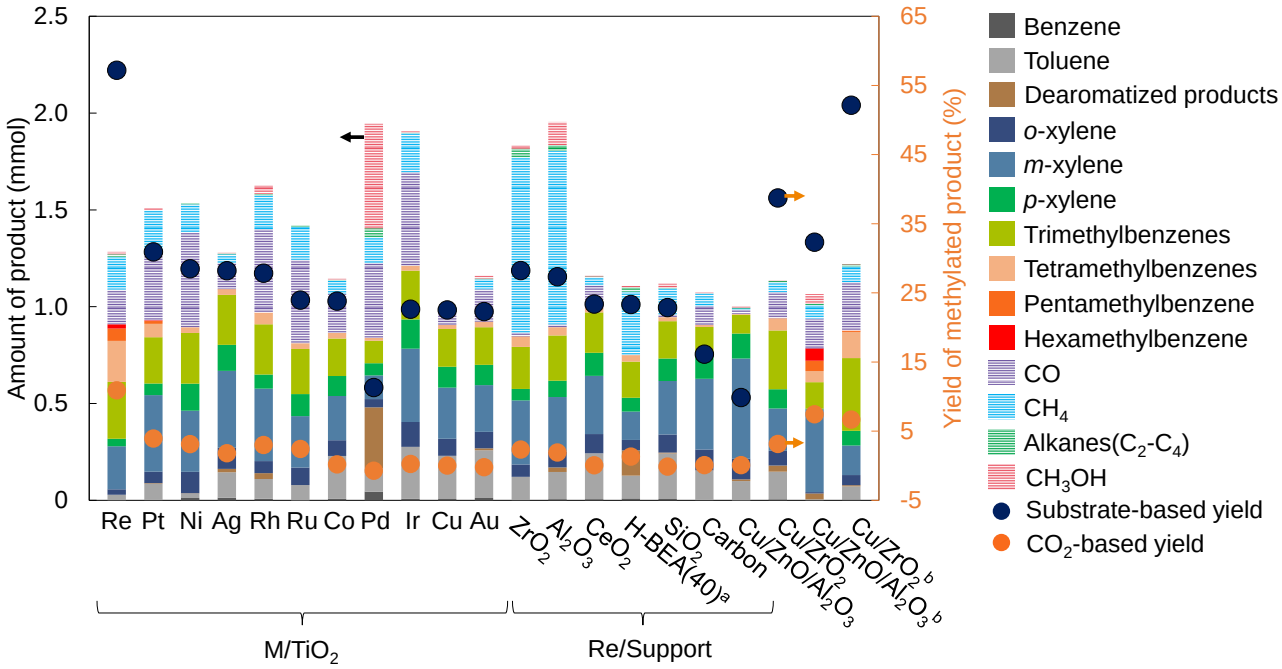

Figure 1. Screening of hydrogenation catalysts for the catalytic methylation of *m*-xylene using CO_2 and H_2. Pre-treatment: 500 °C, 0.5 h under flowing H_2 (20 mL min^{-1}); reaction conditions: 1 wt% of supported metal catalyst (mass adjusted to contain 0.0081 mmol of loaded metal per experiment) with 0.10 g of H-Beta(40), 1.0 mmol of *m*-xylene, CO_2 (1 MPa), H_2 (5 MPa), 240 °C, 20 h. [a]The reaction was performed without H-Beta(40) as a methylation catalyst. [b]0.15 g of catalyst.

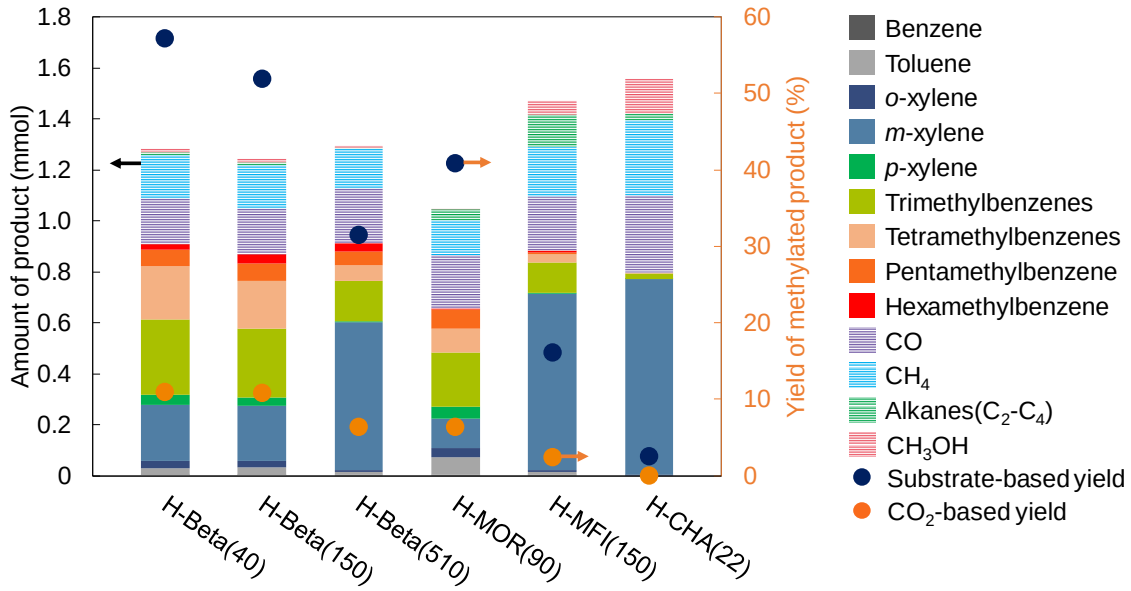

Figure 2. Screening of zeolite catalysts for the catalytic methylation of *m*-xylene using CO_2 and H_2. Pre-treatment: 500 °C, 0.5 h under flowing H_2 (20 mL min^{-1}); reaction conditions: 0.15 g of Re(1)/TiO_2 with 0.10 g of zeolite, 1.0 mmol of *m*-xylene, CO_2 (1 MPa), H_2 (5 MPa), 240 °C, 20 h.

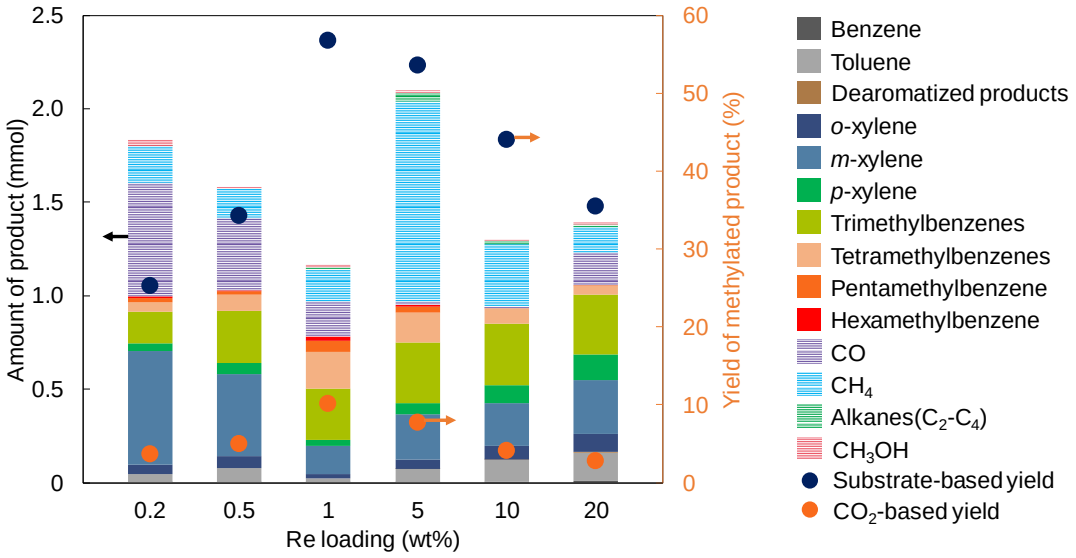

Figure 3. Effect of Re loading on the catalytic methylation of *m*-xylene using CO_2 and H_2. Pre-treatment: 500 °C, 0.5 h under flowing H_2 (20 mL min^{-1}); reaction conditions: 0.0081 mmol of loaded Re with 0.10 g of H-Beta(40), 1.0 mmol of *m*-xylene, CO_2 (1 MPa), H_2 (5 MPa), 240 °C, 20 h.

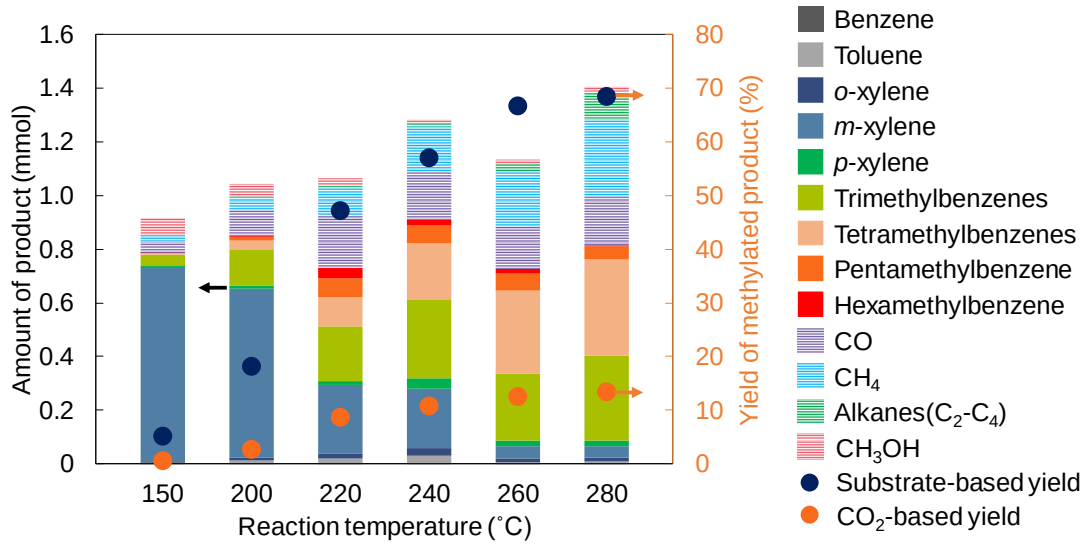

Figure 4. Effect of reaction temperature on the methylation of *m*-xylene using CO_2 and H_2 catalyzed by Re(1)/TiO_2 and H-Beta(40). Pre-treatment: 500 °C, 0.5 h under flowing H_2 (20 mL min^{-1}); reaction conditions: 0.0081 mmol of loaded metal with 0.10 g of H-Beta(40), 1.0 mmol of benzene, CO_2 (1 MPa), H_2 (5 MPa), 20h.

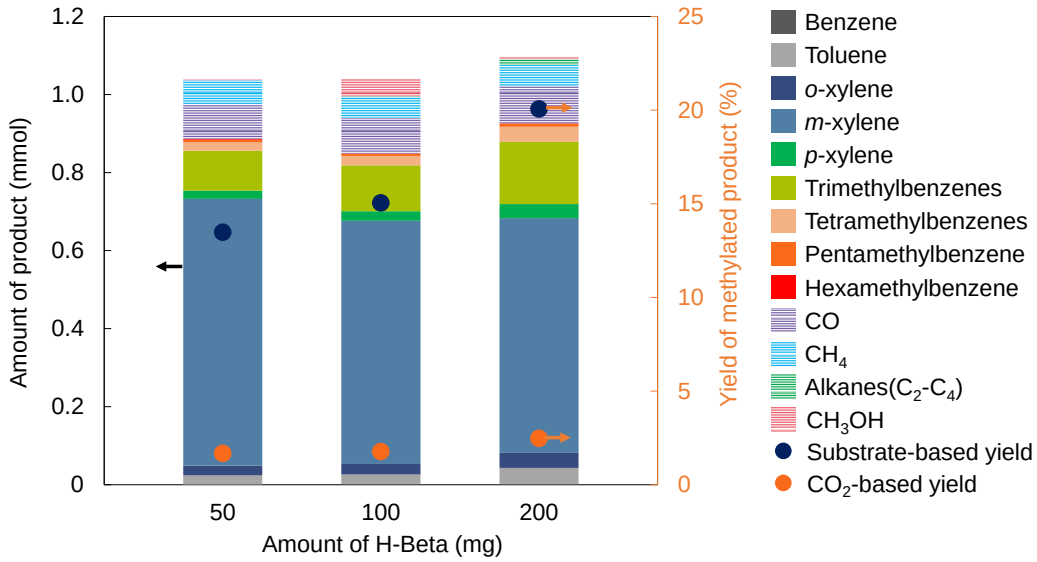

Figure 5. Effect of amount of H-Beta(40) on the catalytic methylation of *m*-xylene using CO_2 and H_2 over Re(1)/TiO_2. Pre-treatment: 500 °C, 0.5 h under flowing H_2 (20 mL min^{-1}); reaction conditions: 0.15 g of Re(1)/TiO_2 with *x* mg of H-Beta(40) (*x* = 50, 100 or 200), 1.0 mmol of *m*-xylene, CO_2 (1 MPa), H_2 (5 MPa), 240 °C, 1 h.

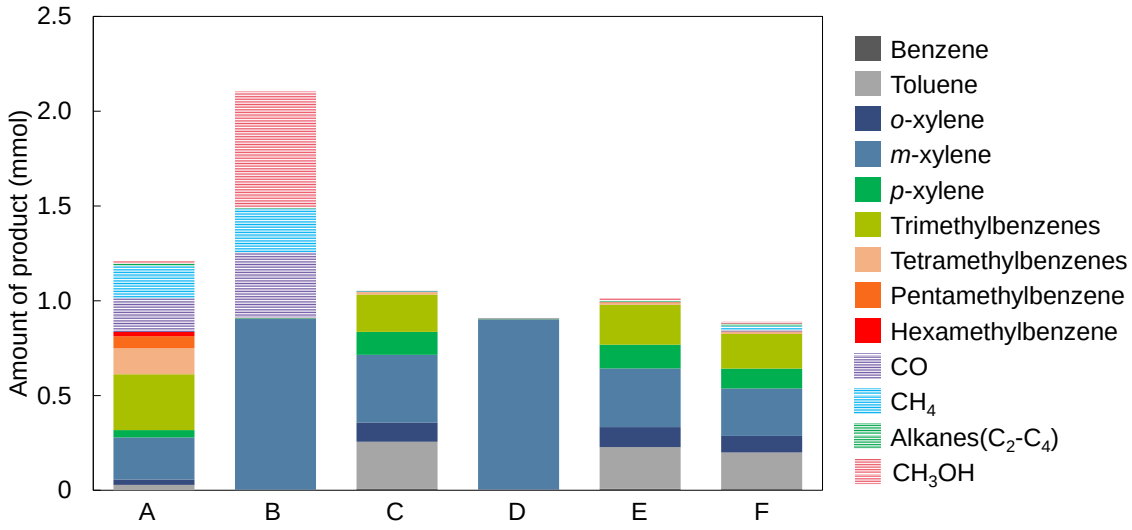

Figure 6. Control experiment for the catalytic methylation of *m*-xylene. Reaction conditions for each run are shown as follows. (A) 0.15 g of Re(1)/TiO_2 with 0.10 g of H-Beta(40), 1.0 mmol of *m*-xylene, CO_2 (1 MPa), H_2 (5 MPa). (B) 0.15 g of Re(1)/TiO_2, 1.0 mmol of *m*-xylene, CO_2 (1 MPa), H_2 (5 MPa). (C) 0.10 g of H-Beta(40), 1.0 mmol of *m*-xylene, CO_2 (1 MPa), H_2 (5 MPa). (D) 0.15 g of Re(1)/TiO_2, 1.0 mmol of *m*-xylene, N_2 (1 MPa). (E) 0.10 g of H-Beta(40), 1.0 mmol of *m*-xylene, N_2 (1 MPa). (F) 0.15 g of Re(1)/TiO_2 with 0.10 g of H-Beta(40), 1.0 mmol of *m*-xylene, N_2 (1 MPa). Pre-treatment: 500 °C, 0.5 h under flowing H_2 (20 mL min^{-1}). All reactions are carried out at 240 °C for 20 h.

3.3.2 Catalytic methylation of toluene

With the optimized catalyst system in hand, we proceeded with the methylation reaction by substituting *m*-xylene with toluene. Several selected hydrogenation catalysts combined with H-Beta(40) were tested for the methylation of toluene using CO_2 and H_2. The results generally follow the same trend as those for the methylation of *m*-xylene, with Re(1)/TiO_2 exhibiting the best performance (**Figure 7**). The performance of other catalysts was underwhelming, with low product yields and strong tendencies to form byproducts, as evident for Pd(1)/TiO_2 with its high yield of dearomatized product. Benchmark experiments identical to those of methylation of *m*-xylene were also conducted using Cu/ZnO/Al_2O_3 and Cu/ZrO_2. The methylation barely proceeded when lesser amount of catalysts (the same amount of loaded metal) was used, showing only limited conversion of toluene. When the amount of catalyst was increased to 0.15 g, high catalytic performances were observed in both catalysts. However, similar to the methylation of *m*-xylene, both of these benchmark catalysts were found to promote dearomatization. On the other hand, neither the formation of dearomatized product nor complete dealkylation to benzene was observed when Re(1)/TiO_2 was used, further cementing its position as a highly selective catalyst for this reaction.

The screening of zeolites was also conducted by pairing Re(1)/TiO_2 with various zeolite catalysts, as shown in **Figure 8**. H-Beta(40) exhibited the best performance, showing a high yield of methylated product with a relatively low amount of byproducts compared with the other zeolite catalysts. However, comparisons of H-Beta with different SiO_2/Al_2O_3 ratios showed that, in the kinetic region (reaction time = 1 h), H-Beta(510) displayed the greatest product formation rate when normalized by the number of protonic sites, as shown in **Figure 9**. This result is attributable to the fact that increasing the SiO_2/Al_2O_3 ratio enhanced the hydrophobic reaction between the zeolite pore surfaces and the substrate (in this case, toluene), thereby leading to a higher product formation rate when adjusted for the number of protonic sites.[53] The same trend was observed for the methylation of benzene using Re(1)/TiO_2 and H-MOR in our previous report.[38]

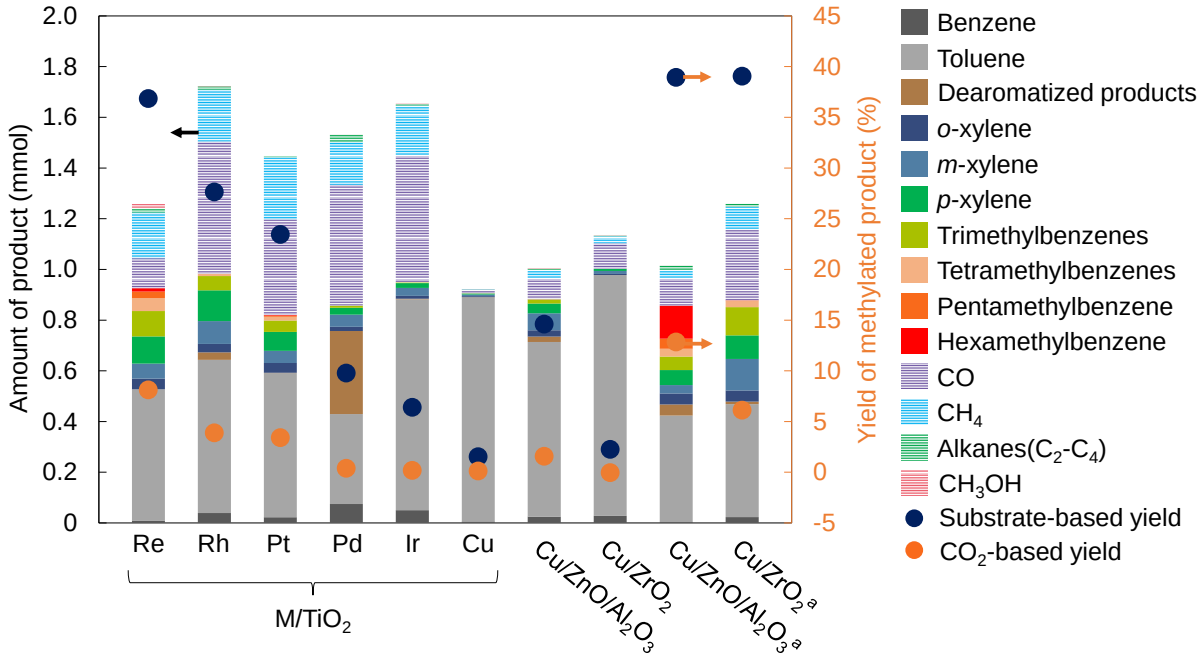

Figure 7. Evaluation of selected hydrogenation catalysts for the catalytic methylation of toluene using CO_2 and H_2. Pre-treatment: 500 °C, 0.5 h under flowing H_2 (20 mL min^{-1}); reaction conditions: 1 wt% of supported metal catalyst (mass adjusted to contain 0.0081 mmol of loaded metal per experiment) with 0.10 g of H-Beta(40), 1.0 mmol of toluene, CO_2 (1 MPa), H_2 (5 MPa), 240 °C, 20 h. [a]0.15 g of catalyst.

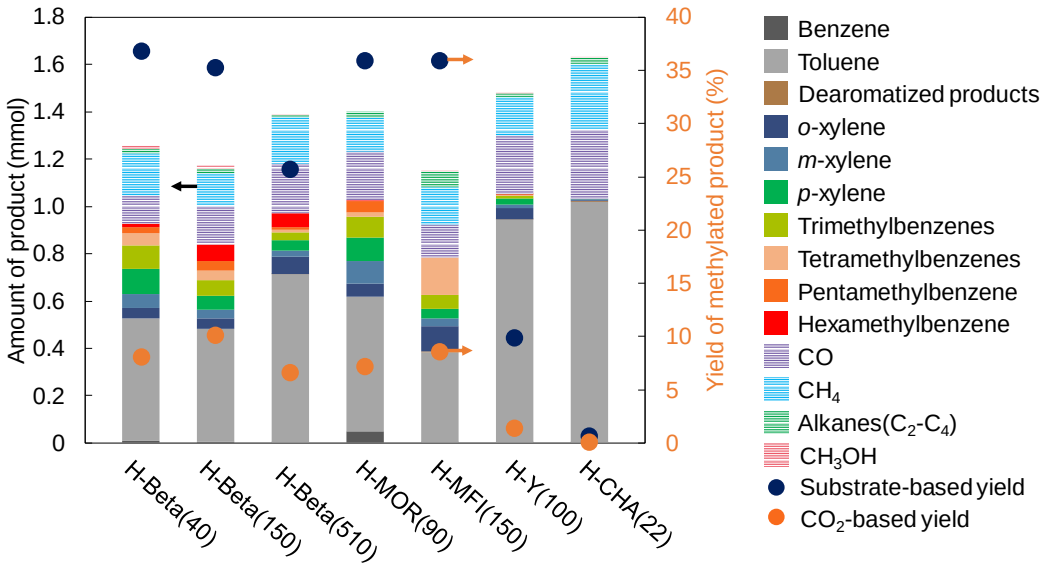

Figure 8. Screening of zeolite catalysts for the catalytic methylation of toluene using CO_2 and H_2. Pre-treatment: 500 °C, 0.5 h under flowing H_2 (20 mL min^{-1}); reaction conditions: 0.15 g of Re(1)/TiO_2 with 0.10 g of zeolite, 1.0 mmol of toluene, CO_2 (1 MPa), H_2 (5 MPa), 240 °C, 20 h.

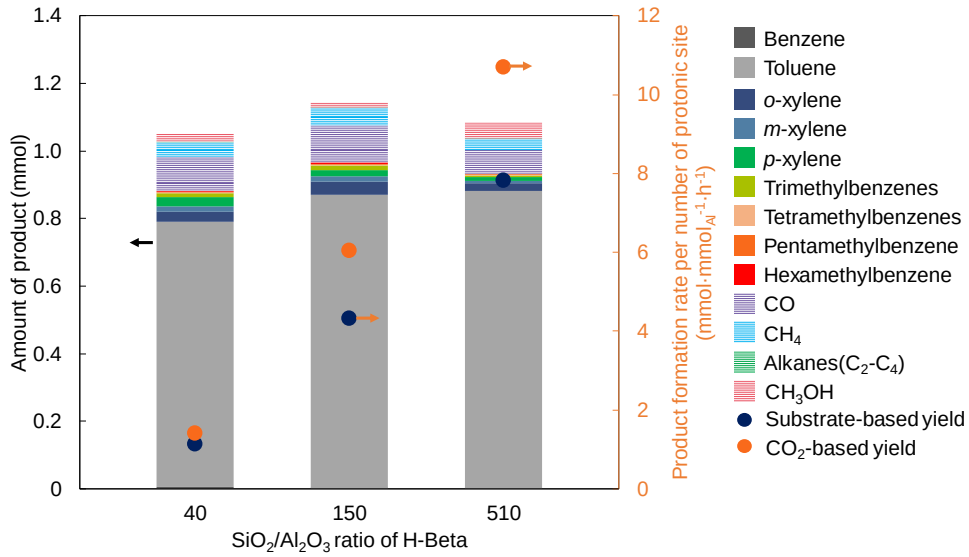

Figure 9. Effect of the SiO_2/Al_2O_3 ratio of H-Beta on the catalytic methylation of toluene using CO_2 and H_2. Pre-treatment: 500 °C, 0.5 h under flowing H_2 (20 mL min^{-1}); reaction conditions: 0.15 g of Re(1)/TiO_2 with 0.10 g of H-Beta, 1.0 mmol of toluene, CO_2 (1 MPa), H_2 (5 MPa), 240 °C, 1 h.

3.3.3 ML-assisted catalyst optimization

In recent years, ML has been gaining popularity in the molecular, materials science, and catalysis communities for use in high-throughput screening or for predicting various physical properties whose mathematical modeling involves complex principles.[54–59] ML methods can not only provide platforms for predictions but also aid in identifying input variables (descriptors) that are important for making predictions. However, despite the overwhelming expectations and future potential of ML, its use in heterogeneous catalysis research is still limited because of the complexity arising from the fact that catalysis is a multidimensional, multiscale, and dynamic event. Most of the previous ML research on heterogeneous catalysis has involved either literature data or theoretical values calculated using density functional theory. Because theoretical models for heterogeneous catalysis with reasonable computational costs are not currently available,[57,60] ML approaches using "real-world" experimental catalysis data, rather than models based on computationally derived (i.e., well-behaved) datasets, would be much more useful. Moreover, although literature data can serve as a rich resource of insightful information for catalyst discovery and design, such an approach is often difficult because sufficient information to describe the whole process has not always been reported. In this regard, statistical analysis based on ML should be carried out using experimental data obtained using the same (or comparable) experimental setup.

In the present study, we used ML techniques to analyze our experimental data related to the methylation of aromatic hydrocarbons using CO_2 and H_2. The data include not only results related to the methylation of *m*-xylene and toluene performed in the present study but also results of our previous work on the methylation of benzene and naphthalene.[38] The total number of datapoints was 328. The CO_2-based methylation rate (mmol g^{-1} h^{-1}) was predicted using descriptors such as the types of supported metals and supports for the hydrogenation catalysts, zeolite type, and various experimental conditions. Note that only controllable input variables were used as descriptors because we aimed to incorporate the obtained insights into our actual experiments. Our ML model based on XGB could predict the target value (CO_2-based methylation rate) with RMSE values of 0.013 mmol g^{-1} h^{-1} (training error) and 0.047 mmol g^{-1} h^{-1} (test error).

Feature importance scores represent the relative impact of an input value on the output value and thus provide useful insights into the underlying chemistry of a system. The feature scores were computed from the XGB model and are shown in **Figure 10A**. The reaction time, amount of hydrogenation catalyst, toluene as a starting substrate, and Re loading were identified as the most influential descriptors. In addition, the SHapley Additive exPlanations (SHAP: version 0.36.0) values[61,62] were also calculated and compared with the feature importance scores (**Figure 10B**). The SHAP approach, which is another method for identifying important variables, enables the identification and prioritization of descriptors and thus can be used to explain the contribution of a given input feature to the target (CO_2-based methylation rate) response. The most important descriptors were the reaction time, amount of hydrogenation catalyst, Re loading, and reaction temperature. The results are similar to those obtained using the feature importance score analysis, confirming the high reliability of the method.

We can also interpret the impact of each descriptor value on the predictions from the SHAP analysis. The most important descriptor, reaction time, negatively influences the CO_2-based methylation rate when it is increased. By contrast, the CO_2-based methylation rate increases with increasing amount of hydrogenation catalyst to some extent. Note that, although H-CHA(22) ranked relatively high, especially in the feature importance score analysis, it was found to negatively affect the methylation yield by the SHAP analysis. In-depth analyses using multiple approaches are necessary to avoid misinterpretations.

To visualize the marginal effect of the descriptor values on the predicted target (CO_2-based methylation rate) response, partial dependence plots (PDPs) were computed for the loading amount of Re, which is an important and controllable descriptor related to catalyst development, as shown in **Figure 11**. The obtained results show that the identified optimal loading amount of Re is in the range 1.2–1.8 wt%. On the basis of this ML analysis, Re/TiO_2 catalysts with an Re loading of 1.3 and 1.8 wt% were prepared (see **Figure 12** for STEM images of $Re(1.8)/TiO_2$ obtained using FEI Titan Cubed G2 60-300) and a series of Re/TiO_2 catalysts were tested for the methylation of benzene using CO_2 and H_2, as shown in **Figure 13**. H-MOR(90), which was found to be the best methylation catalyst for the benzene methylation in our previous study,[38] was used for this purpose. The newly prepared $Re(1.8)/TiO_2$ catalyst exhibited the highest activity among the investigated catalysts, substantially

surpassing the activity of the previously reported Re(1)/TiO_2 catalyst. The catalytic systems using Re/TiO_2 catalysts with a lower loading amount did not exhibit a high product formation rate. However, systems based on Re/TiO_2 catalysts with a higher Re loading were ineffective as hydrogenation catalysts because they generated more CH_4 as a byproduct. Therefore, 1.8 wt% was found to be the optimum Re loading for the current system. To further verify that Re(1.8)/TiO_2 is the superior catalyst, the performance of Re(1)/TiO_2 and Re(1.8)/TiO_2 for both catalytic methylation of *m*-xylene and toluene were investigated. As shown in **Figure 14**, Re(1.8)/TiO_2 outperforms Re(1)/TiO_2, showing overall improved yield and product selectivity, which is consistent with the prediction via ML. These results indicate that analyses such as feature importance analysis and PDPs as well as SHAP can serve as useful tools to identify and quantify important factors (descriptors) to unravel underlying chemical/physical principles and can be used in an efficient catalyst optimization procedure.

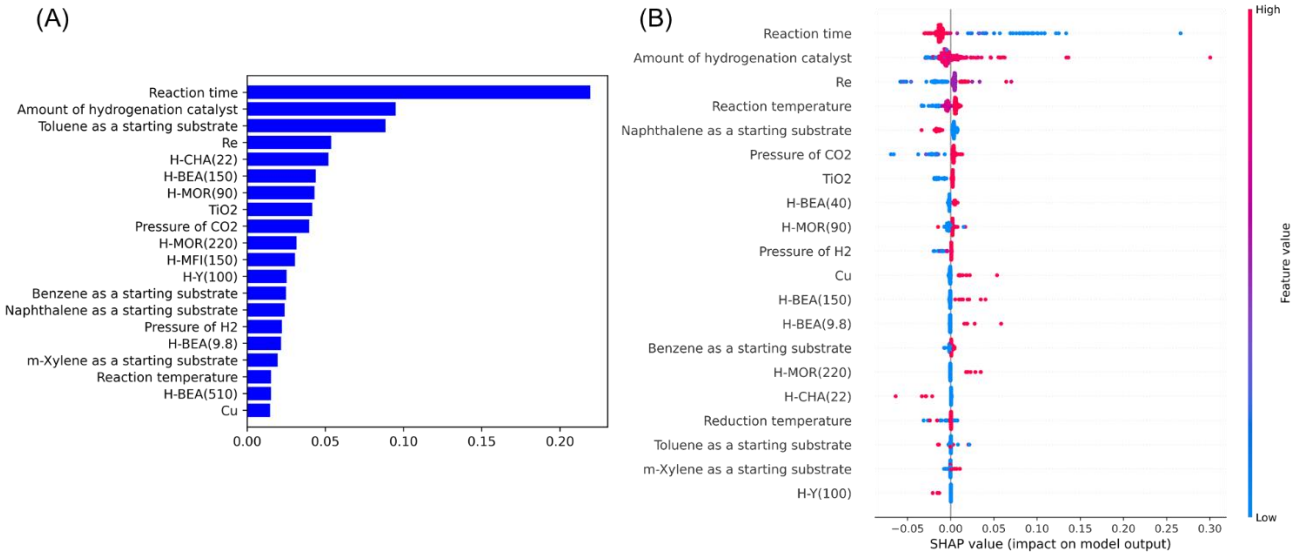

Figure 10. (A) Feature importance scores and **(B)** SHAP values of the 20 descriptors with the greatest contributions in predicting CO_2-based methylation rate using XGB.

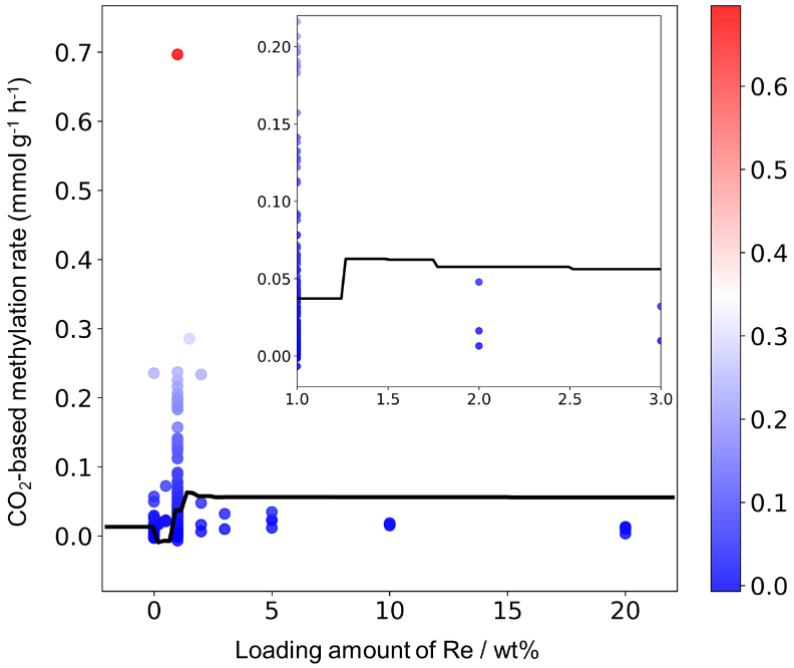

Figure 11. Partial dependence plot (PDP) showing the marginal effect of the loading amount of Re on the CO_2-based methylation rate for the XGB model. The lines correspond to PDPs; scatter plots of the actual values are also shown in the same figure. The inset shows an enlarged figure (Re loading of 1–3 wt%).

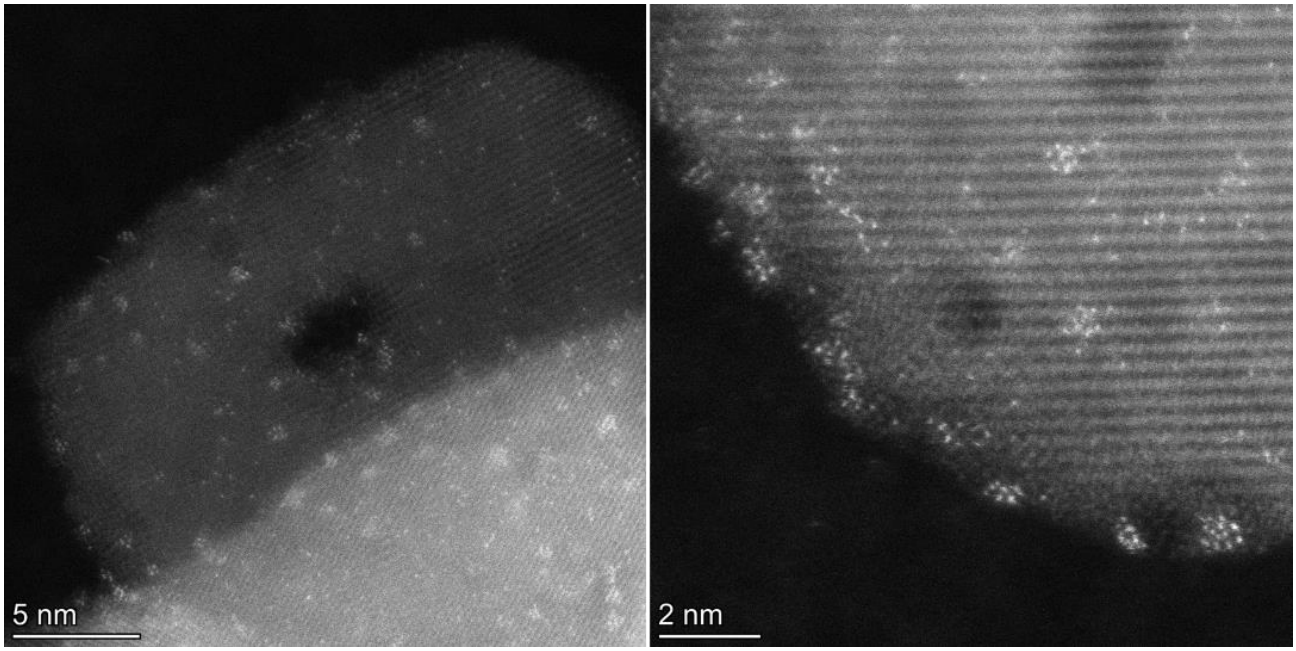

Figure 12. HAADF-STEM images of Re(1.8)/TiO_2.

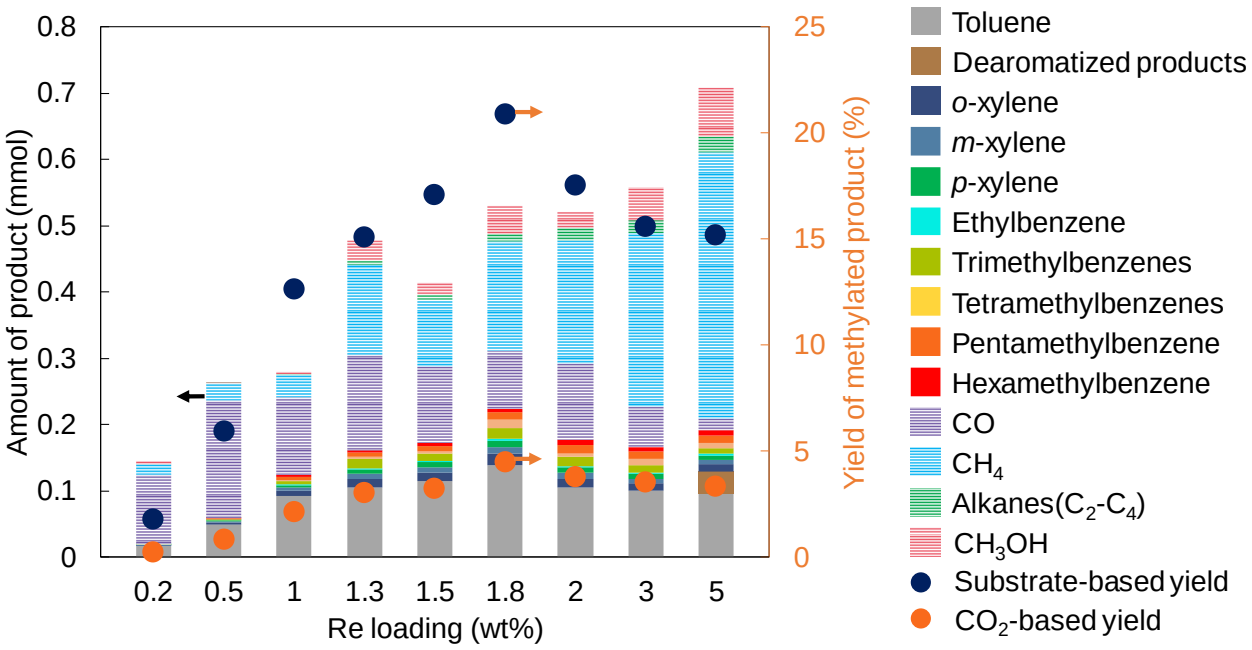

Figure 13. ML-directed optimization of the Re loading for the catalytic methylation of benzene. Pre-treatment: 500 °C, 0.5 h under flowing H_2 (20 mL min^{-1}); reaction conditions: 0.15 g of Re(*x*)/TiO_2 with 0.10 g of H-MOR(90), 1.0 mmol of benzene, CO_2 (1 MPa), H_2 (5 MPa), 250 °C, 1 h.

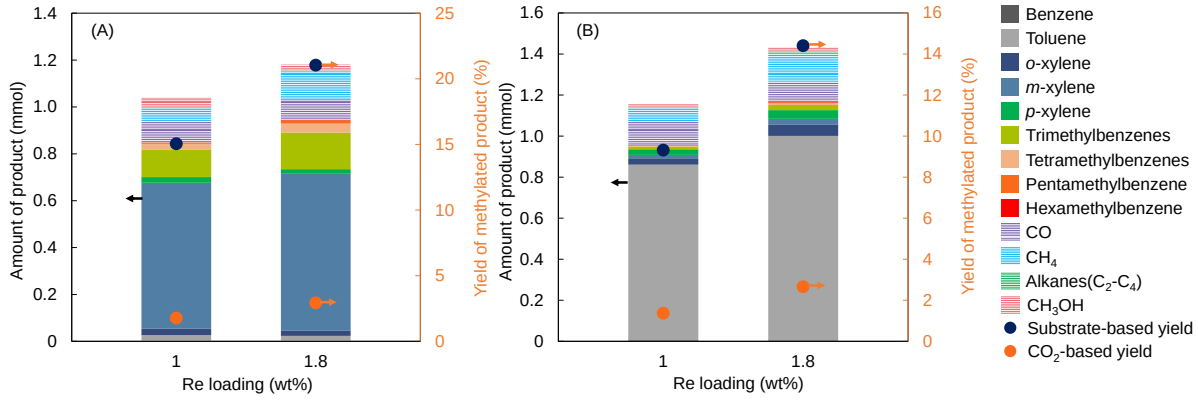

Figure 14. Comparisons of the performance of Re(1)/TiO_2 and Re(1.8)/TiO_2 for the catalytic methylation of (A) *m*-xylene, and (B) toluene using CO_2 and H_2. Pre-treatment: 500 °C, 0.5 h under flowing H_2 (20 mL min^{-1}); reaction conditions: 0.15 g of Re/TiO_2 with 0.10 g of H-Beta(40), 1.0 mmol of substrate, CO_2 (1 MPa), H_2 (5 MPa), 240 °C, 1 h.

3.4 Conclusion

In this work, the synthesis of methylated benzene derivatives via catalytic methylation of *m*-xylene using CO_2 and H_2 was demonstrated. Various combinations of hydrogenation catalysts and zeolites were tested and evaluated for this reaction. The combination of Re(1)/TiO_2 and H-Beta(40) exhibited the best performance, giving a relatively high yield and selectivity of methylated products. This catalyst system was also found to be compatible with the methylation of toluene under completely identical reaction conditions. In addition, ML approaches were used to analyze 328 experimental datapoints on the methylation of benzene, toluene, *m*-xylene, and naphthalene and to improve the performance of the catalytic methylation process. According to the PDP analysis based on the XGB prediction, among the investigated catalysts, the Re/TiO_2 catalyst with a Re loading amount of 1.8 wt% exhibited the best activity toward the methylation of benzene using CO_2/H_2.

3.5 References

(1) Gao, P.; Li, S.; Bu, X.; Dang, S.; Liu, Z.; Wang, H.; Zhong, L.; Qiu, M.; Yang, C.; Cai, J.; et al. Direct Conversion of CO_2 into Liquid Fuels with High Selectivity over a Bifunctional Catalyst. *Nat. Chem.* **2017**, *9*, 1019–1024.

(2) Vogt, C.; Monai, M.; Kramer, G. J.; Weckhuysen, B. M. The Renaissance of the Sabatier Reaction and Its Applications on Earth and in Space. *Nat. Catal.* **2019**, *2*, 188–197.

(3) Zhou, W.; Cheng, K.; Kang, J.; Zhou, C.; Subramanian, V.; Zhang, Q.; Wang, Y. New Horizon in C1 Chemistry: Breaking the Selectivity Limitation in Transformation of Syngas and Hydrogenation of CO_2 into Hydrocarbon Chemicals and Fuels. *Chem. Soc. Rev.* **2019**, *48*, 3193–3228.

(4) Bao, J.; Yang, G.; Yoneyama, Y.; Tsubaki, N. Significant Advances in C1 Catalysis: Highly Efficient Catalysts and Catalytic Reactions. *ACS Catal.* **2019**, *9*, 3026−3053.

(5) Vrijburg, W. L.; Moioli, E.; Chen, W.; Zhang, M.; Terlingen, B. J. P.; Zijlstra, B.; Filot, I. A. W.; Züttel, A.; Pidko, E. A.; Hensen, E. J. M. Efficient Base-Metal NiMn/TiO_2 Catalyst for CO_2 Methanation. *ACS Catal.* **2019**, *9*, 7823–7839.

(6) Ronda‐Lloret, M.; Rothenberg, G.; Shiju, N. R. A Critical Look at Direct Catalytic Hydrogenation of Carbon Dioxide to Olefins. *ChemSusChem* **2019**, *12*, 3896–3914.

(7) Sehested, J. Industrial and Scientific Directions of Methanol Catalyst Development. *J. Catal.* **2019**, *371*, 368–375.

(8) Xiaoding, X.; Moulijn, J. A. Mitigation of CO_2 by Chemical Conversion: Plausible Chemical Reactions and Promising Products. *Energy and Fuels* **1996**, *10*, 305–325.

(9) Saito, M.; Murata, K. Development of High Performance Cu/ZnO-Based Catalysts for Methanol Synthesis and the Water-Gas Shift Reaction. *Catal. Surv. from Asia* **2004**, *8*, 285–294.

(10) Rodriguez, J. A.; Liu, P.; Stacchiola, D. J.; Senanayake, S. D.; White, M. G.; Chen, J. G. Hydrogenation of CO_2 to Methanol: Importance of Metal-Oxide and Metal-Carbide Interfaces in the Activation of CO_2. *ACS Catal.* **2015**, *5*, 6696–6706.

(11) Natte, K.; Neumann, H.; Beller, M.; Jagadeesh, R. V. Transition-Metal-Catalyzed Utilization of Methanol as a C1 Source in Organic Synthesis. *Angew. Chemie - Int. Ed.* **2017**, *56*, 6384–6394.

(12) Álvarez, A.; Bansode, A.; Urakawa, A.; Bavykina, A. V.; Wezendonk, T. A.; Makkee, M.; Gascon, J.; Kapteijn, F. Challenges in the Greener Production of Formates/Formic Acid,

Methanol, and DME by Heterogeneously Catalyzed CO_2 Hydrogenation Processes. *Chem. Rev.* **2017**, *117*, 9804–9838.

(13) Jiang, X.; Nie, X.; Guo, X.; Song, C.; Chen, J. G. Recent Advances in Carbon Dioxide Hydrogenation to Methanol via Heterogeneous Catalysis. *Chem. Rev.* **2020**, *15*, 7984–8034.

(14) Zhong, J.; Yang, X.; Wu, Z.; Liang, B.; Huang, Y.; Zhang, T. State of the Art and Perspectives in Heterogeneous Catalysis of CO_2 Hydrogenation to Methanol. *Chem. Soc. Rev.* **2020**, *49*, 1385–1413.

(15) Tian, P.; Wei, Y.; Ye, M.; Liu, Z. Methanol to Olefins (MTO): From Fundamentals to Commercialization. *ACS Catal.* **2015**, *5*, 1922−1938.

(16) Yarulina, I.; Chowdhury, A. D.; Meirer, F.; Weckhuysen, B. M.; Gascon, J. Recent Trends and Fundamental Insights in the Methanol-to-Hydrocarbons Process. *Nat. Catal.* **2018**, *1*, 398–411.

(17) Artz, J.; Müller, T. E.; Thenert, K.; Kleinekorte, J.; Meys, R.; Sternberg, A.; Bardow, A.; Leitner, W. Sustainable Conversion of Carbon Dioxide: An Integrated Review of Catalysis and Life Cycle Assessment. *Chem. Rev.* **2018**, *118*, 434–504.

(18) Gaikwad, R.; Bansode, A.; Urakawa, A. High-Pressure Advantages in Stoichiometric Hydrogenation of Carbon Dioxide to Methanol. *J. Catal.* **2016**, *343*, 127–132.

(19) Porosoff, M. D.; Yan, B.; Chen, J. G. Catalytic Reduction of CO_2 by H_2 for Synthesis of CO, Methanol and Hydrocarbons: Challenges and Opportunities. *Energy Environ. Sci.* **2016**, *9*, 62–73.

(20) Kuei, C.; Lee, M. Hydrogenation of Carbon Dioxide by Hybrid Catalysts, Direct Synthesis of Aromatics from Carbon Dioxide and Hydrogen. *Can. J. Chem. Eng.* **1991**, *69*, 347–354.

(21) Ni, Y.; Chen, Z.; Fu, Y.; Liu, Y.; Zhu, W.; Liu, Z. Selective Conversion of CO_2 and H_2 into Aromatics. *Nat. Commun.* **2018**, *9*, 3457.

(22) Wang, Y.; Tan, L.; Tan, M.; Zhang, P.; Fang, Y.; Yoneyama, Y.; Yang, G.; Tsubaki, N. Rationally Designing Bifunctional Catalysts as an Efficient Strategy to Boost CO_2 Hydrogenation Producing Value-Added Aromatics. *ACS Catal.* **2019**, *9*, 895−901.

(23) Cui, X.; Gao, P.; Li, S.; Yang, C.; Liu, Z.; Wang, H.; Zhong, L.; Sun, Y. Selective Production of Aromatics Directly from Carbon Dioxide Hydrogenation. *ACS Catal.* **2019**, *9*, 3866–3876.

(24) Zhang, J.; Zhang, M.; Chen, S.; Wang, X.; Zhou, Z.; Wu, Y.; Zhang, T.; Yang, G.; Han, Y.; Tan, Y. Hydrogenation of CO_2 into Aromatics over a ZnCrOx-Zeolite Composite Catalyst. *Chem. Commun.* **2019**, *55*, 973–976.

(25) Xu, Y.; Shi, C.; Liu, B.; Wang, T.; Zheng, J.; Li, W.; Liu, D.; Liu, X. Selective Production of Aromatics from CO_2. *Catal. Sci. Technol.* **2019**, *9*, 593–610.

(26) Li, Z.; Qu, Y.; Wang, J.; Liu, H.; Li, M.; Miao, S.; Li, C. Highly Selective Conversion of Carbon Dioxide to Aromatics over Tandem Catalysts. *Joule* **2019**, *3*, 570–583.

(27) Wang, Y.; Kazumi, S.; Gao, W.; Gao, X.; Li, H.; Guo, X.; Yoneyama, Y.; Yang, G.; Tsubaki, N. Direct Conversion of CO_2 to Aromatics with High Yield via a Modified Fischer-Tropsch Synthesis Pathway. *Appl. Catal. B Environ.* **2020**, *269*, 118792.

(28) Zhou, C.; Shi, J.; Zhou, W.; Cheng, K.; Zhang, Q.; Kang, J.; Wang, Y. Highly Active ZnO-ZrO_2 Aerogels Integrated with H-ZSM-5 for Aromatics Synthesis from Carbon Dioxide. *ACS Catal.* **2020**, *10*, 302−310.

(29) Cabrero-Antonino, J. R.; Adam, R.; Beller, M. Catalytic Reductive N-Alkylations Using CO_2 and Carboxylic Acid Derivatives: Recent Progress and Developments. *Angew. Chemie - Int. Ed.* **2019**, *58*, 12820–12838.

(30) Gredig, S. V; Koeppel, R.; Baiker, A. Comparative Study of Synthesis of Methylamines from Carbon Oxides and Ammonia over Cu/Al_2O_3. *Catal. Today* **1996**, *29*, 339–342.

(31) Gredig, S. V.; Koeppel, R. A.; Baiker, A. Synthesis of Methylamines from Carbon Dioxide and Ammonia. *J. Chem. Soc. Chem. Commun.* **1995**, *46*, 73–74.

(32) Auer, S. M.; Gredig, S. V.; Köppel, R. A.; Baiker, A. Synthesis of Methylamines from CO_2, H_2 and NH_3 over Cu-Mg-Al Mixed Oxides. *J. Mol. Catal. A Chem.* **1999**, *141*, 193–203.

(33) Beydoun, K.; Thenert, K.; Streng, E. S.; Brosinski, S.; Leitner, W.; Klankermayer, J. Selective Synthesis of Trimethylamine by Catalytic N-Methylation of Ammonia and Ammonium Chloride by Utilizing Carbon Dioxide and Molecular Hydrogen. *ChemCatChem* **2016**, *8*, 135–138.

(34) Toyao, T.; Siddiki, S. M. A. H.; Morita, Y.; Kamachi, T.; Touchy, A. S.; Onodera, W.; Kon, K.; Furukawa, S.; Ariga, H.; Asakura, K.; et al. Rhenium-Loaded TiO_2: A Highly Versatile and Chemoselective Catalyst for the Hydrogenation of Carboxylic Acid Derivatives and the N-Methylation of Amines Using H_2 and CO_2. *Chem. - A Eur. J.* **2017**, *23*, 14848–14859.

(35) Tlili, A.; Frogneux, X.; Blondiaux, E.; Cantat, T. Creating Added Value with a Waste: Methylation of Amines with CO_2 and H_2. *Angew. Chemie - Int. Ed.* **2014**, *53*, 2543–2545.

(36) Toyao, T.; Siddiki, S. M. A. H.; Ishihara, K.; Kon, K.; Onodera, W.; Shimizu, K. Heterogeneous Platinum Catalysts for Direct Synthesis of Trimethylamine by N-Methylation of Ammonia and Its Surrogates with CO_2/H_2. *Chem. Lett.* **2017**, *46*, 68–70.

(37) Li, Y.; Yan, T.; Junge, K.; Beller, M. Catalytic Methylation of C-H Bonds Using CO_2 and H_2. *Angew. Chemie - Int. Ed.* **2014**, *53*, 10476–10480.

(38) Ting, K. W.; Kamakura, H.; Poly, S.; Toyao, T.; Siddiki, S. M. A. H.; Maeno, Z.; Matsushita, K.; Shimizu, K. Catalytic Methylation of Aromatic Hydrocarbons Using CO_2/H_2 over Re/TiO_2 and H‐MOR Catalysts. *ChemCatChem* **2020**, *12*, 2215–2220.

(39) Fujita, S.; Hiyoshi, N.; Takezawa, N. Vapor Phase Methylation of Pyridine with $CO\text{-}H_2$ over Metal Catalysts. *Appl. Catal. A Gen.* **1999**, *185*, 323–327.

(40) Lee, S.; Kim, D.; Lee, J.; Choi, Y.; Suh, Y. W.; Lee, C.; Kim, T. J.; Lee, S. J.; Lee, J. K. An in Situ Methylation of Toluene Using Syngas over Bifunctional Mixture of Cr_2O_3/ZnO and HZSM-5. *Appl. Catal. A Gen.* **2013**, *466*, 90–97.

(41) Zhao, X.; Zeng, F.; Zhao, B.; Gu, H. Alkylation Activity of Benzene with Syngas over Cu-Based Catalysts. *China Pet. Process. Petrochemical Technol.* **2015**, *17*, 31–38.

(42) Bai, Y.; Yang, F.; Liu, X.; Liu, C.; Zhu, X. Performance of Bifunctional ZnZr/ZSM-5 Catalysts in the Alkylation of Benzene with Syngas. *Catal. Letters* **2018**, *148*, 3618–3627.

(43) Nakamura, K.; Okuda, A.; Ohta, K.; Matsubara, H.; Okumura, K.; Yamamoto, K.; Itagaki, R.; Suganuma, S.; Tsuji, E.; Katada, N. Direct Methylation of Benzene with Methane Catalyzed by Co/MFI Zeolite. *ChemCatChem* **2018**, *10*, 3806–3812.

(44) Zuo, J.; Chen, W.; Liu, J.; Duan, X.; Ye, L.; Yuan, Y. Selective Methylation of Toluene Using CO_2 and H_2 to Para-Xylene. *Sci. Adv.* **2020**, *6*, eaba5433.

(45) Volanti, M.; Cespi, D.; Passarini, F.; Neri, E.; Cavani, F.; Mizsey, P.; Fozer, D. Terephthalic Acid from Renewable Sources: Early-Stage Sustainability Analysis of a Bio-PET Precursor. *Green Chem.* **2019**, *21*, 885–896.

(46) Degnan, T. F. The Implications of the Fundamentals of Shape Selectivity for the Development of Catalysts for the Petroleum and Petrochemical Industries. *J. Catal.* **2003**, *216*, 32–46.

(47) Niziolek, A. M.; Onel, O.; Floudas, C. A. Production of Benzene, Toluene, and Xylenes from Natural Gas via Methanol: Process Synthesis and Global Optimization. *AIChE J.* **2016**, *62*, 1531–1556.

(48) Tada, S.; Kayamori, S.; Honma, T.; Kamei, H.; Nariyuki, A.; Kon, K.; Toyao, T.; Shimizu, K. I.; Satokawa, S. Design of Interfacial Sites between Cu and Amorphous ZrO_2 Dedicated to CO_2-to-Methanol Hydrogenation. *ACS Catal.* **2018**, *8*, 7809–7819.

(49) Pedregosa, F.; Varoquaux, G. Scikit-Learn: Machine Learning in Python. *J. Mach. Learn. Res* **2011**, *12*, 2825–2830.

(50) Suzuki, K.; Toyao, T.; Maeno, Z.; Takakusagi, S.; Shimizu, K.; Takigawa, I. Statistical Analysis and Discovery of Heterogeneous Catalysts Based on Machine Learning from Diverse Published Data. *ChemCatChem* **2019**, *11*, 4537–4547.

(51) Toyao, T.; Ting, K. W.; Siddiki, S. M. A. H.; Touchy, A. S.; Onodera, W.; Maeno, Z.; Ariga-Miwa, H.; Kanda, Y.; Asakura, K.; Shimizu, K. ichi. Mechanistic Study of the Selective Hydrogenation of Carboxylic Acid Derivatives over Supported Rhenium Catalysts. *Catal. Sci. Technol.* **2019**, *9*, 5413–5424.

(52) Ting, K. W.; Toyao, T.; Siddiki, S. M. A. H.; Shimizu, K. Low-Temperature Hydrogenation of CO_2 to Methanol over Heterogeneous TiO_2-Supported Re Catalysts. *ACS Catal.* **2019**, *9*, 3685–3693.

(53) Sultana Poly, S.; Hakim Siddiki, S. M. A.; Touchy, A. S.; Yasumura, S.; Toyao, T.; Maeno, Z.; Shimizu, K. High-Silica Hβ Zeolites for Catalytic Hydration of Hydrophobic Epoxides and Alkynes in Water. *J. Catal.* **2018**, *368*, 145–154.

(54) Ras, E. J.; Rothenberg, G. Heterogeneous Catalyst Discovery Using 21st Century Tools: A Tutorial. *RSC Adv.* **2014**, *4*, 5963–5974.

(55) Goldsmith, B. R.; Esterhuizen, J.; Liu, J.-X.; Bartel, C. J.; Sutton, C. Machine Learning for Heterogeneous Catalyst Design and Discovery. *AIChE J.* **2018**, *64*, 2311–2323.

(56) Takahashi, K.; Takahashi, L.; Miyazato, I.; Fujima, J.; Tanaka, Y.; Uno, T.; Satoh, H.; Ohno, K.; Nishida, M.; Hirai, K.; et al. The Rise of Catalyst Informatics: Towards Catalyst Genomics. *ChemCatChem* **2019**, *11*, 1146–1152.

(57) Lamoureux, P. S.; Winther, K.; Garrido Torres, J. A.; Streibel, V.; Zhao, M.; Bajdich, M.; Abild-Pedersen, F.; Bligaard, T. Machine Learning for Computational Heterogeneous Catalysis. *ChemCatChem* **2019**, *11*, 3581–3601.

(58) Toyao, T.; Maeno, Z.; Takakusagi, S.; Kamachi, T.; Takigawa, I.; Shimizu, K. Machine Learning for Catalysis Informatics: Recent Applications and Prospects. *ACS Catal.* **2020**, *10*, 2260–2297.

(59) Ma, S.; Liu, Z.-P. Machine Learning for Atomic Simulation and Activity Prediction in Heterogeneous Catalysis: Current Status and Future. *ACS Catal.* **2020**, *10*, 13213−13226.

(60) Grajciar, L.; Heard, C. J.; Bondarenko, A. A.; Polynski, M. V.; Meeprasert, J.; Pidko, E. A.; Nachtigall, P. Towards Operando Computational Modeling in Heterogeneous Catalysis. *Chem. Soc. Rev.* **2018**, *47*, 8307–8348.

(61) Lundberg, S. M.; Lee, S. I. A Unified Approach to Interpreting Model Predictions. *Advances in Neural Information Processing Systems*; 2017; pp 4765–4774.

(62) Lundberg, S. M.; Erion, G.; Chen, H.; DeGrave, A.; Prutkin, J. M.; Nair, B.; Katz, R.; Himmelfarb, J.; Bansal, N.; Lee, S.-I. From Local Explanations to Global Understanding with Explainable AI for Trees. *Nat. Mach. Intell.* **2020**, *2*, 56–67.

Chapter 4

Experimental and Theoretical Investigation of Metal−Support Interactions in Metal-Oxide-Supported Rhenium Materials

4.1 Introduction

The interactions between metals and oxide supports have been extensively studied, but the nature of such interactions often remain a matter of debate in the field of heterogeneous catalysis.[1–5] Metal−support interactions (MSIs) influence the behavior of a catalyst by changing the properties of the metal, its interface, and its perimeter sites.[6–10] The nature of the active sites created by the metal−support environment can be affected by the size, shape, and degree of dispersion of the metal species.[11–15] The MSI also affects the resistance of the metal to sintering, a process that often leads to the deactivation of a catalyst.[16–20] Therefore, understanding how MSIs behave depending on the metal and oxide used is essential for tailoring the activity, selectivity, and stability of oxide-supported metal catalysts.[21–25]

Recent efforts that take advantage of both experimental and computational approaches have shown that the degree of dispersion of a supported metal is governed by the binding energy of the metal atom to the oxide surface.[26–31] Metals that bind strongly to oxide supports are less likely to diffuse over the support surface, and as a consequence, show a high degree of dispersion. Likewise, oxides that bind strongly to the supported metals tend to have dispersed metal species on their surfaces. In order to better understand MSIs, a few simple descriptors based on the fundamental physical properties of the metal atoms and their supports need to be identified. It has been demonstrated that a linear scaling relationship exists between the metal adsorption energy (E_{ads}) and metal−support pair properties, such as the chemical potential of the metal,[32,33] the metal oxidation enthalpy,[34] the heat of formation of metal oxide,[35] the reducibility of the support,[36,37] and the oxide support band gaps.[38] Janik, Senftle, and co-workers employed density functional theory (DFT) to investigate the properties of single adatoms and oxide supports that influence MSIs. They confirmed that the interfacial binding strength is correlated to the physical properties of both the supported metal (e.g., the oxophilicity as measured via the oxide-formation energy) and the oxide support (e.g., the reducibility as measured via the oxygen-vacancy-formation energy).[39] However, despite much research and intensive efforts to elucidate MSIs, a comprehensive understanding of the interaction strength between metal–support pairs is still yet to be obtained. In particular, there are insufficient studies that analyze the trends between electronic structures and experimental observations.

In the present study, a systematic investigation is conducted with the aim of describing the MSIs between Re and oxide supports such as TiO_2, SiO_2, Al_2O_3, MgO, V_2O_5, ZrO_2, Nb_2O_5, and CeO_2. Re was chosen because supported Re catalysts efficiently promote a number of valuable reductive catalytic processes,[40–47] including the hydrogenation of both carboxylic-acid derivatives[48–53] and CO_2.[54–59] Additionally, the excellent catalytic properties of supported Re catalysts are often ascribed to the high dispersion of Re on its oxide support.[60–64] Re (5 wt%) was supported on the oxides listed above and the degree of dispersion of the Re species was compared. In addition to the experimental investigation, computational approaches based on DFT were employed to further understand the origin of the MSIs.

4.2 Experimental section

4.2.1 Materials and catalyst preparation

Anatase TiO_2 (ST-01, 188 $m^2\ g^{-1}$), also known as JRC-TIO-8, was obtained from Ishihara Sangyo, while rutile TiO_2 (JRC-TIO-5: 3 $m^2\ g^{-1}$) was obtained from the Catalysis Society of Japan. SiO_2 (CARiACT Q-10, 300 $m^2\ g^{-1}$) was purchased from Fuji Silysia Chemicals. Al_2O_3 (74 $m^2\ g^{-1}$) was prepared by calcination of boehmite (Catapal B Alumina, Sasol) for 3 h at 900 °C. MgO (JRC-MGO-3-500A, 24 $m^2\ g^{-1}$) and ZrO_2 (JRC-ZRO-5, 194 $m^2\ g^{-1}$) were provided by the Catalysis Society of Japan. V_2O_5 (3 $m^2\ g^{-1}$) was purchased from Sigma-Aldrich. Nb_2O_5 (83 $m^2\ g^{-1}$) was prepared by calcination (500 °C, 3 h) of niobic acid ($Nb_2O_5{\cdot}nH_2O$, HY-340) obtained from Companhia Brasileira de Metalurgia e Mineração (CBMM). CeO_2 (69 $m^2\ g^{-1}$) was prepared by calcination (3 h at 600 °C in air) of CeO_2 (Type A) obtained from Daiichi Kigenso Kagaku.

The Re(5)/support (5 wt% Re) samples were prepared using a simple wet impregnation method by mixing the support material with an aqueous solution of NH_4ReO_4 (Sigma-Aldrich). Typically, 0.36 g of NH_4ReO_4 was added to a glass vessel (500 mL) containing 400 mL of deionized water. After complete dissolution of the NH_4ReO_4 was accomplished via stirring, 4.75 g of the support material was added to the solution, followed by stirring at 200 rpm for 30 min at room temperature. Subsequently, the water was removed from the reaction mixture via evaporation *in vacuo*, followed by drying at 110 °C under ambient pressure for 12 h. The resulting material was calcined for 3 h at 500 °C in air, except for Re(5)/V_2O_5, where the calcination step was omitted to prevent sublimation of the Re species. The amount of Re species contained in the samples were quantified by x-ray fluorescence spectroscopy (XRF; Shimadzu EDX-700 instrument) measurements, and it was confirmed that the amount of Re species supported was almost equal to the amount used for the preparation. Finally, the sample for analysis was prepared via reduction under a flow of H_2 (20 mL min^{-1}) at 500 °C for 0.5 h.

4.2.2 Catalyst characterization and computational methods

X-ray diffraction (XRD) measurements were carried out using a Miniflex 300 (Rigaku) with CuKα radiation. Scanning transmission electron microscopy (STEM) observations were conducted using JEM-ARM200F and FEI Titan G2 electron microscopes.

Periodic DFT calculations were performed using the Vienna ab initio simulation package (VASP, version 5.4.4).[65,66] The Perdew-Burke-Ernzerhof functional revised for solids (PBEsol)[67] was employed in combination with the projector-augmented wave (PAW) method.[68] A kinetic energy cutoff of 400 eV was set for the plane-wave basis sets. Gaussian smearing with a width of 0.2 eV was applied for the occupation of the electronic levels. The Brillouin zone was sampled using Monkhorst-Pack grids of 2×2×1. Van der Waals interactions were described using the dispersion-corrected DFT-D3 (BJ) function.[69] The convergence of force on each atom was set to 0.03 eV $Å^{-1}$.

The surfaces of the metal oxides including MgO(010), θ-Al_2O_3(100), $ZrO_2(11\bar{1})$, CeO_2(111), β-Ga_2O_3(100), anatase TiO_2(101), and V_2O_5(010), were simulated using supercell slab models (**Figure 1**). The repeated slabs along the surface normal direction were separated by a minimum vacuum region thickness of 15 Å. The bottom two layers were fixed at their original bulk positions. The effect of adding Hubbard U was additionally considered based on Dudarev's formulation.[70] The effective U value (denoted as U_{eff}) of $U - J$ was set to be 5 eV for Ce, and 3 eV for Ti, Zr, and V.[71] Moreover, energy calculations using the one-shot HSE06 (Heyd–Scuseria–Ernzerhof) hybrid functional[72,73] were performed with the structure optimized at the GGA(+U) level. The adsorption energy (E_{ads}) of a Re atom on a metal oxide surface is defined as:

$$E_{ads} = E_{A/S} - E_A - E_S$$

where $E_{A/S}$, E_A, and E_S are the electronic energies of the adsorption complex, the free-state adsorbate, and the bare metal-oxide surface, respectively. Also, the differential charge density ($\Delta\rho$) of the supported Re is defined as:

$$\Delta\rho = \rho_{A/S} - \rho_A - \rho_S$$

where $\rho_{A/S}$, ρ_A, and ρ_S are the charge density of the adsorption complex, the free-state adsorbate, and the bare metal-oxide surface, respectively. A Bader-charge analysis was also performed to evaluate the valence state of Re on the surfaces of the metal oxides.

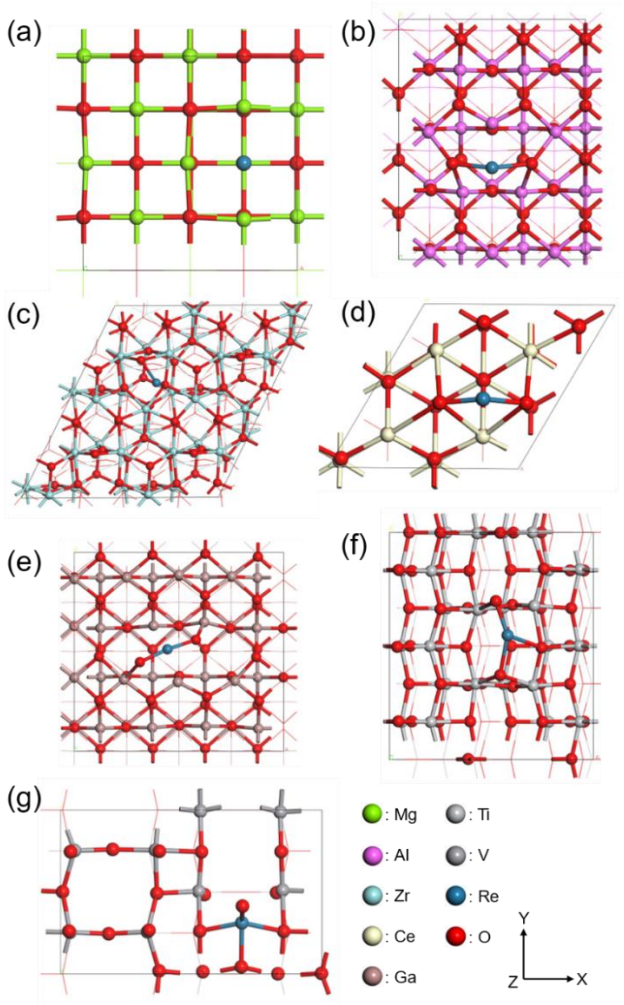

Figure 1. Top views of the slab models used for DFT calculations of the Re adatom on the metal oxide surfaces of (a) MgO(010), (b) θ-Al_2O_3(100), (c) $ZrO_2(11\bar{1})$, (d) CeO_2(111), (e) β-Ga_2O_3(100), (f) anatase TiO_2(101), and (g) V_2O_5(010).

4.3 Results and discussion

4.3.1 XRD and STEM studies

A series of supported Re samples were characterized using XRD and STEM analysis. It should be noted that the samples were exposed to air before the measurements due to the experimental setup. The XRD patterns measured for each sample after H_2 reduction at 500 °C are shown in **Figure 2**. Peaks arising from the metallic Re species, represented using dots, were detected in all samples with the exception of Re(5)/CeO_2, Re(5)/Nb_2O_5, and Re(5)/V_2O_5. This possibly indicates that large Re crystallites that can be detected via XRD are present in Re(5)/SiO_2, Re(5)/TiO_2, Re(5)/Al_2O_3, Re(5)/MgO, and Re(5)/ZrO_2. Peaks arising from the Re species were most pronounced in the Re(5)/SiO_2 XRD pattern, indicating the presence of large Re crystallites. In contrast, only a single Re peak with a significantly lower intensity was observed in the XRD patterns of Re(5)/TiO_2, Re(5)/Al_2O_3, Re(5)/MgO, and Re(5)/ZrO_2, suggesting that the Re in these samples is present in a quantity small enough that it can barely be detected using XRD. It should also be noted here that interference arising from peaks associated with the supports makes identification of the Re peaks difficult and this could be another reason that peaks for the Re species were not observed in patterns for some of the samples. For instance, the most intense peak observed for the crystalline metallic Re at ~43° overlaps with the peaks that arise from supports such as Al_2O_3, V_2O_5, and MgO. In contrast, SiO_2 is amorphous and there was no interference from peaks associated with SiO_2, thus the Re peaks are easily distinguishable. It is furthermore noteworthy that, even though the samples had been exposed to air prior to the measurements, only peaks arising from metallic Re were observed in the XRD patterns and that peaks that could potentially be ascribed to the presence of Re-oxide species were not observed.

High-angle annular dark-field STEM (HAADF-STEM) images and the corresponding particle-size distributions for each sample are shown in **Figures 3** and **4**, respectively. Herein, we will henceforth refer to atomically dispersed Re atoms as a single Re atom[74,75] and to Re species that consist of two to nine Re atoms as sub-nanoclusters. Re clusters/nanoparticles that consist of more than ten atoms were categorized according to their sizes: 0.5-2 nm, 2-4 nm, and >4 nm. Please note that this classification is based on the number of such species including nanoclusters/nanoparticles, and thus, for example, one single Re atom is counted

equally often as one large nanoparticle although the numbers of each constituent Re atom are significantly different. Single-atom Re species were observed in every sample, where they often are the dominant species with the highest fraction in terms of their number. The particle-size distributions show that the presence of larger Re particles (>2 nm) was most prevalent in the Re(5)/SiO_2, Re(5)/Al_2O_3, and Re(5)/MgO samples (**Figure 4**). The Re species on SiO_2 are the most highly aggregated, showing a significantly higher fraction, higher than any other sample, of Re nanoparticles larger than 2 nm. Re(5)/MgO shows a relatively high fraction of single atoms according to the classification employed, i.e., based on the number of the species. However, significantly aggregated Re species with a particle size of >4 nm was also present. Although it is difficult to quantify the number of Re atoms in the aggregated nanoparticles, this result suggests that most of the Re atoms in the sample are aggregated to form large particles. Although no large Re species were observed (>2 nm) in either the Re(5)/TiO_2 or the Re(5)/ZrO_2 samples, these samples have a slightly lower fraction of single-atom Re species. The formation of these relatively large Re nanoparticles on TiO_2 and ZrO_2 can be detected in their XRD patterns via the presence of a Re peak. These findings are consistent with our previous STEM and (*in situ*) XRD and X-ray absorption spectroscopy (XAS) studies on these Re(5)/support (support = TiO_2, Al_2O_3, and SiO_2) samples.[57,64] In those previous studies, Re(5)/SiO_2 was found to have the most highly aggregated Re species of the three samples with a coordination number (CN) of 10.4 for the Re–Re shell.[64] We also found that the extended X-ray absorption fine structures (EXAFS) of Re(5)/TiO_2 and Re(5)/Al_2O_3 contain features associated with both Re–O and Re–Re bonds.[64] The CNs of the Re–O and Re–Re bonds in Re(5)/TiO_2 were determined to be 2.7 and 3.4, respectively, while the CNs of the Re–O and Re–Re bonds in Re(5)/Al_2O_3 were determined to be 2.0 and 8.6, respectively.[64] However, the Re species on the CeO_2, Nb_2O_5, and V_2O_5 supports are among the most highly dispersed, where they are mainly present as either single-atom or sub-nanocluster species, which could be the reason why Re peaks were not observed in their XRD patterns. In order to investigate the effect of the specific surface area of the support materials on the dispersion of Re species, low-specific-surface-area rutile TiO_2 (JRC-TIO-5) supported Re samples (Re(5)/TiO_2 (JRC-TIO-5)) were prepared. Rutile TiO_2 has a different bulk structure from anatase TiO_2, but both exhibit a similar electronic structure, e.g., the EA values for anatase and rutile are 5.20

and 5.45, respectively. These experimental observations indicate that Re dispersed on wide-gap non-reducible oxides[76–78] such as SiO_2, Al_2O_3, and MgO tends to be aggregated whereas Re dispersed on reducible oxide semiconductors such as TiO_2, V_2O_5, ZrO_2, Nb_2O_5, and CeO_2 exhibits a high degree of dispersion without the presence of aggregated species.

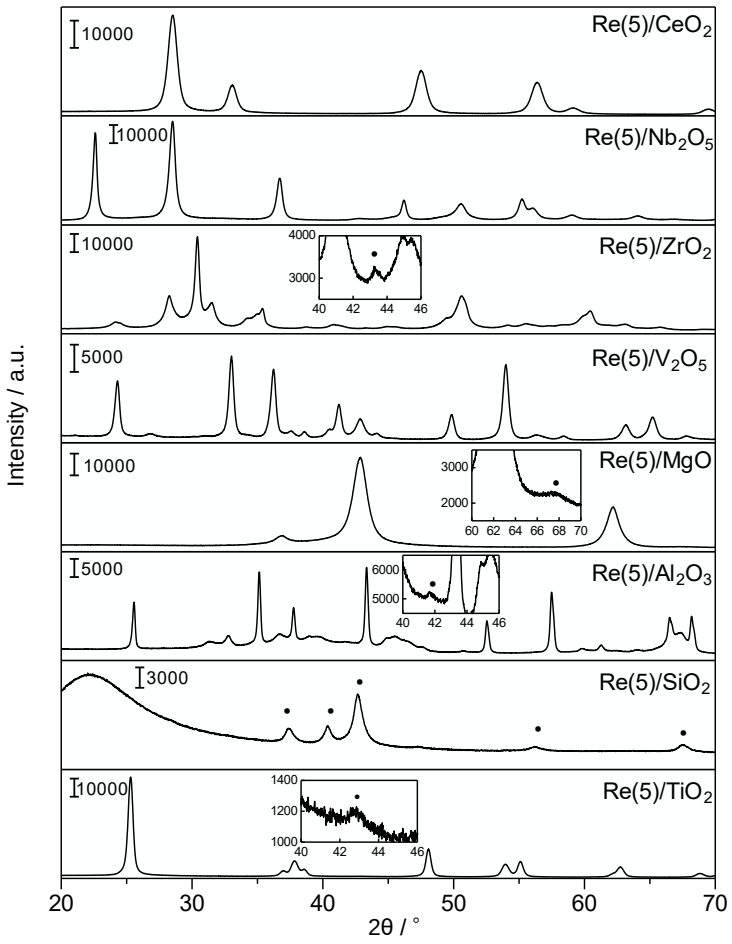

Figure 2. XRD patterns of the Re(5)/support samples (support = TiO_2, SiO_2, Al_2O_3, MgO, V_2O_5, ZrO_2, Nb_2O_5, and CeO_2); Re = 5 wt%.

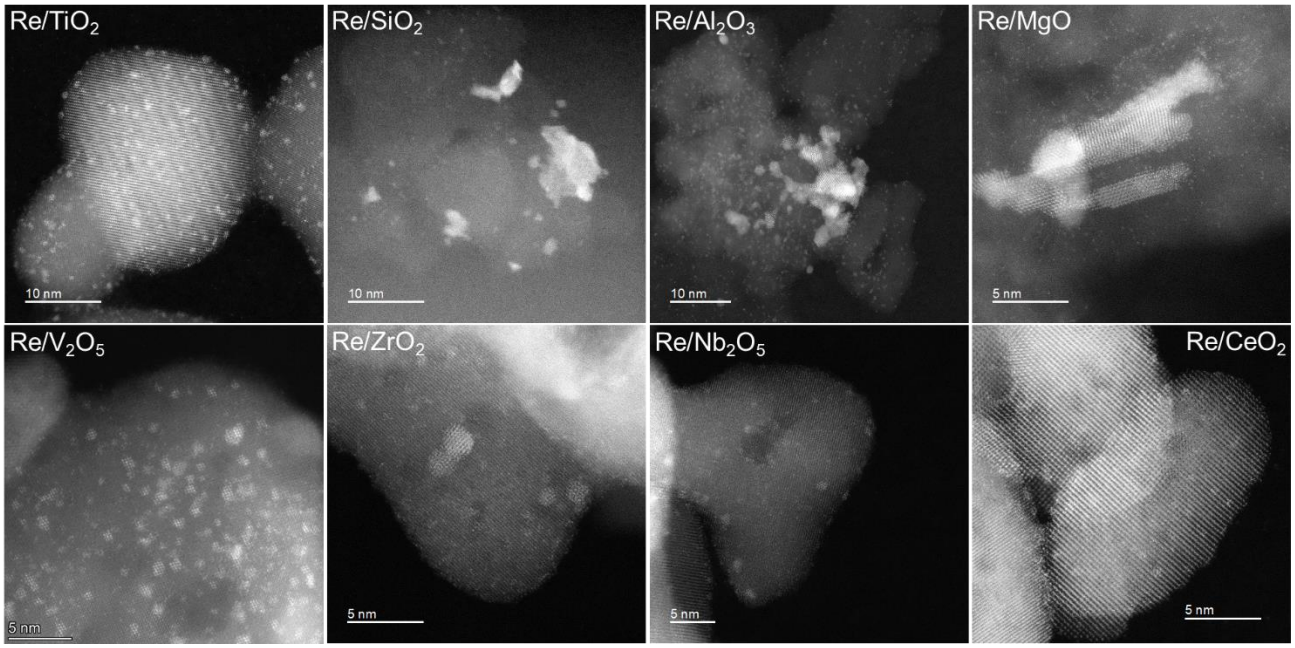

Figure 3. HAADF-STEM images of the Re(5)/support samples (support = TiO_2, SiO_2, Al_2O_3, MgO, V_2O_5, ZrO_2, Nb_2O_5, and CeO_2); Re = 5 wt%.

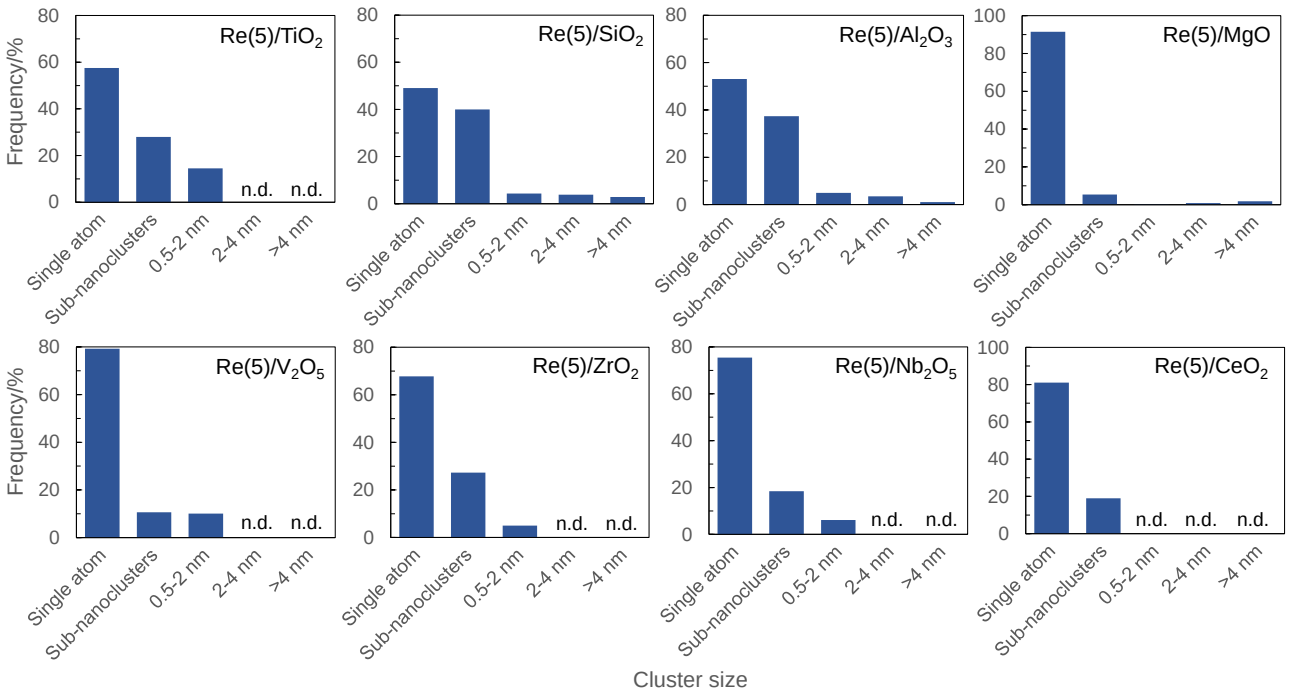

Figure 4. Particle-size distributions of the Re(5)/support samples (support = TiO_2, SiO_2, Al_2O_3, MgO, V_2O_5, ZrO_2, Nb_2O_5, and CeO_2) derived from the STEM observations. Atomically dispersed Re atoms were counted as a single atom, while Re species consisting of two to nine Re atoms were counted as sub-nanoclusters. Re clusters/nanoparticles consisting of more than ten atoms were categorized by their sizes (0.5-2 nm, 2-4 nm, and >4 nm). n.d. denotes “not detected”.

4.3.2 Interactions between Re and oxide supports

Identifying correlations between the degree of dispersion of Re on various supports and the physicochemical properties of both Re and the supports may enable to rationalize the observed degree of Re dispersion and to estimate this for as-yet prepared materials. This would be beneficial for screening of catalyst supports for use in specific applications without incurring significant experimental and/or computational costs. In the computational section of this study, we began by calculating the E_{ads} of a Re atom on the surface of each metal-oxide support using a representative surface model for each individual support. The SiO_2 and Nb_2O_5 surfaces were not modelled due to the uncertainty of their bulk structures (T-phase or TT-phase Nb_2O_5[79] and amorphous SiO_2) and the uncertainty in the surface termination, even for alpha-quartz SiO_2. Instead, Ga_2O_3, another common support, was analyzed. The E_{ads} values of a Re atom on MgO(100), θ-Al_2O_3(100), $ZrO_2(11\bar{1})$, CeO_2(111), β-Ga_2O_3(100), anatase TiO_2(101), and V_2O_5(010) were calculated to be -0.42, -1.80, -4.40, -3.61, -4.52, -4.11, and -6.34 eV, respectively. We found that the supports with less negative E_{ads} values, such as MgO and Al_2O_3, show a low degree of experimentally observed Re dispersion, whereas supports with more negative E_{ads} values, such as ZrO_2, CeO_2, TiO_2, and V_2O_5 show a high degree of experimentally observed Re dispersion. This result is in good agreement with previous computational assessments that the degree to which a metal is anchored to a support is governed by the binding energy of the metal atom; metals that exhibit strong exothermic binding to a support are less likely to diffuse across the support and agglomerate.[80] However, it should be noted that the specific surface area of each support is different and can affect the degree of Re dispersion. The trends observed between the physical properties of the oxide supports, including the O-vacancy-formation energy (E_{Ovac}), electron affinity (EA), ionization potential (IP), bandgap (BG), surface energy (E_{surf}), and electronegativity (EN), were analyzed further. From our previous study, we obtained the values for these properties, which were calculated at the same computational level of theory.[71] It is noteworthy that the EA is the negative of the conduction band minimum (CBM) with respect to the vacuum level, while the IP is the negative of the valence band maximum (VBM) with respect to the vacuum level.[71] The EN was obtained according to the Sanderson definition,[81] which is the geometric mean of Pauling's EN of atoms in the system. The Bader charge of the supported Re was also calculated in this study. These quantities are plotted as a

function of E_{ads} in **Figure 5**. A correlation map of these properties and E_{ads} is shown in **Figure 6** because these physical quantities are highly related to one other, and thus, this is an effective way to understand these very important correlations. The obtained coefficients of determination (R^2 values) for the correlation of E_{ads} with the EA and IP values as well as the Bader charges were greater than 0.8 (**Figure 5**), indicating a strong correlation between these properties and the E_{ads} of a Re adatom. The EA shows the highest R^2 (0.84), suggesting the presence of an electronic interaction between the Re adatom and the conduction band (CB) of the support oxide because the EA essentially corresponds to the position of the CBM with respect to the vacuum level.

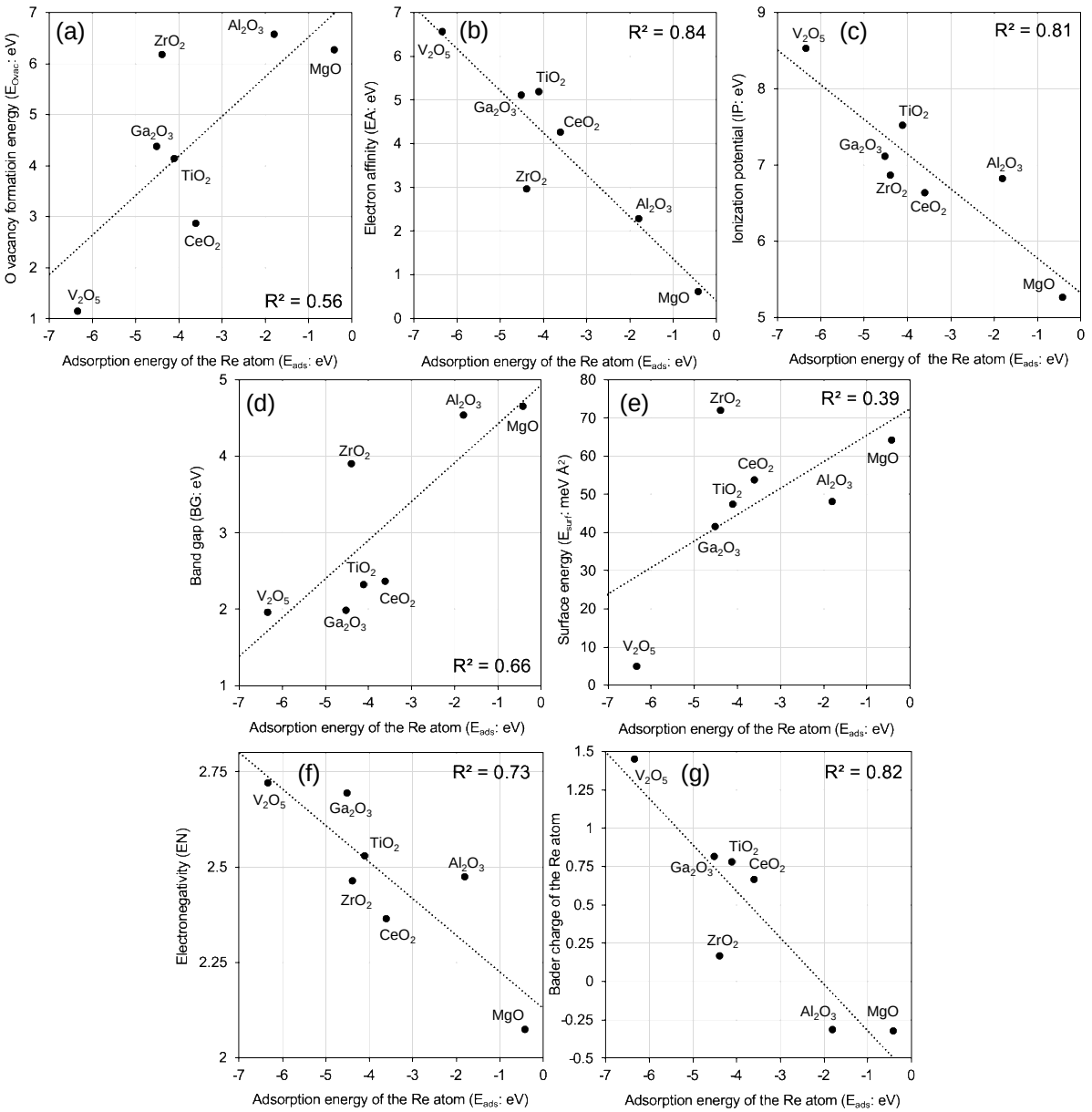

Figure 5. E_{ads} of a Re adatom on various support-oxide surfaces as a function of (a) O-vacancy-formation energy (E_{Ovac}), (b) electron affinity (EA), (c) ionization potential (IP), (d) band gap (BG), (e) surface energy (E_{surf}), (f) electronegativity (EN), and (g) Bader charge.

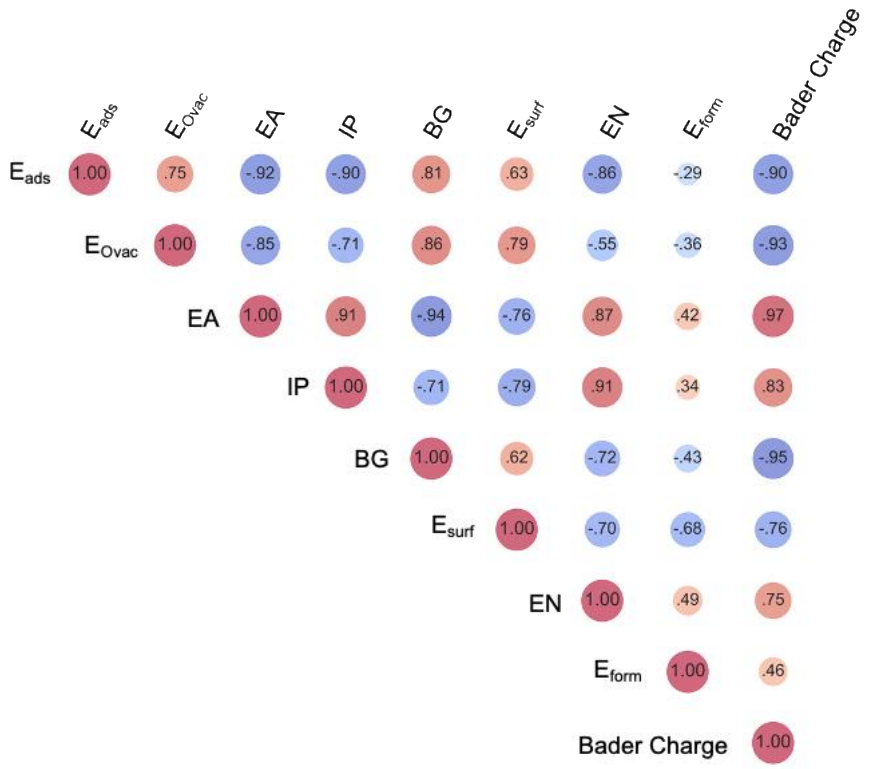

Figure 6. Correlation map of E_{ads} and other physical properties. The correlation coefficients (R) are given by the numbers in the circles.

To obtain further chemical insights into the electronic interactions between Re and the support oxides, a schematic energy diagram of the EA and IP of each metal-oxide support and the work function (WF) of the Re atom is shown in **Figure 7**. Note that the WF value of a Re atom is smaller (the Fermi energy, E_F, is shallower with respect to the vacuum level) than the value obtained in our previous study, at the same computational level of theory, for the most stable surface, i.e. (0001).[84] This is consistent with previous studies on the modelling of WFs where the surface energy is inversely proportional to the WFs via the broken-bond surface density.[85–87] Specifically, the higher coordination to which unsaturated metals are exposed, the smaller the WFs become. In this study, there is a group of support metal oxides that have both an EA that is larger than the WF of the Re atoms, which results in a high E_{ads} of Re (CeO_2, Ga_2O_3, TiO_2, and V_2O_5). As a result, these metal oxides can incorporate electrons from the Re atoms into their conduction bands (CBs) because their CBM are located below the E_F of the Re atom. This suggests that the charge is transferred from Re to the oxide support and therefore these oxides can act as electron scavengers that negatively

increase the E_{ads} by inducing interactions between the Re adatom and the surface. In contrast, there is a second group of metal oxides that have an EA that is smaller than the WF of the Re atoms, which results in a low E_{ads} of Re (MgO and Al_2O_3). These support oxides cannot receive electrons from Re as their CBM positions are far above the E_F of the Re atom and therefore, these metal oxides cannot act as electron scavengers, which results in a low E_{ads} of Re. This is supported by the observation that the Bader charge of a supported Re adatom also shows high correlation with the Re E_{ads} (R^2 = 0.82).

In addition, the differential charge densities of Re supported on two representative surfaces (anatase TiO_2 (101) and MgO(100)) and the Bader charge of the Re adatom, the adjacent Ti center, and O for these systems were calculated using the GGA/PBEsol(+*U*) functional (**Figure 8**). The E_{ads} of Re on TiO_2(101) and MgO(100) were calculated to be -4.11 and -0.42 eV, respectively. These E_{ads} values follow the trends described above: TiO_2(101) exhibits a larger E_{ads} on account of its larger EA (lower position of the CBM), whereas MgO(100) exhibits a smaller E_{ads} due to its smaller EA (higher position of the CBM). A visual representation of the charge transfer upon adsorption of Re on the anatase TiO_2(101) surface demonstrates that the adsorption of Re causes significant charge transfer from the Re adatom to the surface. Charge that initially surrounds the Re adatom redistributes toward the neighboring O and Ti atoms. In contrast, there is almost no donation of charge from the Re adatom to the MgO(100) surface. Similarly, the Bader charge analysis showed that, for Re supported on anatase TiO_2 (110), the Re adatom donates electrons to the adjacent Ti center. On the other hand, for Re supported on MgO (100), the electrons are donated from the adjacent O atom to the Re adatom.

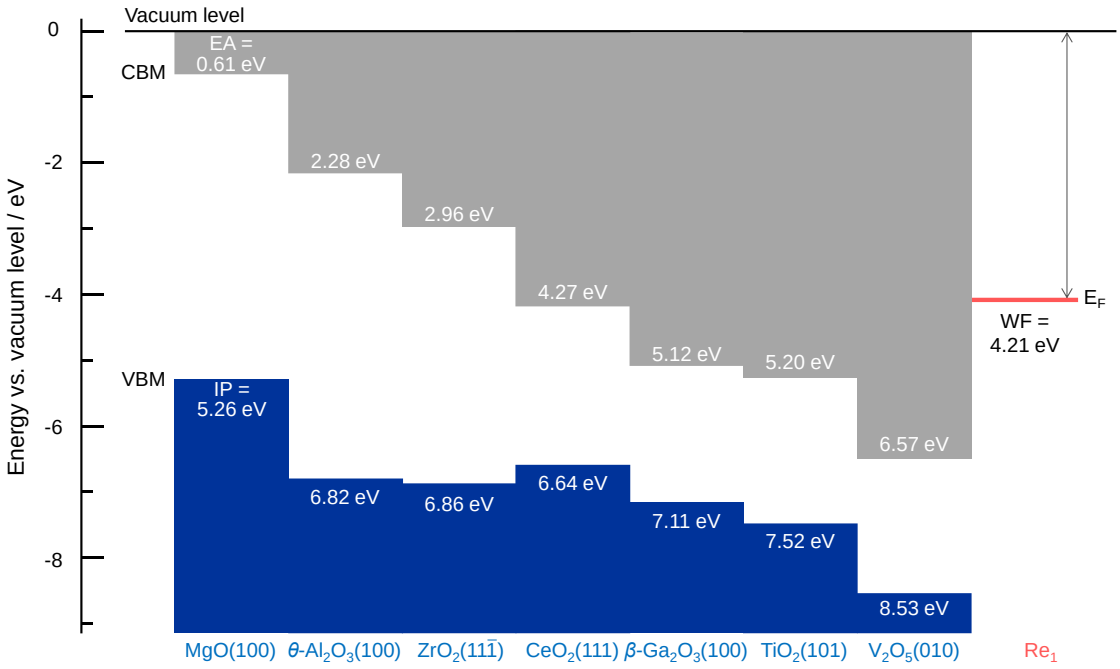

Figure 7. Valance-band maxima and conduction-band minima with respect to the vacuum level (the negatives of the IP and EA, respectively) for the support-oxide surfaces. Also shown is the work function with respect to the vacuum level (the negative of the E_F) for the Re atom (red line) obtained from DFT calculations using the PBEsol functional.

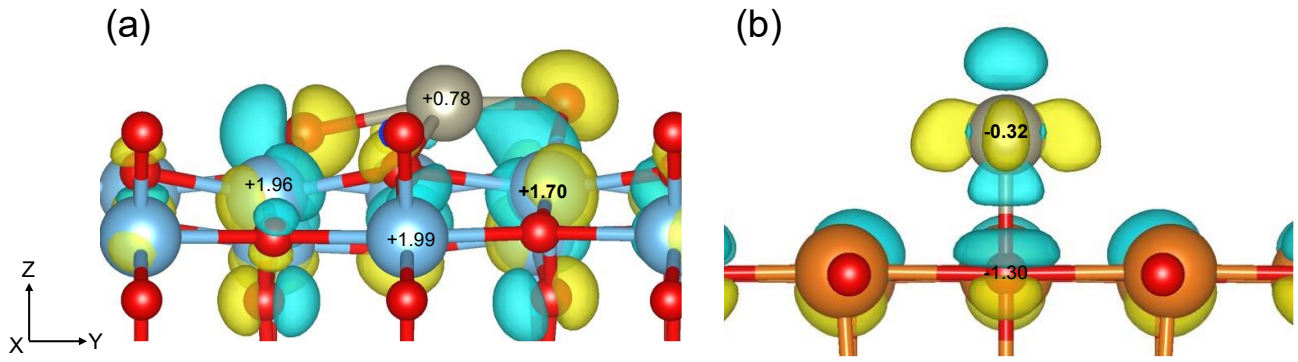

Figure 8. Differential charge densities of Re supported on (a) anatase TiO_2 (110) and (b) MgO(100) surfaces calculated by using the GGA/PBEsol(+*U*) functional. The charge density represented in yellow and blue shows the positive and negative phases, respectively. The numbers represent the Bader charge. The isosurface was set to 0.01 |e|/Bohr^3; light blue: Ti; red: O; orange: Mg; gray: Re.

4.4 Conclusions

We have used a combined experimental and computational approach to investigate the metal−support interactions (MSIs) of Re adsorbed on a series of metal-oxide supports (TiO_2, SiO_2, Al_2O_3, MgO, V_2O_5, ZrO_2, Nb_2O_5, and CeO_2). In their entirety, our investigations suggest that the degree of dispersion and aggregation of the Re atoms on the surface of the oxide supports is correlated to the electronic properties of both species. The position of the conduction band minimum (CBM) of the oxide support, which serves as a proxy for the electron affinity (EA), and the Fermi energy (E_F) of the supported Re, which serves as a proxy for the work function (WF), are of particular importance. Metal-oxide supports that exhibit an EA that is higher than the WF of Re (TiO_2, V_2O_5, and CeO_2) accept electrons from Re into their CB, which induces strong MSIs and results in a relatively high Re-adsorption energy (E_{ads}) that leads to a high degree of dispersion of the supported Re metal. Conversely, metal oxides that exhibit an EA smaller than the WF of Re (MgO and Al_2O_3) do not incorporate electrons from Re into their CB, which induces merely weak MSIs and a correspondingly small E_{ads} for Re. Ultimately, this leads to low degrees of dispersion of the supported Re metal. These fundamental insights into the electronic interactions that govern the degree of dispersion of Re on various metal-oxide supports will most likely be also applicable to other combinations of metals and supports. Our results rationalize experimental observations, elucidate the underlying physics of MSIs, and can thus be expected to guide future studies to create fine-tuned supported metal materials.

4.5 References

(1) Haruta, M. Size- and Support-Dependency in the Catalysis of Gold. *Catal. Today* **1997**, *36*, 153–166.

(2) Freund, H. J.; Pacchioni, G. Oxide Ultra-Thin Films on Metals: New Materials for the Design of Supported Metal Catalysts. *Chem. Soc. Rev.* **2008**, *37*, 2224–2242.

(3) Goodman, E. D.; Schwalbe, J. A.; Cargnello, M. Mechanistic Understanding and the Rational Design of Sinter- Resistant Heterogeneous Catalysts. *ACS Catal.* **2017**, *7*, 7156−7173.

(4) Ro, I.; Resasco, J.; Christopher, P. Approaches for Understanding and Controlling Interfacial Effects in Oxide-Supported Metal Catalysts. *ACS Catal.* **2018**, *8*, 7368−7387.

(5) Fu, J.; Lym, J.; Zheng, W.; Alexopoulos, K.; Mironenko, A. V.; Li, N.; Boscoboinik, J. A.; Su, D.; Weber, R. T.; Vlachos, D. G. C–O Bond Activation Using Ultralow Loading of Noble Metal Catalysts on Moderately Reducible Oxides. *Nat. Catal.* **2020**, *3*, 446–453.

(6) Haruta, M. Spiers Memorial Lecture: Role of Perimeter Interfaces in Catalysis by Gold Nanoparticles. *Faraday Discuss.* **2011**, *152*, 11–32.

(7) Cargnello, M.; Doan-Nguyen, V. V. T.; Gordon, T. R.; Diaz, R. E.; Stach, E. A.; Gorte, R. J.; Fornasiero, P.; Murray, C. B. Control of Metal Nanocrystal Size Reveals Metal-Support Interface Role for Ceria Catalysts. *Science (80-.).* **2013**, *341*, 771–773.

(8) Kudernatsch, W.; Peng, G.; Zeuthen, H.; Bai, Y.; Merte, L. R.; Lammich, L.; Besenbacher, F.; Mavrikakis, M.; Wendt, S. Direct Visualization of Catalytically Active Sites at the FeO-Pt(111) Interface. *ACS Nano* **2015**, *9*, 7804–7814.

(9) van Deelen, T. W.; Hernández Mejía, C.; de Jong, K. P. Control of Metal-Support Interactions in Heterogeneous Catalysts to Enhance Activity and Selectivity. *Nat. Catal.* **2019**, *2*, 955–970.

(10) Kumar, K. B. S.; Whittaker, T. N.; Peterson, C.; Grabow, L. C.; Chandler, B. D. Water Poisons H_2 Activation at the Au−TiO_2 Interface by Slowing Proton and Electron Transfer between Au and Titania. *J. Am. Chem. Soc.* **2020**, *142*, 5760−5772.

(11) Goodman, D. W. Model Studies in Catalysis Using Surface Science Probes. *Chem. Rev.* **1995**, *95*, 523–536.

(12) Mostafa, S.; Behafarid, F.; Croy, J. R.; Ono, L. K.; Li, L.; Yang, J. C.; Frenkel, A. I.; Cuenya, B. R. Shape-Dependent Catalytic Properties of Pt Nanoparticles. *J. Am. Chem. Soc.* **2010**, *132*, 15714–15719.

(13) Liu, L.; Corma, A. Metal Catalysts for Heterogeneous Catalysis: From Single Atoms to Nanoclusters and Nanoparticles. *Chem. Rev.* **2018**, *118*, 4981−5079.

(14) Ghanekar, P.; Kubal, J.; Cui, Y.; Mitchell, G.; Delgass, W. N.; Ribeiro, F.; Greeley, J. Catalysis at Metal/Oxide Interfaces: Density Functional Theory and Microkinetic Modeling of Water Gas Shift at Pt/MgO Boundaries. *Top. Catal.* **2020**, *63* (7–8), 673–687.

(15) Rice, P. S.; Hu, P. Understanding Supported Noble Metal Catalysts Using First-Principles Calculations. *J. Chem. Phys.* **2019**, *151*, 180902.

(16) Hansen, T. W.; Delariva, A. T.; Challa, S. R.; Datye, A. K. Sintering of Catalytic Nanoparticles: Particle Migration or Ostwald Ripening? *Acc. Chem. Res.* **2013**, *46* (8), 1720–1730.

(17) Su, Y. Q.; Liu, J. X.; Filot, I. A. W.; Hensen, E. J. M. Theoretical Study of Ripening Mechanisms of Pd Clusters on Ceria. *Chem. Mater.* **2017**, *29*, 9456–9462.

(18) Iyemperumal, S. K.; Pham, T. D.; Bauer, J.; Deskins, N. A. Quantifying Support Interactions and Reactivity Trends of Single Metal Atom Catalysts over TiO_2. *J. Phys. Chem. C* **2018**, *122*, 25274–25289.

(19) Wang, X.; Van Bokhoven, J. A.; Palagin, D. Atomically Dispersed Platinum on Low Index and Stepped Ceria Surfaces: Phase Diagrams and Stability Analysis. *Phys. Chem. Chem. Phys.* **2019**, *22*, 28–38.

(20) Su, Y. Q.; Zhang, L.; Wang, Y.; Liu, J. X.; Muravev, V.; Alexopoulos, K.; Filot, I. A. W.; Vlachos, D. G.; Hensen, E. J. M. Stability of Heterogeneous Single-Atom Catalysts: A Scaling Law Mapping Thermodynamics to Kinetics. *npj Comput. Mater.* **2020**, *6*, 144.

(21) Nelson, R. C.; Baek, B.; Ruiz, P.; Goundie, B.; Brooks, A.; Wheeler, M. C.; Frederick, B. G.; Grabow, L. C.; Austin, R. N. Experimental and Theoretical Insights into the Hydrogen-Efficient Direct Hydrodeoxygenation Mechanism of Phenol over Ru/TiO_2. *ACS Catal.* **2015**, *5*, 6509–6523.

(22) Mehta, P.; Greeley, J.; Delgass, W. N.; Schneider, W. F. Adsorption Energy Correlations at the Metal-Support Boundary. *ACS Catal.* **2017**, *7* (7), 4707–4715.

(23) Daelman, N.; Marçal, C.-C.; López, N. Dynamic Charge and Oxidation State of Pt/CeO_2 Single-Atom Catalysts. *Nat. Mater.* **2019**, *18*, 1215–1221.

(24) Dietze, E. M.; Plessow, P. N. Predicting the Strength of Metal-Support Interaction with Computational Descriptors for Adhesion Energies. *J. Phys. Chem. C* **2019**, *123* (33), 20443–20450.

(25) Paz-Borbón, L. O.; Buendiá, F.; Garzón, I. L.; Posada-Amarillas, A.; Illas, F.; Li, J. $CeO_2(111)$ Electronic Reducibility Tuned by Ultra-Small Supported Bimetallic Pt-Cu Clusters. *Phys. Chem. Chem. Phys.* **2019**, *21*, 15286–15296.

(26) Strayer, M. E.; Binz, J. M.; Tanase, M.; Kamali Shahri, S. M.; Sharma, R.; Rioux, R. M.; Mallouk, T. E. Interfacial Bonding Stabilizes Rhodium and Rhodium Oxide Nanoparticles on Layered Nb Oxide and Ta Oxide Supports. *J. Am. Chem. Soc.* **2014**, *136*, 5687–5696.

(27) Strayer, M. E.; Senftle, T. P.; Winterstein, J. P.; Vargas-Barbosa, N. M.; Sharma, R.; Rioux, R. M.; Janik, M. J.; Mallouk, T. E. Charge Transfer Stabilization of Late Transition Metal Oxide Nanoparticles on a Layered Niobate Support. *J. Am. Chem. Soc.* **2015**, *136*, 5687−5696.

(28) Liu, J. Catalysis by Supported Single Metal Atoms. *ACS Catal.* **2017**, *7*, 34−59.

(29) Puigdollers, A. R.; Schlexer, P.; Tosoni, S.; Pacchioni, G. Increasing Oxide Reducibility: The Role of Metal/Oxide Interfaces in the Formation of Oxygen Vacancies. *ACS Catal.* **2017**, *7*, 6493–6513.

(30) Qin, R.; Liu, P.; Fu, G.; Zheng, N. Strategies for Stabilizing Atomically Dispersed Metal Catalysts. *Small Methods* **2018**, *2*, 1700286.

(31) Lang, R.; Xi, W.; Liu, J. C.; Cui, Y. T.; Li, T.; Lee, A. F.; Chen, F.; Chen, Y.; Li, L.; Li, L.; Lin, J.; Miao, S.; Liu, X.; Wang, A. Q.; Wang, X.; Luo, J.; Qiao, B.; Li, J.; Zhang, T. Non Defect-Stabilized Thermally Stable Single-Atom Catalyst. *Nat. Commun.* **2019**, *10*, 234.

(32) Campbell, C. T.; Mao, Z. Chemical Potential of Metal Atoms in Supported Nanoparticles: Dependence upon Particle Size and Support. *ACS Catal.* **2017**, *7*, 8460–8466.

(33) Mao, Z.; Campbell, C. T. Predicting a Key Catalyst-Performance Descriptor for Supported Metal Nanoparticles: Metal Chemical Potential. *ACS Catal.* **2021**, *11* (1), 8284–8291.

(34) Campbell, C. T.; Sellers, J. R. V. Anchored Metal Nanoparticles: Effects of Support and Size on Their Energy, Sintering Resistance and Reactivity. *Faraday Discuss.* **2013**, *162*, 9–30.

(35) Nørskov, J. K.; Bligaard, T.; Rossmeisl, J.; Christensen, C. H. Towards the Computational Design of Solid Catalysts. *Nat. Chem.* **2009**, *1*, 37–46.

(36) Noronha, F. B.; Fendley, E. C.; Soares, R. R.; Alvarez, W. E.; Resasco, D. E. Correlation between Catalytic Activity and Support Reducibility in the CO_2 Reforming of Methane over $Pt/Ce_xZr_{1-x}O_2$ Catalysts. *Chem. Eng. J.* **2001**, *82*, 21–31.

(37) Hemmingson, S. L.; Campbell, C. T. Trends in Adhesion Energies of Metal Nanoparticles on Oxide Surfaces: Understanding Support Effects in Catalysis and Nanotechnology. *ACS Nano* **2017**, *11*, 1196–1203.

(38) Tan, K.; Dixit, M.; Dean, J.; Mpourmpakis, G. Predicting Metal-Support Interactions in Oxide-Supported Single-Atom Catalysts. *Ind. Eng. Chem. Res.* **2019**, *58*, 20236−20246.

(39) O'Connor, N. J.; Jonayat, A. S. M.; Janik, M. J.; Senftle, T. P. Interaction Trends between Single Metal Atoms and Oxide Supports Identified with Density Functional Theory and Statistical Learning. *Nat. Catal.* **2018**, *1*, 531–539.

(40) Wang, L.; Ohnishi, R.; Ichikawa, M. Selective Dehydroaromatization of Methane toward Benzene on Re/HZSM-5 Catalysts and Effects of CO/CO_2Addition. *J. Catal.* **2000**, *190*, 276–283.

(41) Chia, M.; Pagán-Torres, Y. J.; Hibbitts, D.; Tan, Q.; Pham, H. N.; Datye, A. K.; Neurock, M.; Davis, R. J.; Dumesic, J. A. Selective Hydrogenolysis of Polyols and Cyclic Ethers over Bifunctional Surface Sites on Rhodium-Rhenium Catalysts. *J. Am. Chem. Soc.* **2011**, *133*, 12675–12689.

(42) Lwin, S.; Li, Y.; Frenkel, A. I.; Wachs, I. E. Activation of Surface ReOx Sites on Al_2O_3 Catalysts for Olefin Metathesis. *ACS Catal.* **2015**, *5*, 6807−6814.

(43) Sandbrink, L.; Klindtworth, E.; Islam, H. U.; Beale, A. M.; Palkovits, R. ReO_x/TiO_2: A Recyclable Solid Catalyst for Deoxydehydration. *ACS Catal.* **2016**, *6*, 677–680.

(44) Cao, J.; Tamura, M.; Hosaka, R.; Nakayama, A.; Hasegawa, J. Y.; Nakagawa, Y.; Tomishige, K. Mechanistic Study on Deoxydehydration and Hydrogenation of Methyl Glycosides to Dideoxy Sugars over a ReOx-Pd/CeO2Catalyst. *ACS Catal.* **2020**, *10*, 12040–12051.

(45) Xu, Y.; Hirano, T.; Kunieda, H.; Hara, Y.; Miyata, Y. Enhancing the Methane Steam Reforming Catalytic Performance of Ni Monolithic Catalysts: Via Ni-Re Surface Alloying. *Catal. Sci. Technol.* **2020**, *10*, 2004–2019.

(46) Yu, Y.; Yi, X.; Zhang, J.; Tong, Z.; Chen, C.; Ma, M.; He, C.; Wang, J.; Chen, J.; Chen, B. Application of ReO_x/TiO_2 Catalysts with Excellent SO_2 Tolerance for the Selective Catalytic Reduction of NO_x by NH_3. *Catal. Sci. Technol.* **2021**, *11*, 5125–5134.

(47) Gothe, M. L.; Silva, K. L. C.; Figueredo, A. L.; Fiorio, J. L.; Rozendo, J.; Manduca, B.; Simizu, V.; Freire, R. S.; Garcia, M. A. S.; Vidinha, P. Rhenium – A Tuneable Player in Tailored Hydrogenation Catalysis. *Eur. J. Inorg. Chem.* **2021**, in press.

(48) Takeda, Y.; Nakagawa, Y.; Tomishige, K. Selective Hydrogenation of Higher Saturated Carboxylic Acids to Alcohols Using a ReOx–Pd/SiO2 Catalyst. *Catal. Sci. Technol.* **2012**, *2*, 2221–2223.

(49) Liu, K.; Pritchard, J.; Lu, L.; Van Putten, R.; Verhoeven, M. W. G. M.; Schmitkamp, M.; Huang, X.; Lefort, L.; Kiely, C. J.; Hensen, E. J. M.; Pidko, E. A. Supported Nickel-Rhenium Catalysts for Selective Hydrogenation of Methyl Esters to Alcohols. *Chem. Commun.* **2017**, *53*, 9761–9764.

(50) Toyao, T.; Siddiki, S. M. A. H.; Touchy, A. S.; Onodera, W.; Kon, K.; Morita, Y.; Kamachi, T.; Yoshizawa, K.; Shimizu, K. TiO_2-Supported Re as a General and Chemoselective Heterogeneous Catalyst for Hydrogenation of Carboxylic Acids to Alcohols. *Chem. - A Eur. J.* **2017**, *23*, 1001–1006.

(51) Toyao, T.; Siddiki, S. M. A. H.; Morita, Y.; Kamachi, T.; Touchy, A. S.; Onodera, W.; Kon, K.; Furukawa, S.; Ariga, H.; Asakura, K.; Yoshizawa, K.; Shimizu, K. Rhenium-Loaded TiO_2: A Highly Versatile and Chemoselective Catalyst for the Hydrogenation of Carboxylic Acid Derivatives and the N-Methylation of Amines Using H_2 and CO_2. *Chem. - A Eur. J.* **2017**, *23*, 14848–14859.

(52) Tomishige, K.; Nakagawa, Y.; Tamura, M. Taming Heterogeneous Rhenium Catalysis for the Production of Biomass-Derived Chemicals. *Chinese Chem. Lett.* **2020**, *31*, 1049–1344.

(53) Huang, X.; Liu, K.; Vrijburg, W. L.; Ouyang, X.; Iulian Dugulan, A.; Liu, Y.; Tiny Verhoeven, M. W. G. M.; Kosinov, N. A.; Pidko, E. A.; Hensen, E. J. M. Hydrogenation of Levulinic Acid to γ-Valerolactone over Fe-Re/TiO_2 Catalysts. *Appl. Catal. B Environ.* **2020**, *278*, 119314.

(54) Xu, Z.; Qian, Z. H.; Tanabe, K.; Hattori, H. Support Effect of Re Catalyst on Methanol Synthesis From CO_2 and H_2 Under a Pressure of 5-Atm. *Bull. Chem. Soc. Jpn.* **1991**, *64*, 1664–1668.

(55) Manyar, H. G.; Paun, C.; Pilus, R.; Rooney, D. W.; Thompson, J. M.; Hardacre, C. Highly Selective and Efficient Hydrogenation of Carboxylic Acids to Alcohols Using Titania Supported Pt Catalysts. *Chem. Commun.* **2010**, *46*, 6279–6281.

(56) Rozmysłowicz, B.; Kirilin, A.; Aho, A.; Manyar, H.; Hardacre, C.; Wärnå, J.; Salmi, T.; Murzin, D. Y. Selective Hydrogenation of Fatty Acids to Alcohols over Highly Dispersed ReO_x/TiO_2Catalyst. *J. Catal.* **2015**, *328*, 197–207.

(57) Ting, K. W.; Toyao, T.; Siddiki, S. M. A. H.; Shimizu, K. Low-Temperature Hydrogenation of CO_2 to Methanol over Heterogeneous TiO_2-Supported Re Catalysts. *ACS Catal.* **2019**, *9*, 3685–3693.

(58) Ting, K. W.; Kamakura, H.; Poly, S.; Toyao, T.; Siddiki, S. M. A. H.; Maeno, Z.; Matsushita, K.; Shimizu, K. Catalytic Methylation of Aromatic Hydrocarbons Using CO_2/H_2 over Re/TiO_2 and H-MOR Catalysts. *ChemCatChem* **2020**, *12*, 2215–2220.

(59) Gothe, M. L.; Pérez-Sanz, F. J.; Braga, A. H.; Borges, L. R.; Abreu, T. F.; Bazito, R. C.; Gonçalves, R. V.; Rossi, L. M.; Vidinha, P. Selective CO_2 Hydrogenation into Methanol in a Supercritical Flow Process. *J. CO2 Util.* **2020**, *40*, 101195.

(60) Okal, J.; Tylus, W.; Kepinski, L. XPS Study of Oxidation of Rhenium Metal on γ-Al2O3 Support. *J. Catal.* **2004**, *225*, 498–509.

(61) Bare, S. R.; Kelly, S. D.; D.vila, F.; Boldingh, E.; Karapetrova, E.; Kas, J.; Mickelson, G. E.; Modica, F. S.; Yang, N.; Rehr, J. J. Experimental (XAS, STEM, TPR, and XPS) and Theoretical (DFT) Characterization of Supported Rhenium Catalysts. *J. Phys. Chem. C* **2011**, *115*, 5740–5755.

(62) She, X.; Brown, H. M.; Zhang, X.; Ahring, B. K.; Wang, Y. Selective Hydrogenation of Trans,Trans-Muconic Acid to Adipic Acid over a Titania-Supported Rhenium Catalyst. *ChemSusChem* **2011**, *4*, 1071–1073.

(63) Ly, B. K.; Tapin, B.; Aouine, M.; Delichere, P.; Epron, F.; Pinel, C.; Especel, C.; Besson, M. Insights into the Oxidation State and Location of Rhenium in Re-Pd/TiO_2Catalysts for Aqueous-Phase Selective Hydrogenation of Succinic Acid to 1,4-Butanediol as a Function of Palladium and Rhenium Deposition Methods. *ChemCatChem* **2015**, *7*, 2161–2178.

(64) Toyao, T.; Ting, K. W.; Siddiki, S. M. A. H.; Touchy, A. S.; Onodera, W.; Maeno, Z.; Ariga-Miwa, H.; Kanda, Y.; Asakura, K.; ichi Shimizu, K. Mechanistic Study of the Selective Hydrogenation of Carboxylic Acid Derivatives over Supported Rhenium Catalysts. *Catal. Sci. Technol.* **2019**, *9*, 5413–5424.

(65) Kresse, G.; Furthmüller, J. Efficient Iterative Schemes for Ab Initio Total-Energy Calculations Using a Plane-Wave Basis Set. *Phys. Rev. B - Condens. Matter Mater. Phys.* **1996**, *54*, 11169–11186.

(66) Kresse, G.; Furthmüller, J. Efficiency of Ab-Initio Total Energy Calculations for Metals and Semiconductors Using a Plane-Wave Basis Set. *Comput. Mater. Sci.* **1996**, *6*, 15–50.

(67) Perdew, J. P.; Ruzsinszky, A.; Csonka, G. I.; Vydrov, O. A.; Scuseria, G. E.; Constantin, L. A.; Zhou, X.; Burke, K. Restoring the Density-Gradient Expansion for Exchange in Solids and Surfaces. *Phys. Rev. Lett.* **2008**.

(68) Blöchl, P. E. Projector Augmented-Wave Method. *Phys. Rev. B* **1994**, *50*, 17953–17979.

(69) Grimme, S.; Ehrlich, S.; Goerigk, L. Effect of the Damping Function in Dispersion Corrected Density Functional Theory. *J. Comput. Chem.* **2011**, *32*, 1456–1465.

(70) Dudarev, S.; Botton, G. Electron-Energy-Loss Spectra and the Structural Stability of Nickel Oxide: An LSDA+U Study. *Phys. Rev. B - Condens. Matter Mater. Phys.* **1998**, *57*, 1505.

(71) Hinuma, Y.; Toyao, T.; Kamachi, T.; Maeno, Z.; Takakusagi, S.; Furukawa, S.; Takigawa, I.; Shimizu, K. I. Density Functional Theory Calculations of Oxygen Vacancy Formation and Subsequent Molecular Adsorption on Oxide Surfaces. *J. Phys. Chem. C* **2018**, *122* (51), 29435–29444.

(72) Heyd, J.; Scuseria, G. E.; Ernzerhof, M. Hybrid Functionals Based on a Screened Coulomb Potential. *J. Chem. Phys.* **2003**, *118* (18), 8207–8215.

(73) Krukau, A. V.; Vydrov, O. A.; Izmaylov, A. F.; Scuseria, G. E. Influence of the Exchange Screening Parameter on the Performance of Screened Hybrid Functionals. *J. Chem. Phys.* **2006**, *125* (22).

(74) Lang, R.; Du, X.; Huang, Y.; Jiang, X.; Zhang, Q.; Guo, Y.; Liu, K.; Qiao, B.; Wang, A.; Zhang, T. Single-Atom Catalysts Based on the Metal-Oxide Interaction. *Chem. Rev.* **2020**, *120* (21), 11986–12043.

(75) Kaiser, S. K.; Chen, Z.; Faust Akl, D.; Mitchell, S.; Pérez-Ramírez, J. Single-Atom Catalysts across the Periodic Table. *Chem. Rev.* **2020**, *120*, 11703–11809.

(76) Helali, Z.; Jedidi, A.; Syzgantseva, O. A.; Calatayud, M.; Minot, C. Scaling Reducibility of Metal Oxides. *Theor. Chem. Acc.* **2017**, *136*, 100.

(77) Pacchioni, G.; Freund, H. J. Controlling the Charge State of Supported Nanoparticles in Catalysis: Lessons from Model Systems. *Chem. Soc. Rev.* **2018**, *47*, 8474–8502.

(78) Rousseau, R.; Glezakou, V. A.; Selloni, A. Theoretical Insights into the Surface Physics and Chemistry of Redox-Active Oxides. *Nat. Rev. Mater.* **2020**, *5* (6), 460–475.

(79) Siddiki, S. M. A. H.; Rashed, M. N.; Ali, M. A.; Toyao, T.; Hirunsit, P.; Ehara, M.; Shimizu, K. Lewis Acid Catalysis of Nb2O5 for Reactions of Carboxylic Acid Derivatives in the Presence of Basic Inhibitors. *ChemCatChem* **2019**, *11*, 383–396.

(80) Campbell, C. T. The Energetics of Supported Metal Nanoparticles: Relationships to Sintering Rates and Catalytic Activity. *Acc. Chem. Res.* **2013**, *46*, 1712–1719.

(81) Sanderson, R. T. Principles of Electronegativity. Part II. Applications. *J. Chem. Educ.* **1988**, *65* (2), 227–231.

(82) Grüneis, A.; Kresse, G.; Hinuma, Y.; Oba, F. Ionization Potentials of Solids: The Importance of Vertex Corrections. *Phys. Rev. Lett.* **2014**, *112* (9), 1–5.

(83) Hinuma, Y.; Grüneis, A.; Kresse, G.; Oba, F. Band Alignment of Semiconductors from Density-Functional Theory and Many-Body Perturbation Theory. *Phys. Rev. B - Condens. Matter Mater. Phys.* **2014**, *90* (15), 1–16.

(84) Hinuma, Y.; Toyao, T.; Hamamoto, N.; Takao, M.; Shimizu, K. I.; Kamachi, T. Changes in Surface Oxygen Vacancy Formation Energy at Metal/ Oxide Perimeter Sites: A Systematic Study on Metal Nanoparticles Deposited on an In2O3(111) Support. *J. Phys. Chem. C* **2020**, *124* (50), 27621–27630.

(85) Wang, J.; Wang, S. Q. Surface Energy and Work Function of Fcc and Bcc Crystals: Density Functional Study. *Surf. Sci.* **2014**, *630*, 216–224.

(86) Ji, D. P.; Zhu, Q.; Wang, S. Q. Detailed First-Principles Studies on Surface Energy and Work Function of Hexagonal Metals. *Surf. Sci.* **2016**, *651*, 137–146.

(87) Tran, R.; Li, X. G.; Montoya, J. H.; Winston, D.; Persson, K. A.; Ong, S. P. Anisotropic Work Function of Elemental Crystals. *Surf. Sci.* **2019**, *687*, 48–55.

(88) Pham, T. D.; Deskins, N. A. Efficient Method for Modeling Polarons Using Electronic Structure Methods. *J. Chem. Theory Comput.* **2020**, *16* (8), 5264–5278.

Chapter 5

General conclusion

In this work, TiO_2-supported Re catalyst was found to be highly active and selective for low-temperature hydrogenation of CO_2 to methanol reaction, which exceeded the activity of performance of the industrial Cu-based methanol synthesis catalyst tested under the reaction condition in this study. The applicability of this methanol synthesis system was further expanded by using one-pot reaction approach which combines methanol synthesis and subsequent methylation of aromatic hydrocarbons for the synthesis of value-added arenes. In the case of catalytic methylation of aromatic hydrocarbons, Re/TiO_2 performed the best by showing the highest yield and selectivity for methylated products, while preventing the dearomatization of aromatic rings. Driven by the desire of utilizing large datasets that we have accumulated over time, optimization of catalyst for above methylation reaction using machine-learning methods was also carried out, where a better performing catalyst in the form of 1.8 wt% Re/TiO_2 was discovered. The origin of the high activity and selectivity of Re/TiO_2 was also found to be partly attributed to the strong metal-support interactions (MSIs) between Re species and TiO_2, particularly the high electron affinity between the two, which enabled high dispersion of Re species loaded on TiO_2. The presence of atomically dispersed Re and Re nanoclusters are believed to be crucial for the catalysis of both reactions. We believe that our findings can facilitate a deeper understanding of supported rhenium catalysts and potentially utilize them in various hydrogenation reaction in real world.